Università degli Studi di Cagliari

DOTTORATO DI RICERCA

Internazionalizzato in Ingegneria e Scienze Ambientali

Ciclo …XXIII……...

TITOLO TESI

Dust signatures observed in atmospheric aerosols and related to radiative transfer algorithms

Settore/i scientifico disciplinari di afferenza

FIS/06 …FIS/07

Presentata da: … Dott.ssa Marzia Boccone……..

Coordinatore Dottorato … Prof. Ing. Roberto Orru'…….

Tutor/Relatore … Prof. Alberto Marini……

Esame finale anno accademico 2010 - 2011

to Beatrice and Lavinia,
above all, you are my life.

ACKNOWLEDGMENTS

This work is part of an international PhD in Engineering and Environmental Science, with no financial grant.

I would like to thank, for their intellectual support:

- **Paolo Antonelli** (SSEC, Space Science and Engineering Center, University of Wisconsin-Madison);
- **Alberto Marini, Francesca Giordano, Mara Pilloni, Teresa Balvis, Francesco Muntoni and the staff of Telegis Laboratory** (Department of Earth Science at the University of Cagliari);
- Professors of the PhD in Engineering and Environmental Science: **Giacomo Cao** and **Roberto Orru'** (PhD coordinators, University of Cagliari), **Alexander Boronin** (Russian Academy of Science), **Ana Isabel Miranda, Filomena Maria Cardoso Pedrosa Ferreira Martins and Alexandra Monteiro** (University of Aveiro), **Mostafa Maalmi** (Ecole Nazionale de l'Industrie Minerale, Rabat), **Paolo Bevilacqua** (Universita' degli Studi di Trieste), **Georgia Valaoras** (Hellenic American University);
- **Students of the International PhD** in Environmental Science and Engineering.

Them all, in different ways and contents, supported me and my research, and I am glad to thank you them.

A special thought to the EUMETSAT, FORGEA and DISAT Staff for the efforts and the many courses that help researchers and knowledge to go on.

Keywords: Remote Sensing, Dust, Algorithm, Mediterranean Sea, Satellites, MODIS, Natural Pollutants, Hydra, PM

CONTENTS

INTRODUCTION

The development of Remote Sensing has not only deeply improved atmospheric knowledge of both Climatology and Environment, but also terrestrial and marine knowledge.
Satellite observation has enlarged and stimulated new studies of spatial and temporal interests that deal with climatologic phenomena in different science, such as Biology, Phisics, Chemistry. Therefore, they try to outline action lists to lower the consequences not only of Global Warming, but also of other important threads, such as the depletion of Biodiversity, Hazardous Weather Conditions, Control Air Quality and so on.
Telegis Laboratory, University of Cagliari, Italy, has produced many PhDs researches on MODIS Spectroradiometer Satellite Data, focusing on Land and Vegetation, Ocean, and now on Air.

Air Pollution

The idea that air could affect our health is not recent. First it was King Edward (UK) who legislated the use of fire in London in 1273; then the industrial revolution and nowadays the so-called Air Pollution comes in many ways.
Air or Atmospheric Pollution are emissions introduced by men, but also by nature, that could affect human health, biological resources, ecosystems, materials, aesthetic values and could have legal consequences on Nations. Think about the restriction of EU Directive 75/2010 on industrial emission.
Air pollution in general is a worldwide problem, with no political borders, since it takes place on different spatial and temporal scales and it is affected by global atmosphere circulations. The increase of air pollution could increase *Acid Rains*, *Photochemical Smog*, the *Ozone Hole*, *Greenhouse Gases* and *Health Effects* due not only to UV rays, but also to *Particle Matter* presence.
Both outdoor and indoor air pollution, is a reality of modern life. Although outdoor air pollution has decreased considerably since the 1970s, thanks to a combination of technological advances and strict legislation, it is still a problem in some populated areas. Moreover it still affect health, particularly in older and/or ill-health people, and children. Carbon dioxide (CO_2) is what many might initially associate with “air pollution” but it is not an air pollutant directly connected to health. Other pollutants generated by man's activities, such as sulphur dioxide (SO_2), ozone (O_3), and particulate are much more relevant to health.

The pollutants that are more important for people are NOx, soot and smoke, CO, SO2, heavy metals, dust, benzene, lead (Pb), particles (PM1, PM2.5 and PM10).

The majority of outdoor air pollution is a consequence of our reliance on motorized transport and on the burning of fossil fuels to generate heat and electricity. Therefore it is generally worse in cities and industrial areas than in rural areas (except for the ozone).

Air pollutants are usually measured by networks of monitoring sites in different countries, each site collects information on specific pollutants. Concentrations of air pollutants are expressed as mass concentrations, mass of the pollutant in milligrams (mg), micrograms (μg) or nanograms (ng) in a given volume of air, usually a cubic metre (m^3).

Concentrations and averages used to express levels of air pollutants are collectively referred to as "metrics".

- **Annual average/mean annual concentration –** The average concentration over a year, calculated by averaging 365 daily averages.
- **Daily average/daily mean/24hr average concentration –** The average concentration over a 24hr period, calculated by averaging 24 hour measurements
- **One hour average/mean –** The average concentration over 60 minutes (assuming measurements are taken more frequently than once an hour) e.g. for SO_2 and NO_2.
- **Peak hourly concentration -** The highest hourly measurement in a 24hr period.
- **Peak hourly average/mean –**The average peak hourly concentration, calculated by averaging peak hourly concentrations over a specified time period e.g. day, month or a year. ··
- **Running 8hr average/mean –** The hourly average of 8 concurrent hourly measurements. These 8 hour blocks run concurrently e.g. midnight till 8am, 1am till 9am, 2am till 10 am etc.· This averaging metric is used to monitor ozone and it is used to calculate the **peak running 8hr average**, which for ozone usually occurs between 10am and 6pm.

Air quality model are products that help governances to build air quality forecast and risk assessment charts in order to alarm people and to minimize health diseases.

Natural sources of pollutants, such as Sahara desert dust outbreaks or ashes from forest fires or volcanoes, in many cases, could increase the bad air quality forecast, and measurements of PM limit values could exceed the European Law Recommendations. In such a case the country has to pay the Community a fee, if evidence that the excess is due to a natural pollutant is not brought to the European Court.

The goal to control air quality could be reached studying pollution sources, dispersions with atmospheric model, occurring chemical reactions and finally studying air depositions.
Excesses of air quality limit value represent breaches to Community Laws which can have significant legal consequences for the European Member States. For some existing limit values, such as those listed in the directive 1999/30/EC (First Daughter Directive), an excess, caused by particular natural sources, can be ignored to ensure compliance with Community Laws. Article 2.15 of the First Daughter Directive defines *natural events* as volcanic eruptions, seismic and geothermal activities, wild-land fires, high wind events, atmospheric resuspension, and transport of natural particles from dry regions. The next air quality directive will likely extend this principle to natural (i.e. non anthropogenic) sources of pollution in general as long as the *natural contribution* can be quantified and documented.
Particle Matters (PM) emission sources are sea-spray, soil moved by wind, biogenic aerosols, volcanic emissions, forest fires, and anthropogenic sources.
The EU legislation give limits for mobile emission, there are several concerning Euro X limitation for private cars (gasoline and diesel).
In order to control road transport emissions there are common efforts on engine technologies, reducing traffic in big city centre, the use of Pb and S free fuel, promoting the use of renewable energy and of alternative fuel. A cure strategy is post combustion treatment.
The aim of the present PhD work is to present a new way to approach radioactive transfer on air when dust episodes occur, and to start a research group able to inform - supporting quality and quantity data - on natural sources of air pollution. Such a group should be capable of interacting with other government and regional organizations such as ARPAS (thanks to monitoring activities in site stations or mobile devices), and POLARIS enterprise, that deals with Environmental Science and Air quality.

Mediterranean Sea Temperature

The Mediterranean Sea area is affected by dust. In 1990, it was postulated that heightened greenhouse effect had probably contributed to an increase in temperature and salinity of the deep waters of the western Mediterranean Sea. During the period 1959-1997, changes are shown in Fig.1 from 0.13°C (temperature) to 0.04 *psu* (salinity).

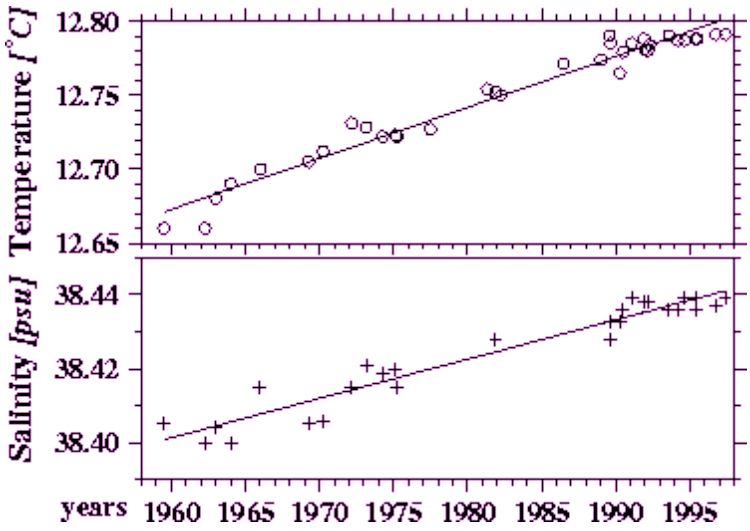

Fig.1 Temperature and salinity trends observed in the deep water of the Algero-Provençal basin over the 1959-1997 period. Each point represents a mean value for data acquired at a depth of between 2000 to a maximum of 2700 *m* ; However, the trends concern the entire deep water from a depth of about 800 *m*. Hydrological stations from 1959 to 1994; 1995-1997 data were acquired by CNRS/Insu ships.

These changes were assumed to be imported from the eastern basin and man-induced. Temperature and salinity increases mostly occurred in the eastern Mediterranean where they were the main causes of hydrographic events observed in 1993 and 1995. The characteristics of deep waters are acquired at the surface; resulting from air-sea exchanges and winter formation of dense water in different northern areas of eastern and western basins. Furthermore, the effect is quantifiable as well as its consequences on air temperature and freshwater budget in the Mediterranean area, where recurrent droughts and freshwater availability are already a problem. The Mediterranean appears as a scaled down model for the study of ocean circulation and environment: air-sea interaction, the monitoring of climatic and environmental evolutions, changes with consequences for the Mediterranean ecosystem, marine circulation and the global change. The point is that the temperature of both air and water increases when the wind blows south, south-west and south-east, from Maghreb to Southern Europe countries and Mediterranean Sea, and meteorological conditions drag dust all over, both air and ocean.

The Saharan desert is the world's most important natural source of dust. In the Mediterranean

Sea we can detect between 10 to 20 dust cases per years. In the low Mediterranean region, nearby North Africa dust spots, cases are normally more frequent and stronger than in the upper regions during winter, spring, summer and autumn.

Energy Balance

Meteorological observations from space are made through electromagnetic radiations leaving the atmosphere. Outgoing radiations from earth to space vary in accordance with wavelengths for the Energy Planck function which depends on wavelengths themselves and on the absorption by atmospheric gases of differing molecular structures. Energy transfer from one place to another is accomplished by any of the three processes. Conduction is the transfer of kinetic energy of atoms or molecules, travelling at varying speeds, among themselves, due to contact. Convection is the physical displacement of matter in gases or liquids. Radiation is the process whereby energy is transferred across space without the necessity of a medium.

Satellite Remote Sensing

Remote sensing is the observation of a target by a device separated by some distance. With satellites for meteorological research, remote sensing has been largely confined to passive detection or radiation emanating from Earth-Atmosphere system. Satellite remote sensing can provide long time series of observations of atmospheric dust, which can help evaluating the importance of different sources. Using data from the Moderate Resolution Imaging Spectroradiometer (MODIS) could be useful to combine different radiation bands, and not only to identify specific dust sources.

The measurements of aerosols, that are suspended particles in the atmosphere such as dust from the Sahara desert, are an important element in describing energy transmission through the atmosphere. Aerosols are a significant source of uncertainty in climate modeling since they affect cloud microphysics by acting as condensation nuclei; thereby they affect cloud radioactive properties, the hydrological cycle and atmospheric dynamics. They also interact directly with solar radiation, thus affecting the radiative balance. Estimative emissivity of dust is 0.75 between 3.5-3.9 μm, 0.97 between 10.3-11.3 μm and 11.5-12.5μm, so the studied algorithm focuses on

those bands.

The first part/purpose of this study is to use MODIS data and to develop an algorithm able to show dust by combining spectral bands into a scatter plot or RGB plot. The spectral bands were chosen among the emissivity bands of dust. The second part/purpose is to develop a draft model or a simulation pattern to combine MODIS Satellite data and other information from different spectroradiometers or devices operating on Meteorological Satellites already launched and operative over the Earth.

Natural Pollutants: PM

The main pollutants sources are: Nature, Agriculture, Industry, and Traffic .

The primary pollutants are CO, NOx, SOx, PM, TSH, HC, VOC, C6H6, PAH, CO2 and PM.

Wind blow, long range transported mineral dust and sea salt are the most important natural sources contributing to aerosol loading in Europe. They mainly affect air quality standards in Mediterranean area countries, as they are close to arid and semi-arid regions of North Africa. IPCC (Intergovernmental Panel on Climate Change) estimated, for 2000, emissions of 1800 Tg/yr for soil dust and 1500 Tg/yr for sea salt in the Northern hemisphere, with more than 95% in the coarse fraction of PM (> 1 μm).

For the PM classifications, mainly because particle matter is interesting for the present dust research, we can use the aerodynamic diameter (ex: PM10 with diameter equal or less than 10 μm or PM2.5 with diameter equal or less than 2.5 μm) or the Tri-Modal distributions (ultrafine, fine and coarse). They are both dimension classifications, not chemical ones, since the last are more expensive. PM could deeply affect human health and the PM reduced dimensions could reach the deepest recesses of lungs and cause several respiratory diseases.

PM emissions sources are sea spray, soil moved by wind, biogenic aerosols, volcanic emissions, forest fires, and anthropogenic sources. PM from vehicle, cars, transportation should be more controlled and measured, not only on land, but also on sea and air, and in particular vessel, shipping transport and aviation transport.

The EU legislation gives limits to mobile emission, there are many Euro x limitation for private cars (gasoline and diesel).

In order to control road transport emissions there is a common trend of modifying engine technology, reducing traffic in big city centre, the use of Pb and S free fuel, renewable energies

and alternative fuel. A cure strategy is post combustion treatment.

The importance of diesel engine and the main problem related to that fuel is PM emission, a mixture of solid and liquid emission. Different kind of engines and catalysts based on different physical and mechanical properties that are used to decrease PM emissions have been already presented: Three Way Catalyst improves efficiency, NSR catalyst is capable of storing NOx on a BaO support and the Diesel Particulate Filter (honeycomb) is the best to reduce particulate emissions of diesel engine.

According to the definition of Directive 1999/30/EC some mentioned sources of PM must be considered as natural in origin; nevertheless it is common opinion among experts and Member State representatives that a review of this definition, concerning the possibility to subtracting the natural contribution, is necessary.

Different aerosol sources, not specifically mentioned in the legislation, could additionally be considered as natural sources and should be included in the definition, whereas sources of particles formed by the interaction of natural and anthropogenic compounds, as well as natural emissions that can be controlled to some extent by appropriate human measures, should not be subtracted from PM levels.

In addition to emissions from volcanic, seismic or geothermal activities, and dust intrusion (which the current work deals with), the following sources have been identified as natural: Sea-salt, Primary Biological Aerosol Particles (PBAPs), biomass burning and forest fires, Secondary Organic Aerosol (SOA), and re-suspended particles.

In the present research case, since it will deal with the presence of dust over the Mediterranean region, it could be interesting to focus on the interaction between the presence of dust and temperature of the sea surface that could affect the presence of phytoplankton, the major source of food for aquatic species. It also crucial to investigate the interaction between the presence of dust and the variation of the local rainfall, or the interaction between the dust presence and human breathing problems. Hopefully the results should be useful for policy makers.

1. PART ONE - GENERAL PROBLEM

1.1 OUR CHANGING ATMOSPHERE

Earth's climate is significantly moderated by the atmosphere's interaction with incoming and outgoing radiations. The atmosphere scatters and absorbs radiation coming from the sun, affecting the way energy reaches the surface. The radiation that reaches the surface is partly reflected, partly absorbed and partly re-radiated as heat. The atmosphere can absorb and scatter this outgoing radiation as well, creating a balance between incoming and outgoing energy. Changes in the balance are called radioactive forcing, and many atmospheric characteristics contribute to this forcing including clouds, water vapors and aerosols. Cloud and water vapors play a changing role in radioactive forcing, alternatively warning and cooling the Earth. To develop such a complex cause/effect relation requires precise measurements of cloud properties: area of coverage, droplet size, cloud top altitude and temperature, liquid water content and so on. MODIS near-daily global coverage combined with its high spatial and spectral resolution will vastly improve scientists' understanding of clouds and atmosphere. Clouds are also important because they often obscure the Earth's surface. At the time of any single satellite overpass, the Earth scene below MODIS, may be covered with clouds, but the same areas are not to be cloudy every day, and researchers can combine or composite data over many days to produce weekly, monthly or seasonal cloud cleared productions, that can be used as input to global change models.

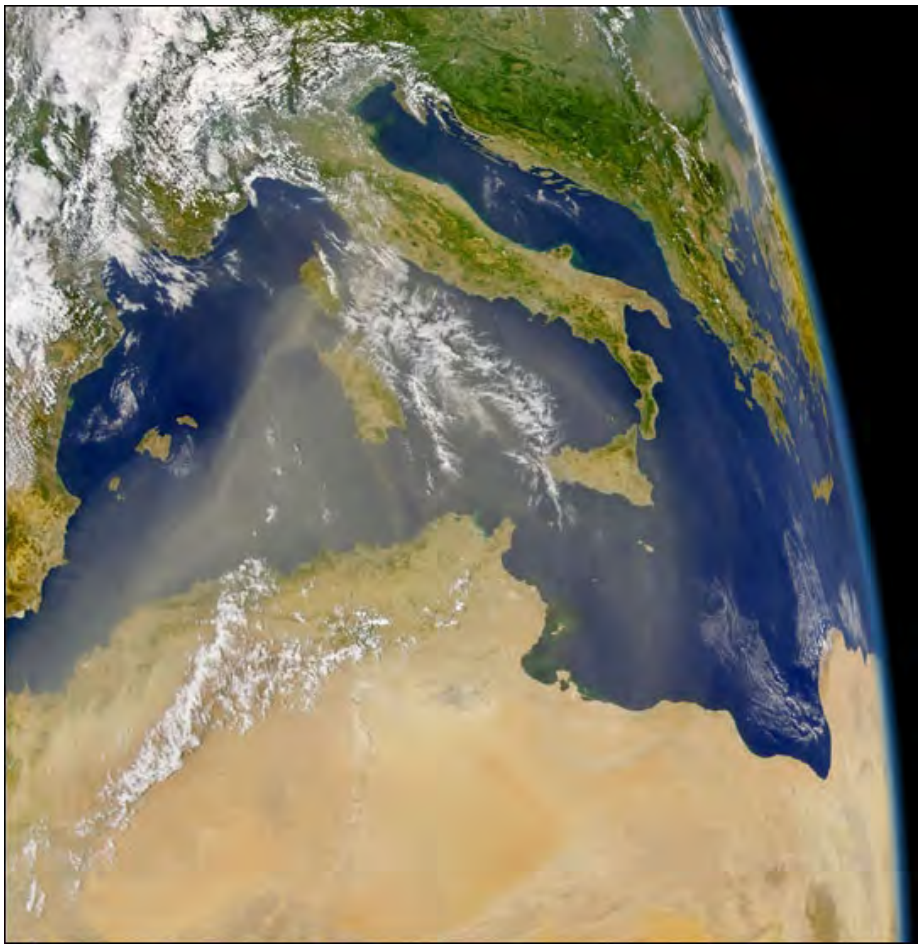

Fig.2 – Dust and Clouds over the Mediterranean Region

In addition to its observations of clouds, MODIS also measure aerosols, which influence climate both directly and indirectly. Aerosols, which include dust, sea salt, volcanic emissions, smoke from forest fire, and some kind of pollution, directly affect the amount of sunlight that reaches the Earth by scattering and absorbing incoming radiations. Radiation scattering by light-colored particles tends to cool the Earth's surface, and absorption by dark-colored particles tends to warm the atmosphere. Aerosols can simultaneously cool the surface but warm the atmosphere. However recent studies suggest that soot from fossil fuel and biomass burning may contaminate more aerosols than scientists previously thought, and that the warming of the atmosphere by these black-carbon aerosols might enhance the cooling effect at the Earth's surface. The resulting atmospheric heating could alter global air circulation and rainfall patterns across the world.

In addition to their direct interaction with sunlight, aerosols also influence climate indirectly with clouds. When water evaporates from the Earth's surface, it spreads into the atmosphere. Without aerosols, water vapors would continue to disperse until been distributed throughout the

atmosphere, and there would be no clouds nor rain. This is because water vapors need a surface which to condense on, or to form liquid droplets. Aerosols provide this surface, serving as a seed attracting condensation.

Increasing concentrations of aerosols may increase condensation by providing more surfaces on which raindrops can form, but clouds formed from manmade aerosols differs from naturally formed clouds. Man-made clouds are smaller and more numerous from the natural ones, clouds containing lots of man-made aerosols contain a larger number of smaller liquid water drops, and those clouds are brighter than those with larger drops (natural), meaning that they reflect more solar radiation back into space. This increased brightness has a cooling effect, which might be expected to counteract a CO2 induced warming trend. However, small drops often evaporate before they can fall from the sky as rain. One possible outcome of increasing aerosol pollution could be more clouds, but less rain.

MODIS multi spectral data on aerosol and cloud properties will be combined with data from other sensors on the Aqua spacecraft to give scientists a better understanding of the relationship between clouds, precipitation and aerosols. MODIS will also improve their understanding of the effect of these atmospheric characteristic on regional and global radioactive forcing; understanding that, is essential for modeling and predicting the consequences of global change.

At a global scale, the Sahara desert is the most important source of mineral aerosols. It is estimated that, in the Saharan dust region, every year, about several hundred million tons of desert are exported to the tropical North Atlantic Ocean and to the Mediterranean Sea. Aerosol optical properties classified the Mediterranean Sea as one of the areas with the highest aerosol optical depths in the world, which mostly occurs during Saharan dust outbreaks.

Long range transport of desert dust mainly takes place in the free troposphere, where the aerosol lifetime is of the order of two weeks. As a consequences, ground-based and space –borne passive remote sensing, which provide columnar estimates of the aerosol loading, cannot be used to accurately quantify the radioactive effects of mineral dust particles. In addition, when visible wave lengths are used in the retrieval, thin dust plumes often remain undetected over continents because of poor knowledge of the surface reflectance characteristics, which vary according to daytime and season.

We can calculate back trajectories arriving at various heights using Hysplit Model (Draxler and Hess, 1998; http://www.arl.noaa.gov/ready/hysplit4.html)

With regard to the volcanic eruption occurred in Iceland in April 2010, Eyjafjallajökull, a now-

active volcano in southern Iceland, erupted first in late March, and has erupted again, ejecting significant volcanic ashes into the atmosphere. Iceland is at an enough high latitudes (between 63 and 66.5 degrees North Latitude) that views from geostationary satellites are not as helpful in diagnosing evolving events such as ash clouds, as they would be for lower-latitude events. Meteorologists instead rely on polar orbiters to observe the atmosphere surrounding the eruption.

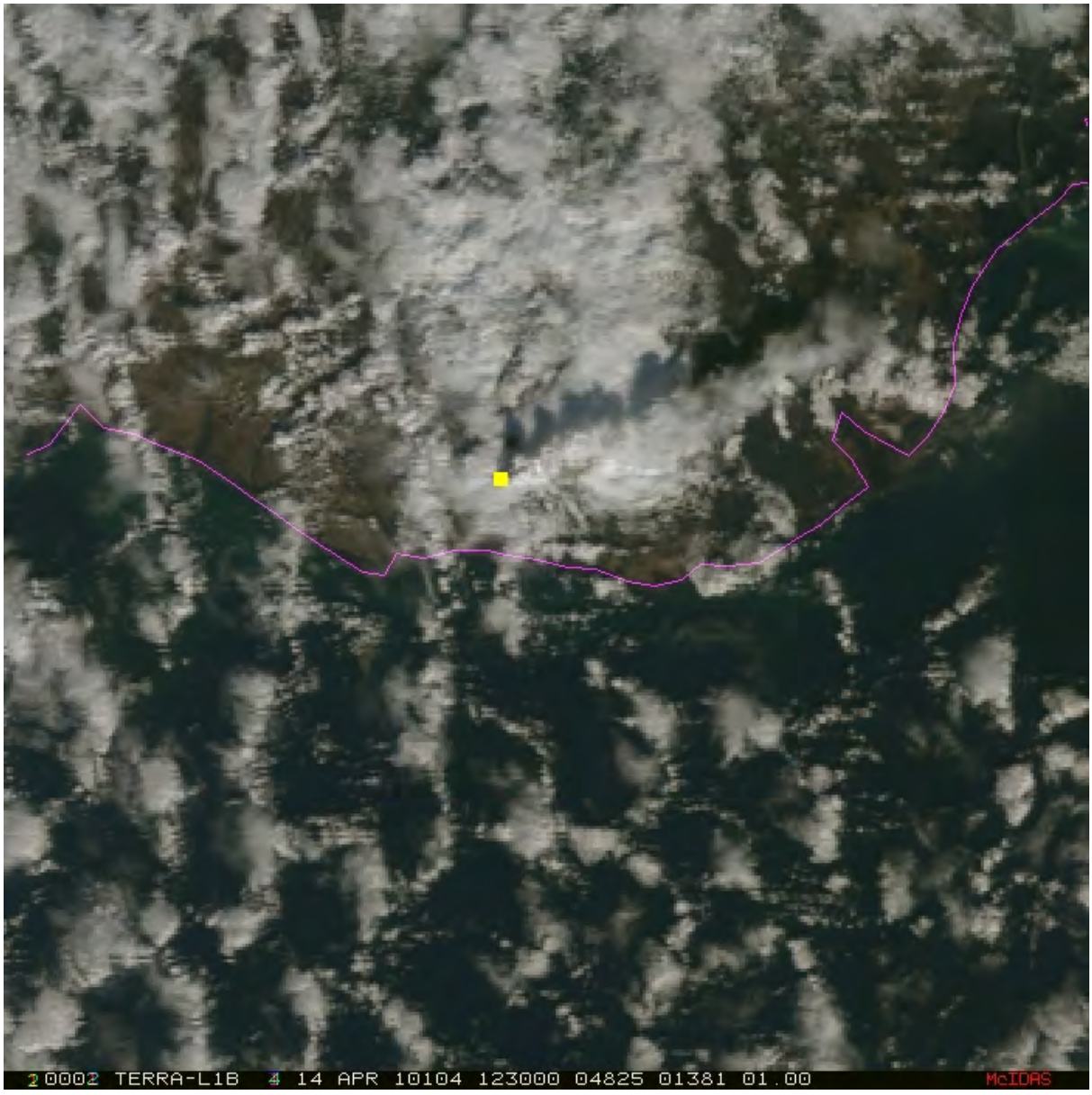

Fig.3: A Terra overpass allowed MODIS to image the eruption, shown as a true color composite

Ashes from volcanoes are a significant aviation hazard if they are drawn into jet turbines. For that reason, all flights at London's Heathrow (and at other airports throughout northern Europe)

had been grounded as of mid-afternoon London time on April the 15th, 2010. The volcanic ash clouds were visible from satellite. The imagery above shows 10.8- and 12.0-micron imagery from a NOAA-18 pass at 0342 UTC on April the 15th, 2010. The volcanic plume is visible as colder cloud tops arcing eastward from Iceland towards northern Scotland. The color enhancement in the loop shows that the 12.0-micron image has colder brightness temperatures than the 10.8-micron image. For example, the coldest point (red pixels) just off the coast of Iceland have 12.0-micron brightness temperatures of 212.6 K; 10.8-micron temperatures in that region are closer to 214.5 K. This difference in temperature arises because volcanic ashes have a lower emissivity at 12.0 microns than at 10.8 microns. Thus, proportionally less radiations compared to blackbody are been emitted at 12.0 microns than at 10.8 microns. When that emitted radiations are detected by the satellite, the proportionally smaller values at 12.0 microns yield cooler blackbody temperatures.

A McIDAS image of a 500-meter resolution Aqua MODIS Red/Green/Blue (RGB) composite using channels 01/04/03 (below) shows a beautiful view of the volcanic ash plume streaming southward on April the 17th, 2010. The tiny village of Skógar, as well as the Mýrdalsjökull Glacier are annotated on the image. As an aside, it is interesting to note that a great deal of lightning were observed associated with the volcanic ash clouds.

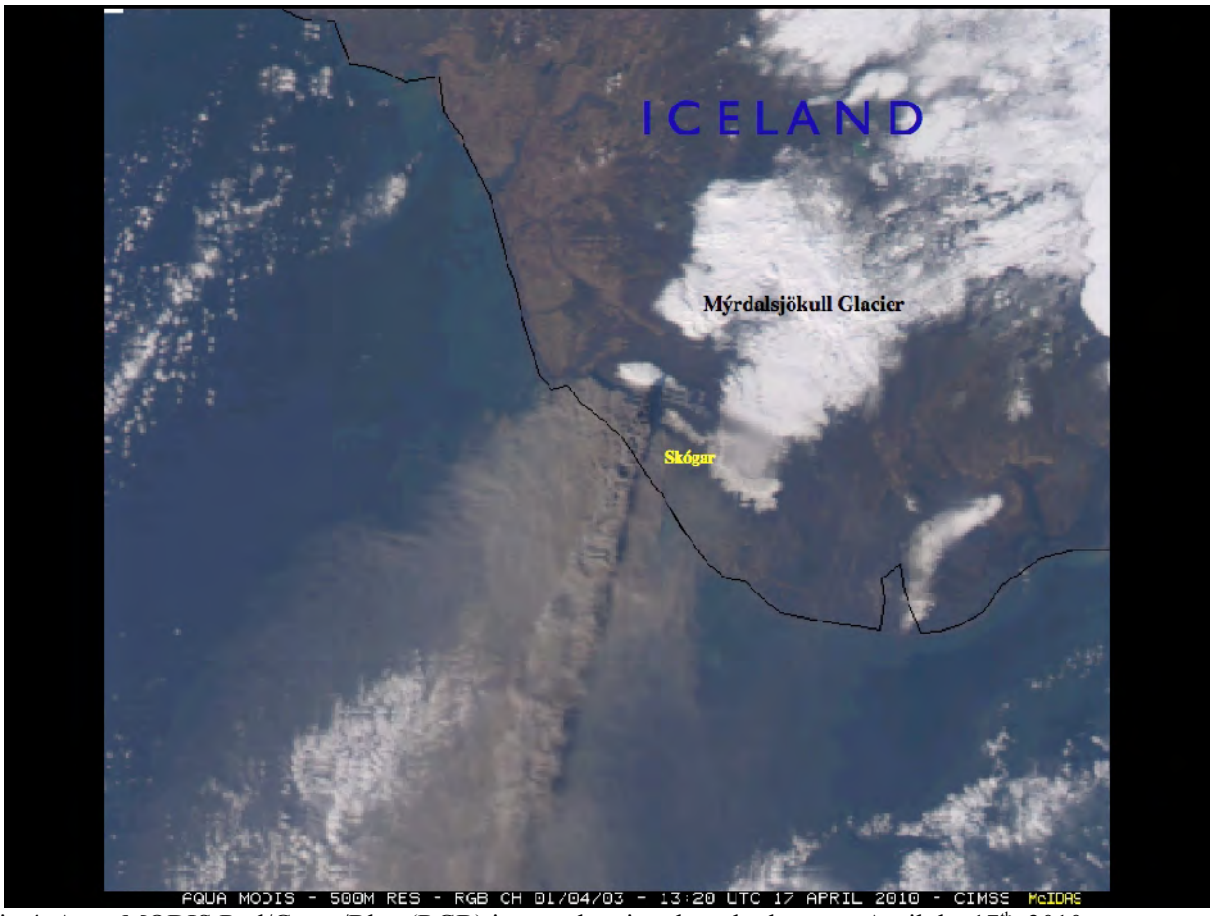

Fig.4: Aqua MODIS Red/Green/Blue (RGB) image showing the ash plume on April the 17th, 2010

1.2 DUST OVER MEDITERRANEAN SEA

The Sahara is the world's largest source of Aeolian soil dust and it probably accounts for almost half of all the Aeolian material in oceans worldwide. This large quantity of dust generation indicates the importance of the geomorphologic process of Aeolian deflation and abrasion in modeling the landscape of parts of the Sahara. The role of dust in environmental change, the source area from which the dust is derived, the strength of the Saharan dust source, the transport paths of material from the desert, the rates at which Saharan dust is being deposited, the nature of that material and the changing rates of dust provision in response to long and short-term climatic changes, all are important to study the dynamics of local and global climate changes.

As we have already highlighted, one environmental consequence of atmospheric dust loadings is their significance for climate through a range of possible influences and mechanisms. They may

affect air temperatures through the absorption and scattering of solar radiation. Saharan dust modifies short wave solar radiations transmitted to the Earth's surface and long wave infra red radiations emitted to space. However, the balance between these two tendencies determine whether this phenomenon creates cooling or warming, and it depends, in part on such variables as the size distribution of dust particles, and in part on their chemical composition. It is also possible that dust may affect climate through its influence on marine primary productivity and there is some evidence that dust may cause ocean cooling. Changes in atmospheric temperatures and in concentrations of potential condensation nuclei may affect convectional activity and cloud formation, thereby modifying rainfall amounts. Saharan dust aerosols influence the nutrient dynamics and bio-geochemical cycling of both terrestrial and oceanic ecosystems.

One of the most important advances required to understand the production of Saharan dust is to identify the major source areas. A recent method to detect dust source regions is the Total Ozone Mapping Spectrometer (TOMS), and an Aerosol Index (AI) has been calculated, which is linearly proportional to the aerosol optical thickness. AI values indicates the intensity of aerosols amount (which contains dust), not the whole dust flux. The TOMS data confirm the Bodelè depression of central Sahara region as the most important intense source region of dust in the world (AI values exceed 30). The importance of Bodelè region as a dust source relates to various factors. Firstly the region is very dry (17mm annual rainfall), but is fed by silt alluvia by streams draining from the Tibesti Massif.

The following table indicates maximum mean values for major dust sources

Maximum mean AI values for most significant global dust sources determined by TOMS	
Location	**>**
Bodelè Depression of Central Sahara	30
West Sahara in Mali and Mauritania	24
Arabia (Southern Oman/Saudi border)	21
Eastern Sahara (Libya)	15
Southwest Asia (Makran Coast)	12
Taklamakan/ Tarim basin	11
Ethosha Pan (Namibia)	11
Lake Eyre Basin	11
Mkgadikgadi Basin (Botswana)	8
Salar de Uyuni (Blivia)	7
Great Basin of the USA	5

Table 1: AI values for dust region

Saharan dust is regularly transported from its source areas along three main transport paths:

- westward over the North Atlantic Ocean (NAO) to North America and South America;
- northward across the Mediterranean to Southern Europe and sometimes as far as Scandinavia;
- along easterly trajectories across the eastern Mediterranean to the Middle East.

The winds that transports this dust are regular features of local climates.

Observing European trajectories we can notice that Saharan dust is often deposited in precipitation over southern Europe and it has been reported since ancient times. Individual events can be large, such as the dust fall in March 1991, which covered at least 320.000km^2, stretching from Sicily to Sweden and Finland. The Saharan source strength for dust transport to Europe was estimated at 80-120 million tonnes/year. A major source area for transport to western Europe was identified in southern Algeria. Another source is in western Sahara-Southern Morocco. These sources have been confirmed by back trajectory analysis for dust deposited over Northeastern Spain.

Estimates of dust deposition rates exist for a number of sites at several distances from the Sahara, there is a tendency for rates to be lower at a further distance from the potential sources. Thus, values for Western Europe are less than 1 g m^{-2}. Further south, in NE Spain, a value of 5,1 g m^{-2} is recorded, while over Sardinia, Corsica, Crete and the SE Mediterranean, most values are between 10 and 40 g m^{-2}.

A model that uses dust concentration data, indicates deposition rates for the Mediterranean of 3-14 g m^{-2} per year. The highest values in the model are at 10-20°N and 20-10°W, with a value of 30,8 g m^{-2}. Particle size characteristics of Saharan dust transported in central Mediterranean are between 2-11 μm. and the most frequent elements of dust over Italy are:

SiO_2, Al_2O_3, Fe_2O_3, MgO, CaO, K_2O.

What emerges from the present data is that European dust are dominates by SiO_2 and Al_2O_3, a characteristic they share with North American and Chinese ones. The dominance of SiO_2 probably reflects the importance of quartz in Aeolian dust. Overall, the gross composition of Saharan dust appears to be comparable to that of other regions to the gross mean composition of the all minerals of the World.

Over recent decades, meteorological stations and data on atmospheric dust, has been noticed storms and events changing in frequencies and strenght from Sahara to Southern Europe Countries. Increases in dust storm frequency concurrent with drought periods have been noted

in the Sahelian zone since the mid-1960s.

The meaning is that Natural Pollutant are increasing such as the Industrial or Antrophogenic.

Human exposure to some high concentrations of pollutants could deeply affect environment and nature, as well as, health and cause breath diseases.

The Decreto Ministeriale n.60 of April the 2nd, 2002 is an Italian law, that is the result of the European Directive 75/2008 on air pollutant concentration values. It stresses on the importance of different limit values for each pollutant. Therefore, not only a single region should have an air quality forecasting system, but also nations should implement one, as a good starting point to evaluate environmental conditions and policy law planning to prevent and monitor different pollutant concentrations. The goal is to give to public opinion and people real information on human and environmental safety linked to concentration levels of pollutants. Such a forecast system is also needed to monitor soil and water to favor a whole view of the problem.

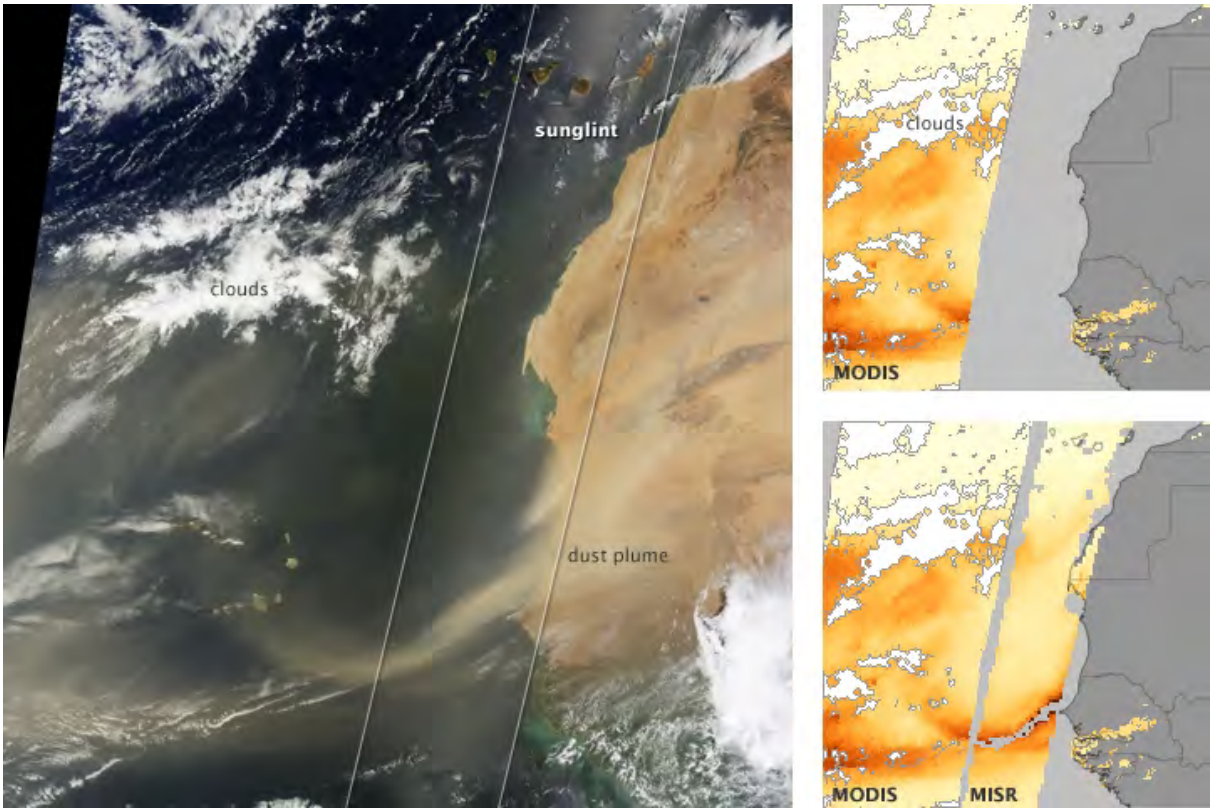

Fig 5: A photo-like image from Terra's Moderate Resolution Imaging Spectroradiometer (MODIS) on July the 12th, 2009 (left), shows a dust storm in progress and reveals where dust plumes are thick or thin. But scientists who want to know, for example, whether dust storms will affect sea surface temperatures during hurricane season need more than pictures; they need numbers—dust concentrations at different locations and altitudes, and particle sizes—that can be fed into weather and climate models.

Dust that blows off the Sahara Desert and over the Atlantic Ocean can neutralize acid rain, reduce sea surface temperatures by reflecting incoming sunlight, carry fungal and bacterial diseases to distant continents, foul Caribbean coral reefs, and stimulate the growth of ocean phytoplankton by delivering iron, which is often lacking in ocean waters far from land.

Satellites are among the most important tools Earth scientists have for monitoring the number, intensity, and spread of desert dust around the globe. This panel of images shows how scientists use observations from two different sensors on NASA's Terra satellite to track dust storms off West Africa.

To translate pictures into numbers, scientists create a scale (index) of how transparent the air was when the satellite observed it. To make this index, called aerosol optical thickness, scientists must know things like the intensity of incoming sunlight, how a "clean" atmosphere would scatter or absorb light, and how much light the satellite sees reflected by the surface.

Over the ocean, there is a portion of all MODIS images where sun glint—the mirror-like reflection of the Sun off the water—makes it impossible for scientists to calculate how transparent the air is. It occurs in the spot where the angle of incident sunlight is roughly the same as MODIS' angle of view. The sun glint area has to be left empty (missing data, gray) in MODIS aerosol optical thickness images (top right).

A second sensor on Terra, the Multi-angle Imaging Spectroradiometer (MISR), doesn't see an area as wide as MODIS does, but it has multiple cameras that view the surface at different angles. Multiple viewing angles mean that MISR always has several views of the surface that aren't affected by sun glint, and scientists can calculate aerosol optical thickness across the entire field of view (except for where there are clouds or where the dust is so thick that the surface is completely blocked from view).

By combining measurements from both sensors (bottom right image), NASA scientists get a more complete picture of the concentration and transport of Saharan dust. These results can improve how dust aerosols are represented in climate, weather forecast, and transport models. Similar measurements of aerosol particles like smoke and urban pollution, taken by Terra, have been incorporated into U.S. regional air quality forecasts.

2. PART TWO - METEOROLOGICAL SATELLITES

2.1 A SHORT STORY

Sputnik was the first Satellite, launched by the Soviet Union on October the 4th, 1957, and provided the first space views of our planet's surface and atmosphere. Then, the US accelerated its program to launch the first meteorological satellite TIROS-1 on April the 1st, 1960: a great help for meteorological measurements over a global scale area of such a satellite platform was realized.

Many programs from different countries has been launched and are currently operative.

During the past forty years NOAA (National Oceanic and Atmospheric Administration - US), and NASA (National Aeronautics and Space Administration - US) have established a remote sensing capability on both polar and geostationary platforms that have proven useful in monitoring and predicting severe weather and climate trends.

For the present work, data collected from MODIS (see 2.2, next chapter), and from a device over two Satellites, Terra and Aqua, have been used .

Terra (http://terra.nasa.gov/) is a multi-national, multi-disciplinary mission involving US in partnerships with the aerospace agencies of Canada and Japan, and managed by NASA's Goddard Space research Center. It is part of a series of satellites specially designed to study the complexities of the global change. On February the 24th, 2000, Terra began collecting what will ultimately become a new, 15-year global data set which to base scientific investigations about our complex home planet on. Together with the entire fleet of EOS (Earth Observing System) spacecraft, Terra is helping scientists to unravel the mysteries of climate and environmental change.

Aqua (http://aqua.nasa.gov/), Latin for water, is a NASA Earth science satellite mission named after and for the large amount of information that the mission will be collecting about the Earth's water cycle, including evaporation from the oceans, water vapor in the atmosphere, clouds, precipitations, soil moisture, sea ice, land ice, and snow cover on the land and ice.

Aqua mission is a part of the EOS spacecraft, together with Terra.

Aqua was launched on May the 4th, 2002, and has six Earth-observing instruments on board, collecting a variety of global data sets.

2.2 MODIS

MODIS (Moderate Resolution Imaging Spectroradiometer) is a key instrument onboard Terra (EOS AM) and Aqua (EOS PM) satellites. Terra's orbit around the Earth is timed so that it passes from north to south across the equator in the morning, while Aqua passes south to north over the equator in the afternoon. Terra MODIS and Aqua MODIS are viewing the entire Earth's surface every 1 to 2 days, acquiring data in 36 spectral bands, or groups of wavelengths. These data will improve our understanding of global dynamics and processes occurring on the land, in the oceans, and in the lower atmosphere. MODIS is playing a vital role in the development of validated, global, interactive Earth system models able to predict global changes accurately enough to assist policy makers in making sound decisions concerning the protection of our environment.

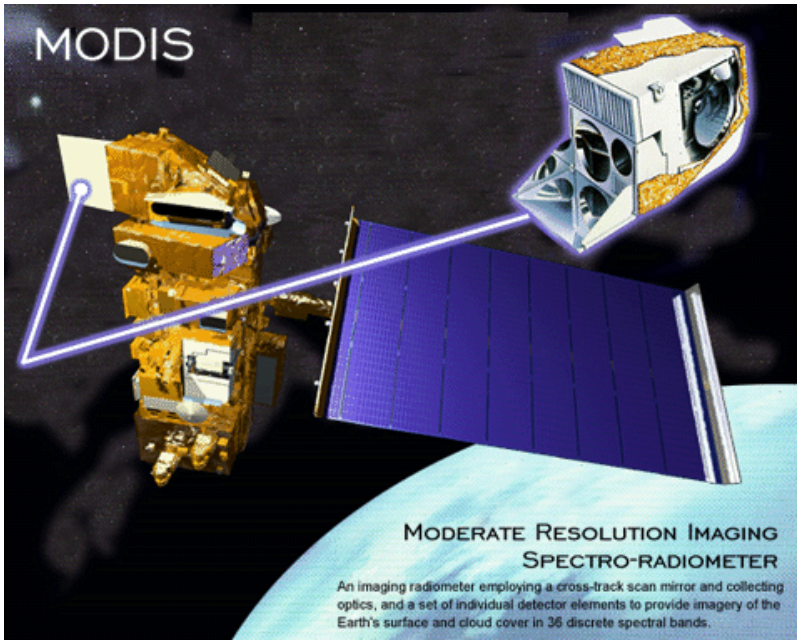

Fig 6.- MODIS

2.2.1 Instrument

MODIS is operating on both the Terra and Aqua spacecraft. It has a viewing swath width of 2,330 km. Its detectors measure spectral bands between 0.405 and 14.385 µm, and it acquires data at three spatial resolutions: 250m, 500m, and 1,000m. MODIS data are transferred to ground stations thanks to broadcasting and several antennas spread all over the

world. The numerous data products derived from MODIS observations describe features of the land, oceans and the atmosphere that can be used to study processes and trends both on local and global scales.

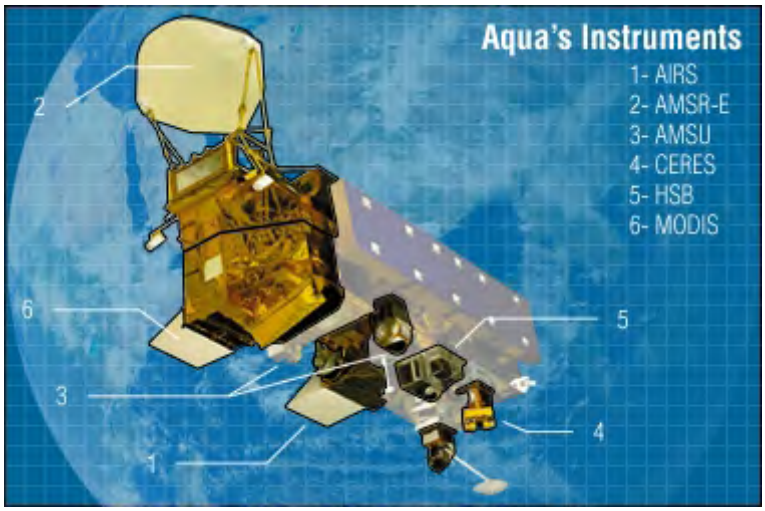

Fig.7 – MODIS on Aqua Satellite (6)

2.2.2. Data Products

There are many standard MODIS data products that scientists are using to study global changes. These products are being used by scientists in a variety of disciplines, including oceanography, biology, and atmospheric science.

2.2.3. Broadcast

One of the unique features of the MODIS instrument is its Direct Broadcast capability. In addition to storing data for later download at designated intervals, MODIS immediately broadcasts the raw data it collects on the chances that someone on the ground below is listening. The Terra MODIS instrument was one of the first satellite to constantly broadcast data for anyone with the right equipment and software to download them, free of charge.

The MODIS direct broadcast system began with Terra on Monday, April the 24th, 2000, and for Aqua on July the 12th, 2002. Both broadcast full-time, except for when passing over any of NASA's Deep Space Network antennas that are actively tracking a remote spacecraft. It has been estimated that this event will occur less than two hours per day. Generally, spacecraft collect data and store them on board until it passes over a ground station, set up to receive the

data, at which point it transmits the data in one large batch. This avoids losing data taken when the spacecraft is out of sight of any ground stations, such as when it is over the ocean. But the advantage to continually broadcasting the data is that many sites have antennas and other necessary equipment to receive and process MODIS Direct Broadcast data. The data stream carries the data from all 36 spectral bands for the entire MODIS field of view. The data can be directly transmitted from the spacecraft to ground stations equipped with an average 3m or larger X-band receiving system and appropriate hardware and software. The Overpass Predictor can be used to determine when there will be a Terra or Aqua spacecraft overpass at any location that may have a MODIS Direct Broadcast receiving station. The University of Cagliari can acquire this information from the SeaWifs Antenna located at Monserrato compound, *Cittadella Universitaria*. All the information is processed by the Terascan System

Fig 8.- The Antenna was located at the Department of Physics, Cittadella Universitaria, Monserrato, Cagliari.

2.2.4. Design

The MODIS instrument provides high radiometric sensitivity (12 bit) in 36 spectral bands ranging in wavelength from 0.4 μm to 14.4 μm. The responses are custom tailored to the individual needs of the user community and provide exceptionally low out-of-band response. Two bands are imaged at a nominal resolution of 250 m at nadir, with five bands at 500 m, and the remaining 29 bands at 1 km. A ±55-degree scanning pattern at the EOS orbit of 705 km achieves a 2,330-km swath and provides global coverage every one to two days. The Scan Mirror Assembly uses a continuously rotating double-sided scan mirror to scan ±55-degrees and is driven by a motor encoder built to operate at 100 percent duty cycle throughout the 6-year instrument designed life. The optical system consists of a two-mirror off-axis a focal telescope, which direct energy to four refractive objective assemblies; one for each of the VIS, NIR, SWIR/MWIR and LWIR spectral regions to cover a total spectral range of 0.4 to 14.4 μm. A high-performance passive radioactive cooler provides cooling to 83K for the 20 infrared spectral bands on two HgCdTe Focal Plane Assemblies (FPAs). Novel photodiode-silicon readout technology for the visible and near infrared provides unsurpassed quantum efficiency and low-noise readout with exceptional dynamic range. Analog programmable gain and offset and FPA clock and bias electronics are located near the FPAs in two dedicated electronics modules: the Space-viewing Analog Module (SAM) and the Forward-viewing Analog Module (FAM) . A third module, the Main Electronics Module (MEM) provides power, control systems, command and telemetry, and calibration electronics. The system also includes four on-board calibrators as well as a view to space: a Solar Diffuser (SD), a v-groove Blackbody (BB), a Spectroradiometric calibration assembly (SRCA), and a Solar Diffuser Stability Monitor (SDSM). The first MODIS Flight Instrument, ProtoFlight Model or PFM, is integrated on the Terra (EOS AM-1) spacecraft. Terra was successfully launched on December the 18th, 1999. The second MODIS flight instrument, Flight Model 1 or FM1, is integrated on the Aqua (EOS PM-1) spacecraft; it was successfully launched on May the 4th, 2002. These MODIS instruments will offer an unprecedented look at terrestrial, atmospheric, and ocean phenomenology for a wide and diverse community of users throughout the world.

2.2.5. Terascan System

The TeraScan software suite runs under White Box and Red Hat Enterprise Linux, and has received security certification from the U.S. Navy. SeaSpace TeraScan(R) systems are the

world's most complete end-to-end solutions for receiving, processing, archiving, and distributing satellite data. TeraScan(R) is a powerful, extensible tool, meeting all the needs for each known direct downlink satellite. TeraScan's standard products and add-on options are the building blocks for every remote sensing enterprise.

2.2.6. Features

Images are displayed line-by-line during satellite overpass

Automated pass scheduling

User-selected areas of interest (AOI)

GUI script builder to generate a wide variety of data products

Interactive rubber sheet image navigation

Full-featured image visualization

Full import/export capability

2.2.7. Benefits

1. From total automation to complete interactivity, scripted operation gives complete control
2. Select from standard scripts or create the user's own data product
3. Intuitive GUIs allow users to see pass swaths in more than 20 map projections
4. Users can set their own rules based on priorities, and resolve pass conflict.
5. Far more efficient and highly selective data capture and processing:
    - Easily build and modify scripts for MODIS, AVHRR and other sensor data products;
    - Tune image geo-location accuracy for improved data fusion with other sources of imagery;
    - Image arithmetic, user defined data layers, time-series animation, and much more;
    - Select from over 20 file formats for import and export, including HDF, netCDF, GEOTIFF, and many more;
    - Export directly into third party environments such as ERDAS® and ENVI®.

3. PART THREE – DATA PROCESSING

3.1. METEOROLOGICAL OBSERVATIONS AND ABSORPTION BANDS

Meteorological observations from space are made through the electromagnetic radiation leaving the atmosphere. Outgoing radiation from Earth to space varies with wavelength for two reasons:

a) Planck function dependence on wavelength;

b) absorption by atmospheric gases of differing molecular structure (CO2, H2O, O3 …).

Thanks to absorbing bands of the constituents gases of the atmosphere, vertical profiles of atmospheric parameters can be derived. Sampling in the spectral region at the centre of absorption band yields radiation from the upper levels of the atmosphere, while radiation from below has already been absorbed by the atmospheric gas; sampling in the spectral regions away from the centre of the absorption band yields radiation from successively lower levels of the atmosphere. Away from the absorption band, there are the windows to the bottom of the atmosphere. The IRIS Infrared spectroradiometer, in 1969, first observed surface temperatures of 320 K in the 11 micron band of the spectrum and tropopause emissions of 210 K in the 15 micron band. As the spectral region moves toward the centre of the CO^2 absorption band, the radiation temperature decrease due to the decrease of temperature with altitude in the lower atmosphere.

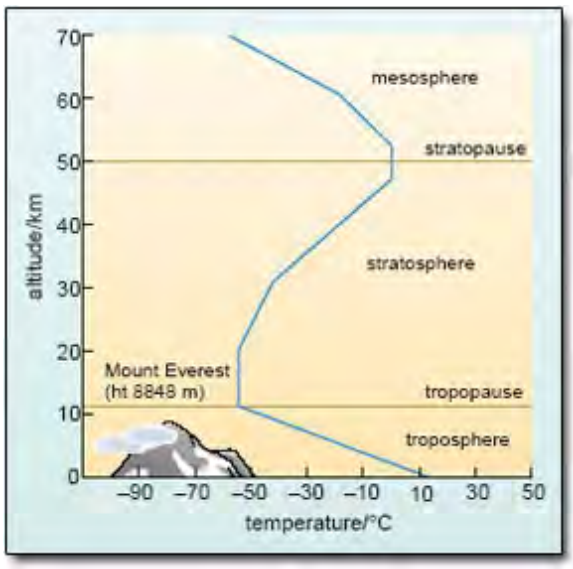

Fig. 9: Temperature Profile: Relation between temperature and altitude on Earth

The characteristic temperature profile of the atmosphere produces a vertical structure like a series of concentric shells. The successive regions or spheres are separated by pauses where the change in temperature with altitude switches from decreasing to increasing, or vice versa. The outer more-rarefied reach of the atmosphere (up to 100 km or so) are not included.

A carefully selection of spectral bands in and near an absorbing band has suggested that multispectral observation could yield information about the vertical structure of atmospheric temperature and moisture. The concept of profile retrieval is based on the fact that atmospheric absorption and transmittance are highly dependent on the frequency of the radiation and on the amount of the absorbing gas. At frequencies close to the centers of the absorbing bands, a small amount of gas results in considerable attenuation in the transmission of the radiation; therefore most of the outgoing radiation arises from the upper levels of the atmosphere. At frequencies far from the centers of the bands, a relatively large amount of the absorbing gas is required to attenuate transmission; therefore the outgoing radiation arises from the lower levels of the atmosphere.

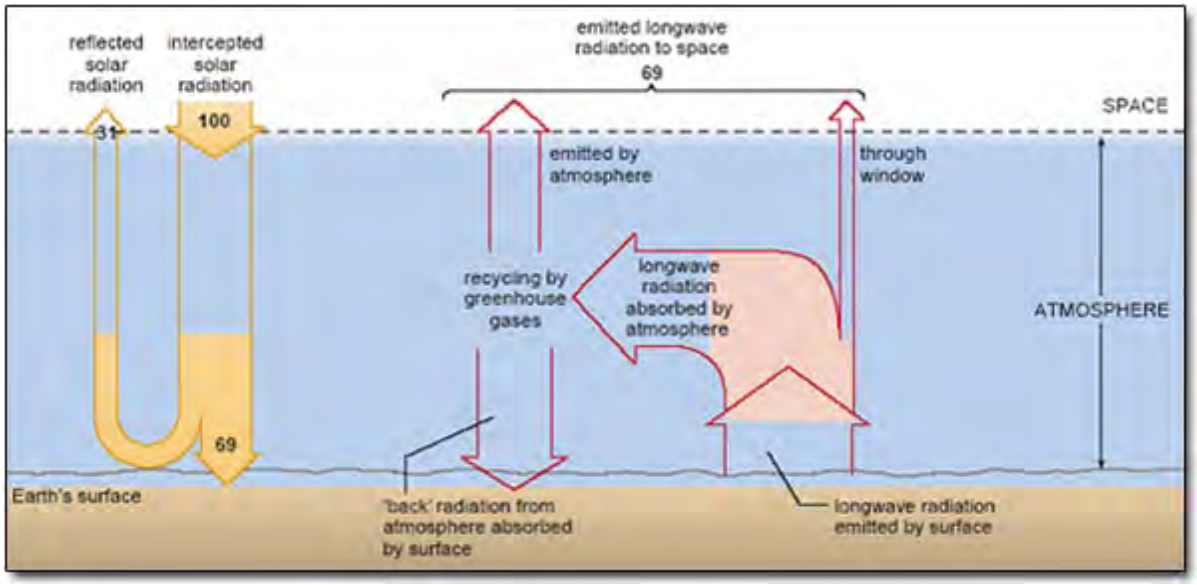

Fig 10: Schematic representation of the globally average radiation balance for an Earth-like planet with an atmosphere that absorbs and re-emits (downward and upward) long-wave radiation from the surface. As it can be observed, 69 units of solar radiation are absorbed by the planet and 69 units of long-wave radiation go back out to space. However, this overall radiation balance is now at the top of the atmosphere, not at the surface, which receives an extra input of energy trough the back radiation from the atmosphere.

It is important to remind that dust moves around in the atmosphere following **meteorological conditions** and patterns, infact Eulerian-Lagrangean back-scatter methods and Chemistry-Transport Parallel models use this information to develop trajectories for dust and other Particle Matter. The first, Eulerian-Lagrangean back-scatter method, is used to find the centre of dust origin or Spot, the second, Chemistry-Transport Parallel model, is useful for air quality forecast or simulation, and it especially used around the most populated area.

Outgoing radiations from earth to space vary in accordance with wavelengths for the Energy Planck function which depends on wavelengths themselves and on the absorption by atmospheric gases of differing molecular structures.

A *blackbody* is an object which absorbs all the light which hits it: hence the name "blackbody". It also emits radiation, in a very particular manner. The exact amount of energy emitted at a particular wavelength **lambda** is given by the Planck function:

$$B_\lambda(T) = \frac{2hc^2/\lambda^5}{e^{hc/\lambda kT} - 1}$$

Bλ(T) is the energy (Joules) emitted per second per unit

λ is the wavelength per steradian from one square meter of a perfect blackbody at temperature T

T is the temperature of the blackbody

h is Planck's constant = 6.63 x 10^(-34) J*s

c is the speed of light = 3.00 x 10^(8) m/s

λ is the wavelength

k is Boltzmann's constant = 1.38 x 10^(-23) J/K

Energy transfer from one place to another is accomplished by any of the three following processes:

Conduction, Convection and Transmission .

Let's compare the absorption bands of the Earth radiation by the atmosphere (due to molecules and particles) and see were MODIS and other sensors (VII, RS) could work.

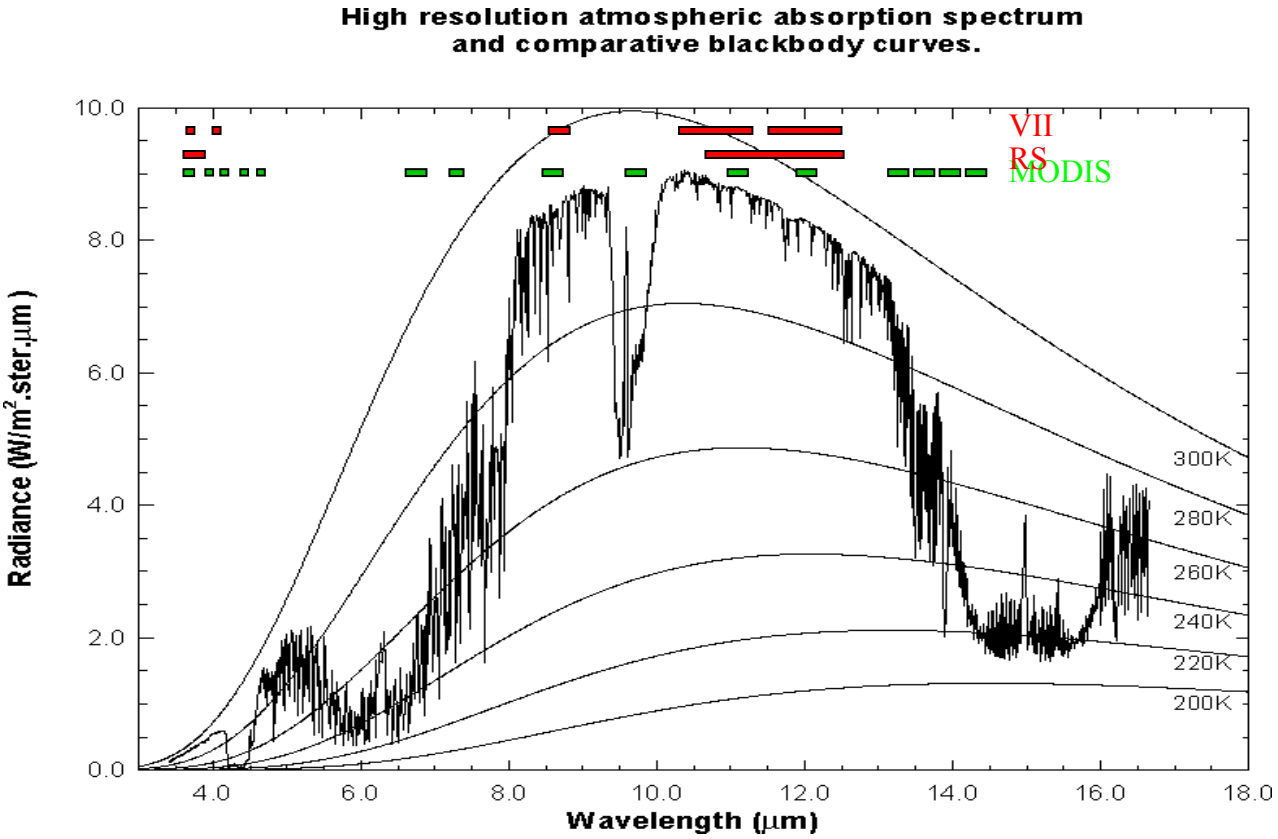

Fig 11 Radiance Atmospheric Absorption Vs Wavelength and comparison between blackbody curves.

3.2. HYDRA

We used the freeware multispectral data analysis toolkit, HYDRA (HYperspectral data viewer for Development of Research Application). In fact, various spectral channels combination were visualized to detect an algorithm for dust over Mediterranean region, and also multiple channel combinations and scatter plots that help to detect Particle Matter (PM).
The software HYDRA can be used for such environmental studies but also for others, especially used to process and manage Meteorological Satellite Data, such as MODIS, SEVIRI and AIRS data.

3.3 TERASCAN

The TeraScan is an integrated system of hardware and software designed for automated reception of data from meteorological/environmental satellites and for processing the data into images and data overlays. The data files for these images and overlays are of a special format called Terascan Data Format (TDF) and can be displayed with the TeraScan viewer called TeraVision. TDF files (also referred to as datasets) can also be converted to picture products in various graphics formats. Both TDF products and picture products can be automatically distributed to any number of local or off-site destinations across the network.
The TeraScan is a versatile system that can be configured for the reception and processing of many different types of data from many different types of satellites, including the X-band-transmitting polar-orbiting satellites. The TeraScan can also generate products that are a mixture of data from different satellites. The types of data that the TeraScan can receive and process are listed below:
MODIS, Oceansat, SAR, AVHRR, SeaWiFS, OLS, MVISR, GOES, HRI, GMS, WEFAX, NESDIS and many others from lot of Meteo Satellites.
The SeaSpace produces several different configurations of its TeraScan system, each geared to a particular satellite telemetry or combination of telemetries. The hardware configuration of our particular system is documented in the drawings and parts lists provided in the *TeraScan System As-Built Specifications* (hardcopy documentation) that was delivered with our system:

- Antennas for satellite signal interception:
    - for high-resolution data reception from geostationary satellites, a large (3.8m-diameter) fixed-direction antenna is used;

    - for high-resolution data reception from polar-orbiting satellites, a tracking antenna is used, its size depends on the telemetry to be received. Tracking antennas are enclosed in a radome to protect from the weather.
- Receivers for tuning to the correct satellite signal frequency and separating the sensor data (the baseband) from the RF carrier (the latter function is known as *demodulation*).
- Bit synchronizers for regenerating the bit stream against noise, converting the digital data format to NRZ-L, if necessary, and extracting the *clock*, a timing pulse added to the signal on the satellite to enable synchronization of the reception system with the satellite transmitter.
- Frame synchronizers for dividing the continuous bit stream into meaningful data blocks called *frames*.
- Computer workstations with TeraScan software for scheduling and controlling data reception and for processing data into products, and displaying and distributing data and data products; they can include tape drives or other storage devices for archiving data.
- Global Positioning System (GPS) antennas to supply position and time to the system.
- Uninterruptible power supplies (UPS) to protect the system from power surges and to keep the system up and running in the event of a power outage.
- Interfaces to shipboard navigation, for shipboard systems.

3.4 ERDAS SUITE

ERDAS provides a global geospatial solution, designed for desktop and enterprise use. Its solutions cannot only be used across the enterprise, but outside it as well, extending information to and from the field, to business partners and across the Web. A geospatial business system meets the full spectrum of an organization's requirements, transforming geospatial data into information useful for decision-making processes. The specific components and capabilities include:

- Authoring: Transforming source data into products, including orthos, terrain, features, maps, 3D data, land cover data and processing models
- Managing: Finding, describing, cataloging and publishing data and web services.

- Connecting: Linking users within an organization, allowing the rapid sharing of content throughout the organization or business to business.
- Delivering: Subscription, mobile and web services which contain value-added content delivered to a variety of domain-specific and business applications.

ERDAS IMAGINE performs advanced remote sensing analysis and spatial modeling to create new information. In addition, with ERDAS IMAGINE, the user can visualize the results in 2D, 3D, movies, and on cartographic quality map compositions.

The core of the ERDAS IMAGINE Suite was designed to match with the user's geospatial data production needs: from IMAGINE Essentials, through IMAGINE Advantage and on to IMAGINE Professional. Optional add-on modules providing specialized functionalities are also available to enhance the user's productivity and capabilities.

4. PART FOUR - CASE STUDY

4.1. - STUDY AREA

This presented method could be applied over every part of the world, but to show the methodology we have chosen the South West Mediterranean area, because of the increase of mean seasonal temperature, desertification and frequent dust episodes during rainfalls. In fact, the presence of dust could increase mean seasonal temperature, but also sea surface temperature and general desertification.

Tunisia, Libya, and the nearby areas consist of two climatic belts, with the Mediterranean influence in the north and the Saharan one in the south. Temperatures are moderate along the coast, with an average annual reading of 18° C (64° F), and hot in the south inland The summer season in the north, from May through September, is hot and dry; the winter, which extends from October to April, is mild and characterized by frequent rains. Temperatures at Tunis range from an average minimum of 6° C (43° F) and maximum of 14° C (57° F) in January, to an average minimum of 21° C (70° F) and maximum of 33° C (91° F) in August.

Precipitations in the northern region reach a high of 150 cm annually, while rainfalls in the extreme south is averagely less than 20 cm a year.

Libya climate has marked seasonal variations influenced by both the Mediterranean Sea and the desert. Along the Tripolitania coast, summer temperatures reach between 40 and 46° C (104– 115° F); farther south, temperatures are even higher. Summers in the north of Cyrenaica range from 27 to 32° C (81–90° F). In Tobruk (Tubruq), the average January temperature is 13° C (55° F); July, 26° C (79° F). The ghibli, a hot, dry desert wind, can change temperatures from 17 to22° C (30–40° F) in both summer and winter.

Rainfall varies from region to region. Rain generally falls in a short winter period and frequently causes floods. Evaporation is high, and severe droughts are common. The Jabal Akhdar, region of Cyrenaica, receives a yearly average of 40 to 60 cm (16–24 in). Other regions have less than 20 cm (8 in), and the Sahara has less than 5 cm (2 in) a year.

In the current work we present the general climatology of the studied Area - South West Mediterranean - choosing two nearby local climatological data areas, Tripoli and Djerba (Libya and Tunisia).

Tripoli lies at the western extremity of Libya, close to the Tunisian border. The dominant climatic influence in Tripoli, a coastal lowland city, is the Mediterranean Sea. The city enjoys warm summers and mild winters with an average July temperature of 22 °C (72 °F) to 29 °C (84 °F). In December temperatures have reached as low as 1 °C (34 °F), but the average remains at between 9 °C (48 °F) and 18 °C (64 °F).

The average annual rainfall is less than 400 mm (15,7 inch). Table 1 below shows climatologic data for Tripoli.

Table 1: Weather data for Tripoli

month	jan	feb	mar	apr	may	jun	jul	aug	sep	oct	nov	dec	year
aver H °C (°F)	16 (61)	17 (63)	19 (66)	22 (72)	24 (75)	27 (81)	29 (84)	30 (86)	29 (84)	27 (81)	23 (73)	18 (64)	23 (73)
aver L °C (°F)	8 (46)	9 (48)	11 (52)	14 (57	16 (61)	19 (66)	22 (72)	22 (72)	22 (72)	18 (64)	14 (57)	9 (48)	15 (59)
precip mm (inch)	81 (3.2)	46 (1.8)	28 (1.1)	10 (0.4)	5 (0.2)	3 (0.1)	0 (0)	0 (0)	10 (0.4)	41 (1.6)	66 (2.6)	94 (3.7)	384 (15.1)

Djerba is a beautiful island of Tunisia and it is well known for its mild Mediterranean climate. Average temperature are nearly the same of Tripoli's, but precipitation is lower.

Table 2 below shows climatologic data for Djerba.

Table 2: Weather data for Djerba

Month	jan	feb	mar	apr	may	jun	jul	aug	sep	oct	nov	dec	year
aver H °C (°F)	16 (61)	18 (64)	20 (67)	22 (72)	26 (78)	26 (83)	32 (89)	32 (90)	30 (86)	26 (79)	21 (70)	17 (63)	24 (75)
aver L °C (°F)	9 (48)	9 (49)	11 (52)	13 (56)	16 (62)	20 (67)	22 (71)	23 (73)	22 (71)	18 (65)	14 (57)	10 (50)	16 (60)
precip mm (inch)	28 (1.1)	20 (0.8)	19 (0.8)	13 (0.5)	5 (0.2)	1 (0)	0 (0)	3 (0.1)	19 (0.8)	53 (2.1)	34 (1.3)	36 (1.4)	231 (9.1)

While Fig.12 shows the two precipitations related together.

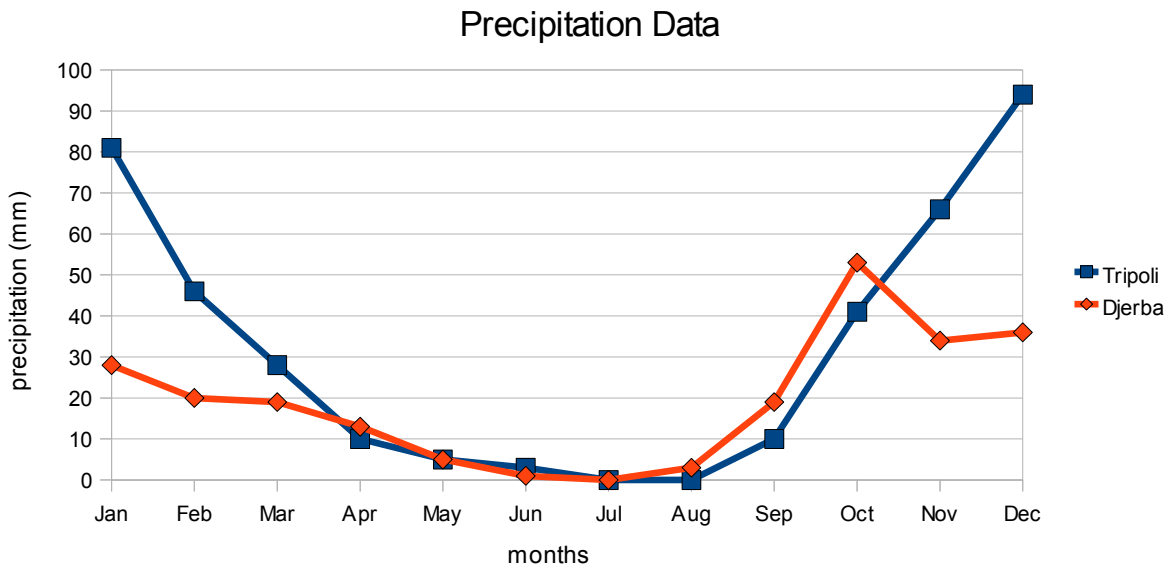

Fig 12- Monthly precipitation charts of Tripoli and Djerba

4.2. - DATA

The picture below shows the general studied area about 41N, 7W, 17E, 35S. And the Reflectance/Brightness Temperature curve of the RGB combination bands versus wavelengths.

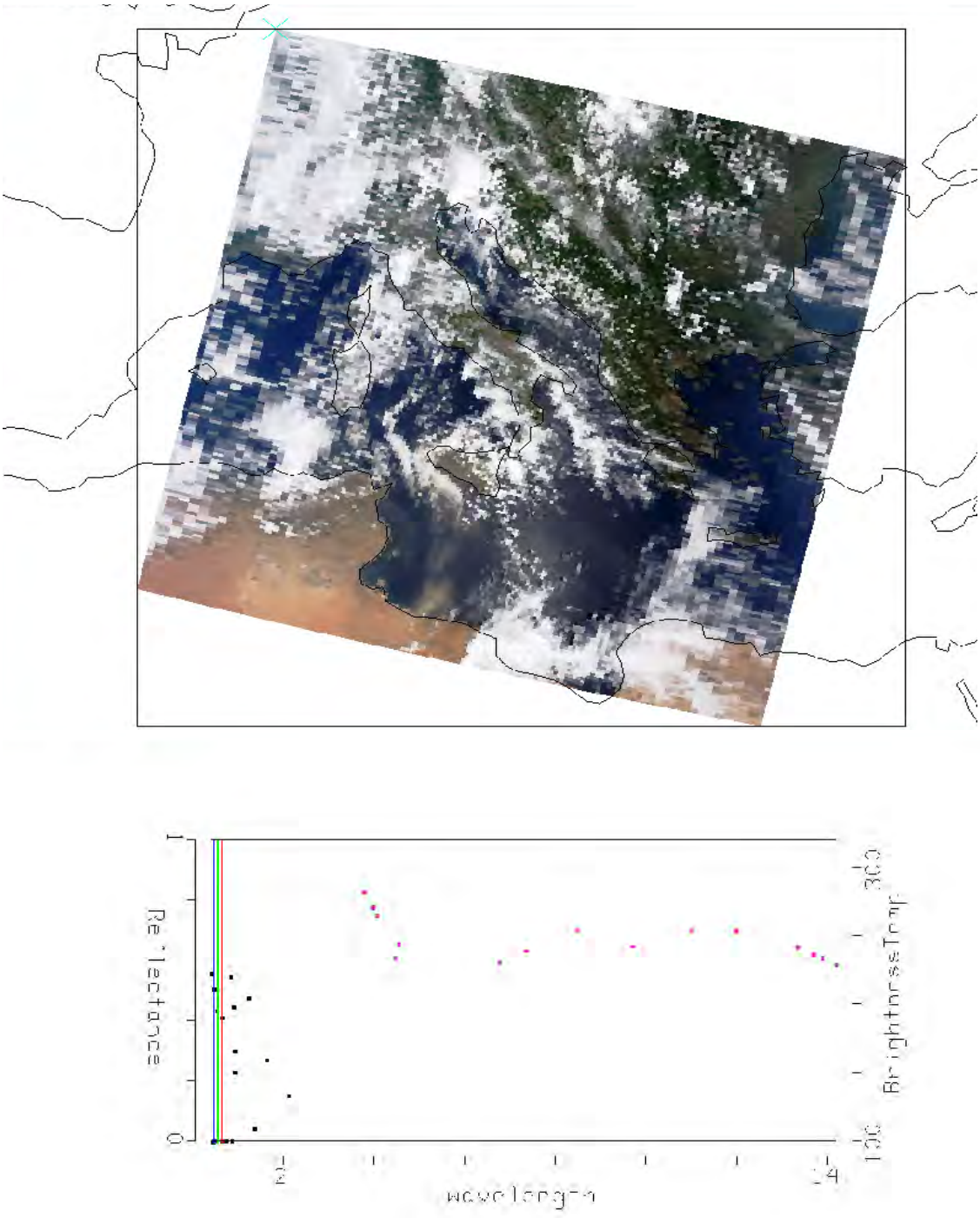

Fig. 13 - Up, RGB image of the Studied Area, date: July the 14th, 2007, and down, the corresponding Reflectance/Brightness Temperature (BT) versus wavelengths: the RGB bands are respectively the first, the second and the third by the left of the diagram.

4.3. - ALGORITHM

4.3.1. Building the Algorithm

The Moderate Resolution Imaging Spectroradiometer (MODIS) is an Earth Observing System (EOS) facility instrument that is currently flying, but in retirement age, aboard the Terra and Aqua spacecraft. Terra began collecting data on February the 24th, 2000, Aqua, a counterpart of Terra, has been launched on May the 4th, 2002 and began collecting data on June the 22nd, 2002. MODIS is a scanning spectro-radiometer with 36 spectral bands between 0.645 and 14.235 μm. Bands 1 – 2 are sensed with a spatial resolution of 250 m, bands 3 –7 at 500 m, and the remaining bands 8- 36 at 1 km.

You can download rough data or processed data from some link to NASA institute or, if you have an Antenna, you can directly broadcast on your own.

For the present study,MOD021KM level 1b data at 1km of spatial resolution and with calibrated radiances, from MODIS sensor on Terra has been used. The general program focuses on the Mediterranean Area, due to desertification and dust episodes. So the case study shows the image of Tunisia/Libya region on July the 14th, 2007.

Since the particulate material of the Sahara/Sahel is mainly constituted by quartz, calcite, dolomia and clay minerals, the direct analysis of Ca, Al2O3, Fe2O3, K, Mg and indirect determination of Si (3*Al2O3 = SiO2) and $CO3^2$ (1.5*Ca + 2.5 * Mg = $CO3^2$) allows the determination of the material load distributed by the Sahara. Estimative emissivity of dust is 0.75 between 3.5-3.9 μm, 0.97 between 10.3-11.3 μm and 11.5-12.5μm, so the studied algorithm focuses on those bands combinations, that are 20 (3.7 μm) , 29 (8.5 μm), 31 (11 μm) and 32 (12 μm) MODIS Channels.

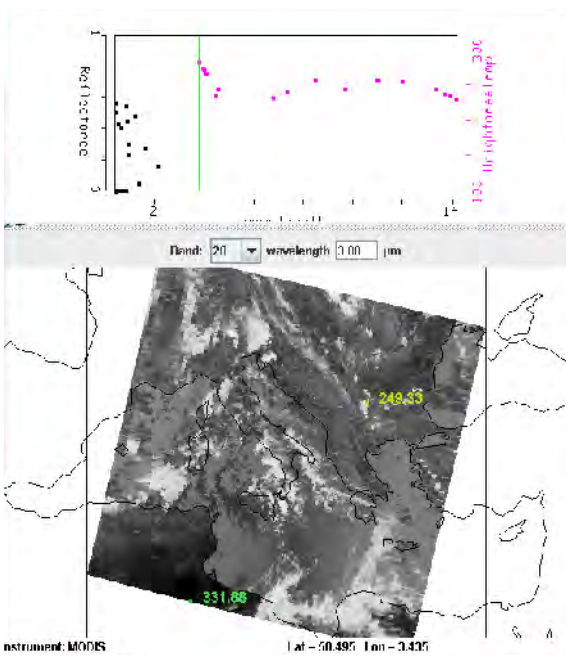

3.a

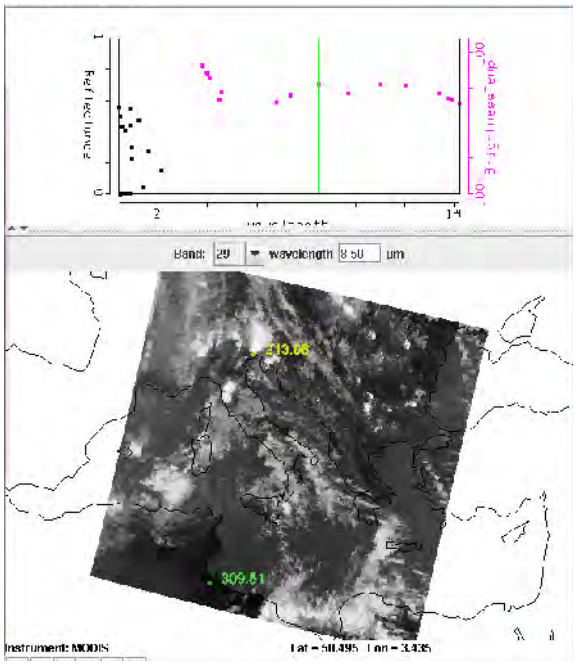

3.b

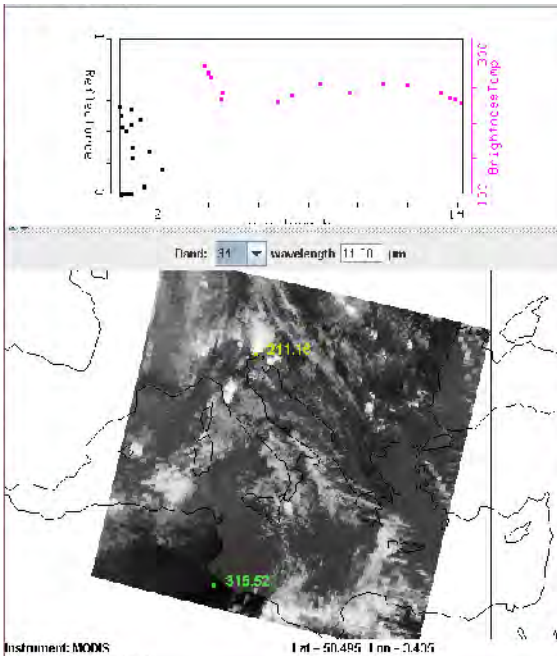

3.c

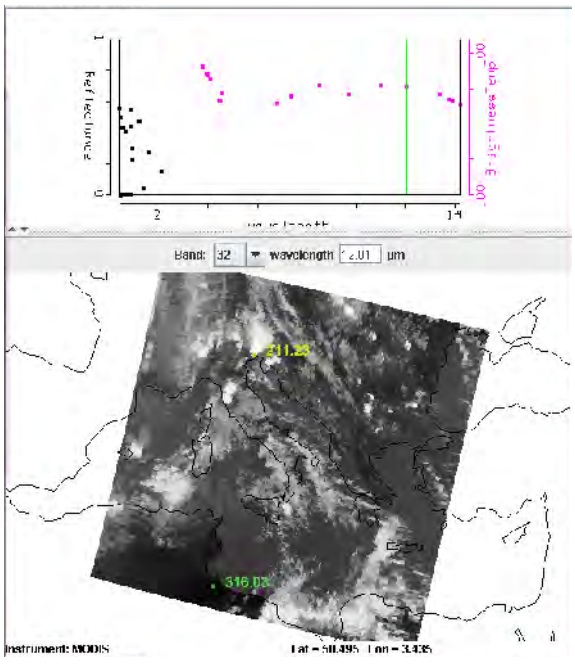

3.d

Fig. 14 - MODIS images of bands: 3.a. 20 (3.7 µm), 3.b. 29 (8.5 µm), 3.c. 31 (11 µm) and 3.d. 32 (12 µm). Visualized using HYDRA-Multichannel-Viewer.

The present study firstly performed three linear combination, that are:
X= 20 – 31 (3.7-11μm), Y= 29 – 31 (8.5-11 μm) and Z= 31 – 32 (11 - 12μm).

4.3.2. METODOLOGY TO THE CASE STUDY

The first linear combination bands performed using HYDRA is X= 20 - 31 (3.7-11μm):

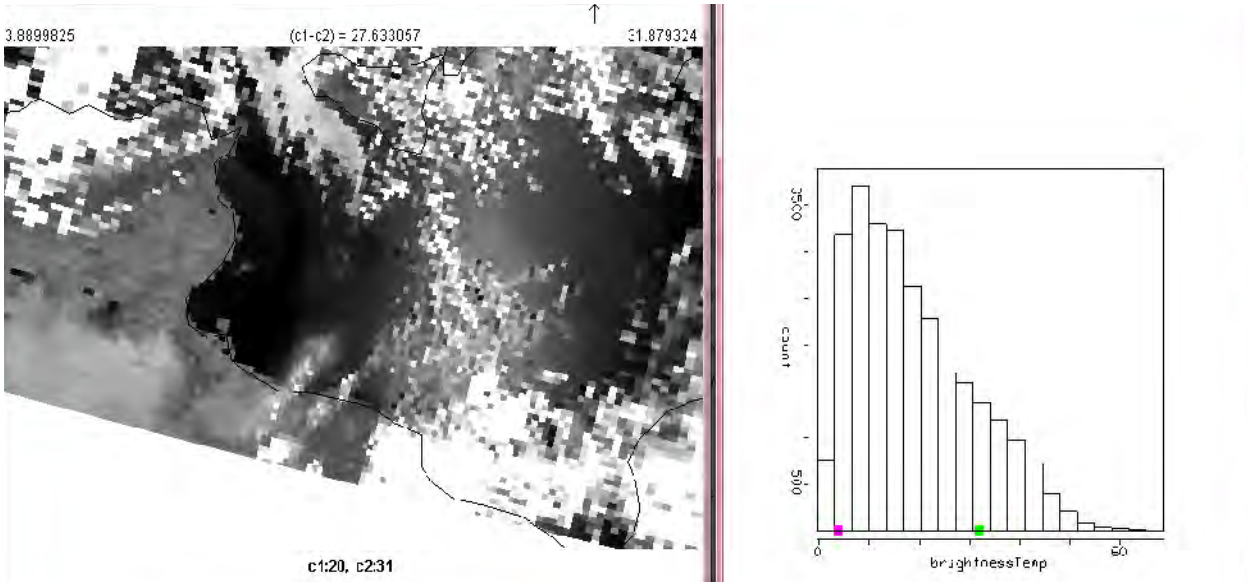

Fig. 15 – Image of the linear combination bands X=20-31 (3.7-11μm). Here the selected zone has the Brightness Temperature (BT) between 3.89 and 31.88. Dust, in the elliptic line, has BT between 10-30, that corresponds to 3000-3500 counts on the diagram (right), and very bright and white in the picture (left).

The second linear combination bands is Y= 29 - 31 (8.5-11 μm) in the same area:

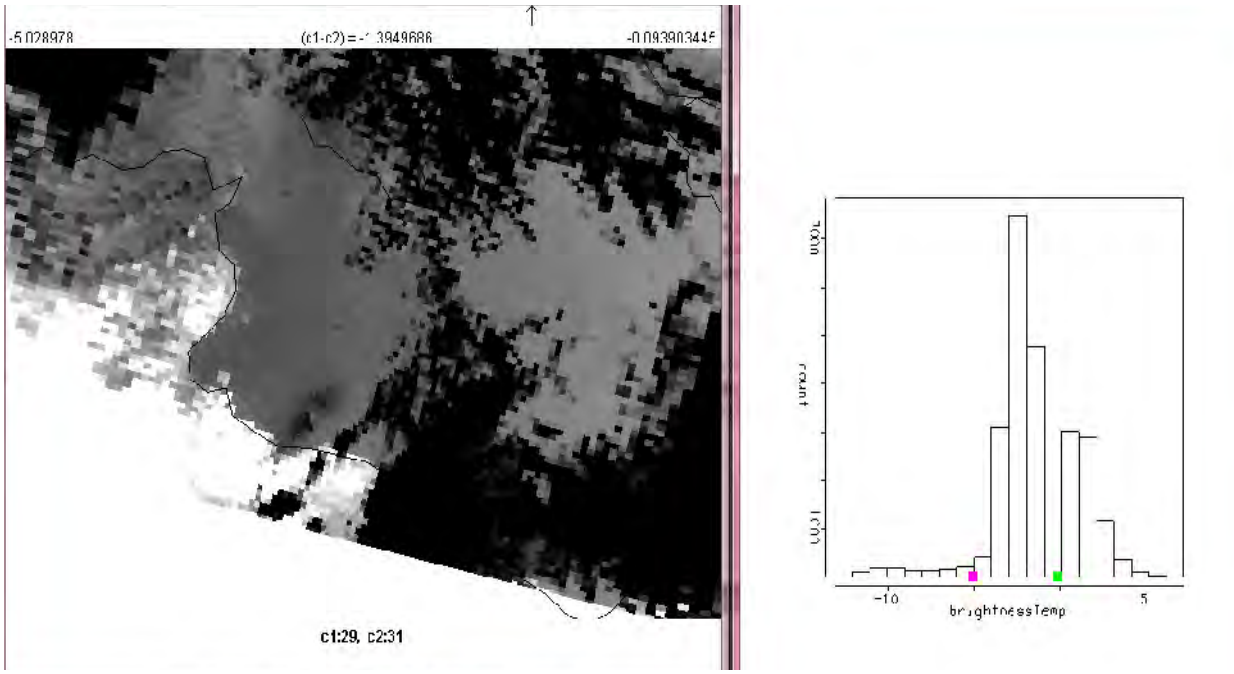

Fig. 16 – Image of the linear combination bands Y=29-31 (8.5-11 μm). Here the selected zone has Bright Temperature between - 5.03 and - 0.10.

The third linear combination bands is Z= 31 – 32 (11 - 12μm):

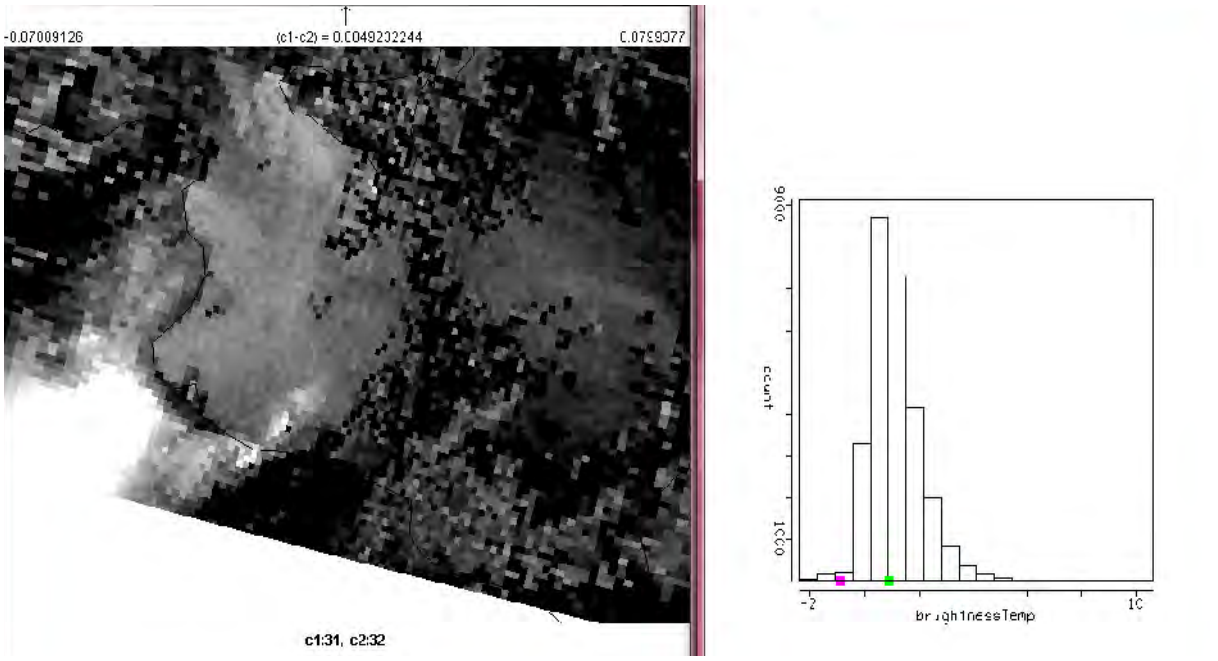

Fig. 17 – Image of the linear combination bands Z=31-32 (11 - 12μm). Here the selected zone has Bright Temperature between - 0.87 and 0.88. The figure shows the same dust area of the combination X and Y, and in this image there is the point with highest BT, about -0.91.

Using HYDRA also allowed the comparison of the first two linear combination bands, X= 20 - 31 (3.7-11µm) and Y= 29 - 31 (8.5-11 µm) in a Scatter Plot in order to see what happens in the dust area zone marked with the elliptic line:

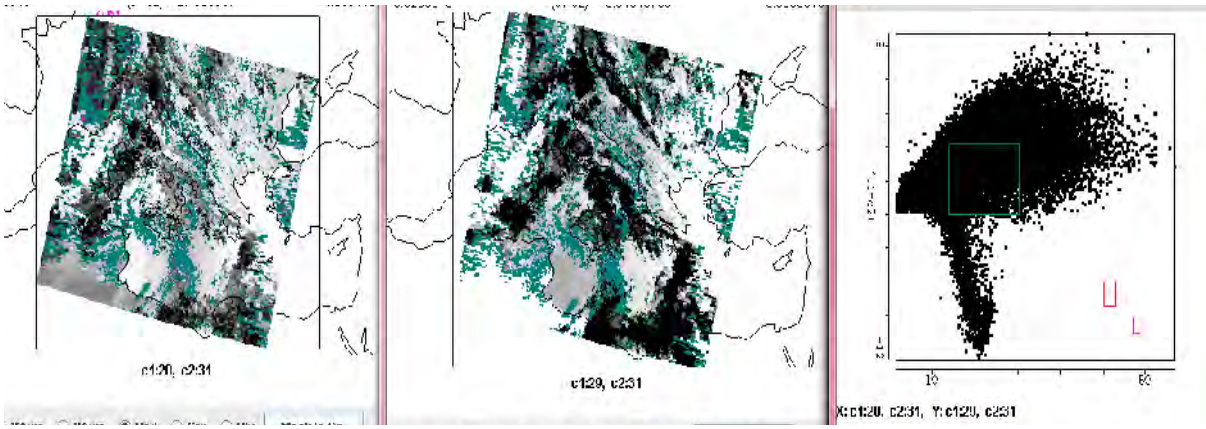

Fig. 18 - Image of the Scatter Plot of the two linear combination bands, X= 20 - 31 (3.7-11µm) and Y= 29 - 31 (8.5-11 µm). Here it is possible to see the dust area zone related to bands 20, 29 and 31. In the Scatter Plot on the left there are the corresponding values which also contain the dust area zone.

Using HYDRA also allowed the comparison of all combination bands (X, Y and Z) in a RGB plot, where the three combination above are X, Y, Z like R, G, B:

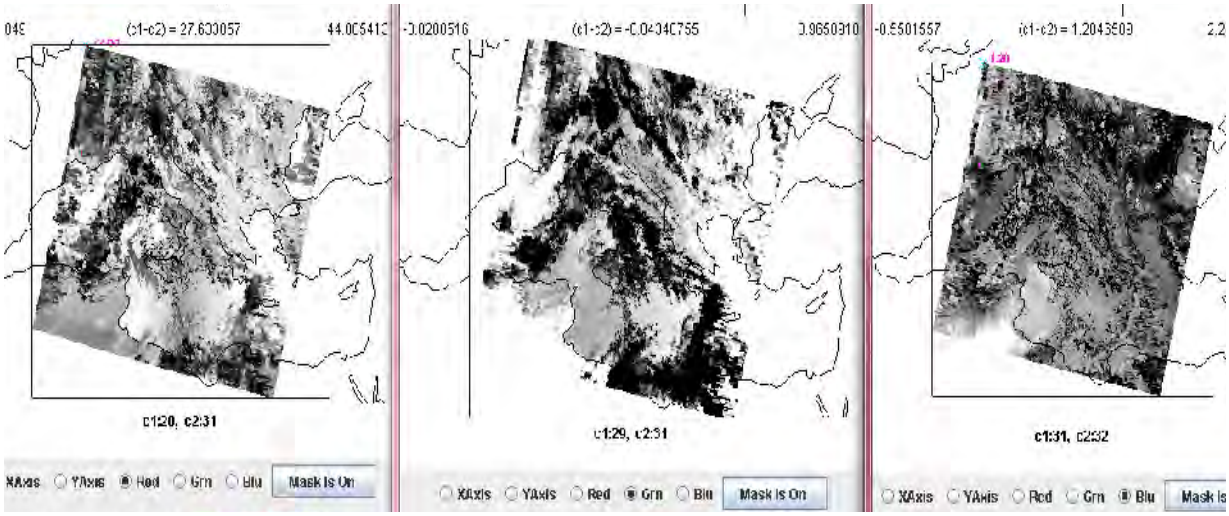

Fig. 19 - Image of the Three linear combinations selected as X, R and Y, G and Z, B using HYDRA multichannel viewer.

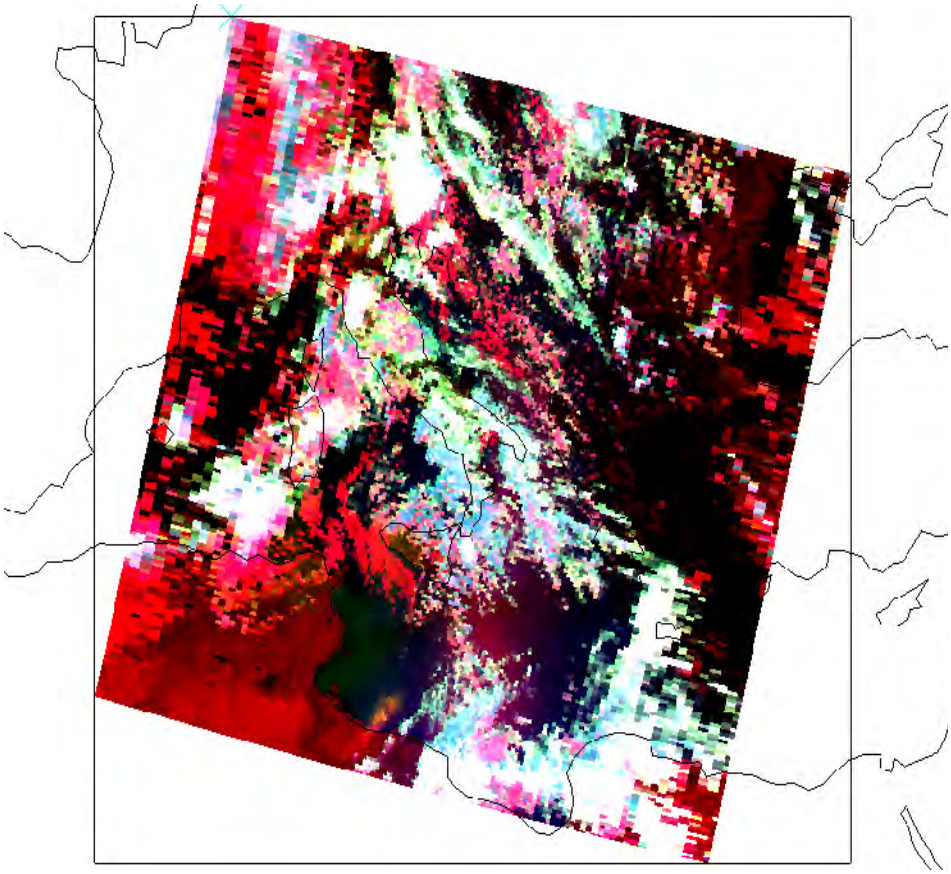

Fig. 20 – RGB Plot of the three combinations X, Y, Z. The plum of the dust area is in the same place of the RGB true colors. Here the lower and upper values of the color scale were chosen as: 6.68 - 27.194 for Red [X= 20 – 31 (3.7-11μm)]; -2.10 - 1.26 for Green [Y= 29 – 31 (8.5-11 μm)]; -26.45 - 5.48 for Blue [Z= 31 – 32 (11 - 12μm)].

The great concentration of dust leaving the land is following weather conditions.
The data image choosed is clear by high clouds, even thought there are some ice clouds on the right.

4.4. RESULTS

Therefore, the studied algorithm focuses on those MODIS combination bands, that are 20, 29, 31 and 32 MODIS Channels.
Firstly: development of three linear combinations that are:
band X= 20 – 31 (3.7-11μm);

band Y= 29 – 31 (8.5-11 μm);

band Z= 31 – 32 (11 - 12μm).

Secondly: comparison of all those combination bands in a Scatter Plot where the three combination above are X,Y,Z.

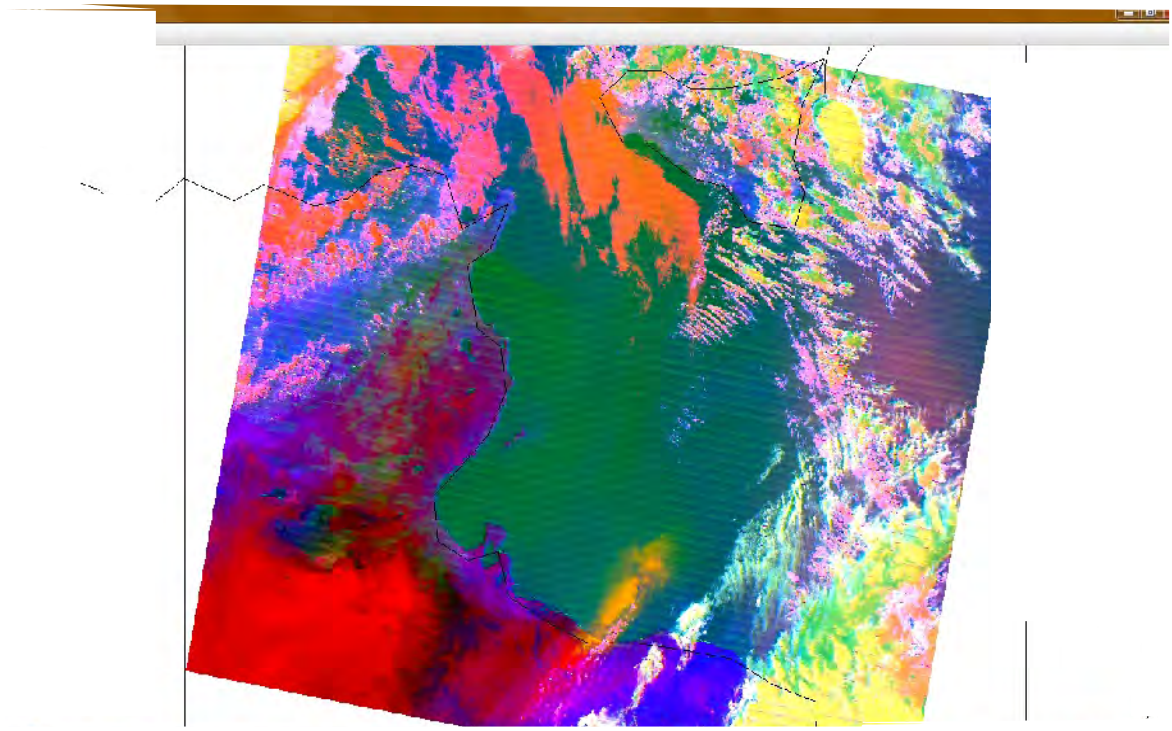

Fig. 21 - Scatter Plot X,Y,Z of three linear combination Modis bands

Table 4. Colour Table of PM Saharan Dust presence							
Colour	**Green**	**Blue**	**Purple**	**Red**	**Yellow**	**White**	**Dark Yellow**
R	0	30	45-55	220-255	248-255	236	**200-255**
G	108	0	64	0-2	242-255	255	**112-165**
B	50	251	155	0-2	96-113	178	**0-60**
meanings	Ocean mainly		Desert land - low Clouds		Top Clouds – little presence of Aerosols		**PM Saharan Dust**

The buffer in dark yellow is dust leaving the Sahara desert to the Mediterranean sea, the white on the right is a cloud, but also dust is transported by clouds.

The great concentration of dust is the dark yellow spot.

Mainly because of the chosen combination bands, above all the G range and the Z= 31 – 32 bands, that gives a difference only in presence of dust, otherwise are equal to zero in presence

of only clouds, but also over soil/land. So the box RGB of Dark Yellow is very important to discriminate dust in atmosphere.

The present study has focused on the detection of dust of the Saharan desert, which is a significant source of uncertainty in climate modeling of this area of interest; since dust affects cloud microphysics by acting as condensation nuclei, thereby affecting cloud radioactive properties, the hydrological cycle and atmospheric dynamics.
The location of anthropogenic and natural aerosols is an important consideration in the study of their impact on local climate, so **the searched algorithm focuses on the MODIS bands corresponding to the mentioned emissivity bands of dust, Sahara dust.**
Starting on estimative emissivity of dust, the presented algorithm focuses on linear combination of those bands using MODIS spectro-radiometer images with spatial resolutions of 1Km.
The searched algorithm helps scientists to easily detect dust without any other processed data, and it could be used to see dust over other regions and studied areas.
With the final comparison between Scatter plot and RGB, it can easily be sorted out where there is the largest amount of dust while the RGB gives an idea of the scatter of dust near and far the largest part of it.

4.5. CONCLUSIONS

Re-suspended and transported African desert dust particles have a strong impact on atmospheric visibility and aerosol composition as well as on PM levels in particular in Southern Europe, and Mediterranean Area Regions. The contribution of transported Saharan dust may reach more than 60% of total PM10 in Mediterranean countries during a strong pollution event, on average the 26% of the central Mediterranean surface was covered by Saharan Dust in the year 2001.
Dust emission is caused by the wind blowing above dry and scarcely vegetated soils of North Africa regions, where particles with diameter of ten to hundreds micrometers are present. These particles, that can be lifted into the atmosphere, travel long distance throughout the troposphere reaching Mediterranean Area States, and South European Countries.

Natural episodes of high PM levels are more frequent in spring/summer periods, when meteorological and climatic conditions are good for the transport of dust from North Africa into eastern Mediterranean areas (mostly in spring) and into western Mediterranean regions (mostly in summer).

To estimate the contribution of Natural Sources to PM in Italy, the Italian CNR – Institute of Atmospheric pollution in Rome - uses a 3-step procedure:

a) the mixing properties of the lower boundary layers are initially evaluated by means of natural radioactivity (radon progeny) concentration measurements. Starting from natural radioactivity values, Atmospheric Stability Indexes can be developed, which give for each day the probability, from the meteorological point of view, for the occurrence of an atmospheric pollution event. The mixing properties of the lower atmosphere are the key factor in determining PM concentration levels (during dust events an increase in PM10 has been experienced;

b) the daily average ratio among the number of particles from the coarse to the fine ranges is evaluated. An increase of this ratio indicates that a natural event is occurring;

c) the further chemical characterization of particles with the analysis of metals, ions and carbon compounds, allow the identification of the main sources, in particular sea-spray (Na^+ and Cl^-) and crustal materials (Al, Si, Ca, K, Fe). Natural events can be identified from an increase of the coarse-to-fine ratio, and the nature of the event is detected by chemical analysis.

Although spatial data and quantitative models describing BioVOC emissions are available, they give no information regarding their contribution to pollutant levels at a certain time at a certain place in Europe, since the composition of ambient air is influenced not only by the strength of the respective sources but by a variety of other factors. Current models describing these processes do not reach the appropriate spatial and time resolution. Thus, with the help of the Satellite Imagery, an analytical method, that discriminates between natural and anthropogenic contributions to organic aerosol, is a precondition for both the qualification and the quantification of monitored PM levels and, above all, for a model validation.

The dust can be easily discriminated, using Satellite Data. However, other organic aerosols, formed from natural and anthropogenic precursor gases, are difficult to measure and discriminate.

Satellite observations, together with modeling and ground base measurements could be useful

to control and study those natural -pollutants -dust events.
In a first step, MODIS data, the satellite data broadcasted whenever events occur, could be used to locate dust in a cheaper way, thanks to a proper algorithm focusing on the emission property of dust. Furthermore it could also determine the main concentrations of dust.
But Meteorology, Satellite imagery and modeling tools, have, all three, to be used to detect natural PM/Dust episodes.

4.5.1 Numerical esteem of Dust

To make a numerical esteem of the quantity of dust moving inside or aside meteorological clouds, a simple assume on MODIS DATA pixels has been used: every single pixel is bidimensional and measures 1km x 1km. if it is used a three dimensional pixel of 1km x 1km x 1km, in which the density of dust is constant and equal to the bidimensional.
Customizing 5 levels of density dust in 3D pixels, the results are in the table below:

Table 5. Dust density levels customized			
Level	Density	Density per 3D pixel	Pixel colour over ocean
1	1 µg/m^3	1 kg/km^3	Almost the same of the ocean
2	*50 µg/m^3	50 kg/km^3	Ocean color is a bit dirty
3	100 µg/m^3	100 kg/km^3	Start to discriminate dust over ocean
4	1 mg/m^3	1000 kg/km^3	Dust cover almost, but not entirely, the ocean
5	10 mg/m^3	10000 kg/km^3	Pixel reaching the color of desert land

* EU Daily Limit Value for PM10

In the dust plum seen, when Hydra and the algorithm are applied, the dust level is 4 and 5, both on land and ocean. It could be that a mean value of 5 mg/m^3,i.e. 5000 kg/km^3 is transported on Troposphere by meteorological and climatologic conditions.

4.6 FUTURE

The algorithm has been tested on almost 20 MODIS data, but several of them where incomplete. In fact, not all the 36 bands were detected.

Therefore, since at least bands 20, 29, 31 and 32 were necessary, 6 images were collected and processed (attached at the end of the present work).

A number of methods for the estime of total PM to natural sources are available and some are implemented by certain Member States.

Above is presented the 3-step used by CNR in Italy. The apportionment may be done using different methodologies, such as the use of a routine method, the use of information in parallel from background stations, and the use of advanced tool implemented by research groups.

During the last two years of my personal PhD, after accumulating the state of the arts on Satellite's Spectroradiometers and the study of meteorological Physics below radioactive transfer in the atmosphere, I personally contacted two groups, one from University of L'Aquila, ITALY and one from Laboratoire de Meteorologie Dynamique Ecole Polytechnique, Palaiseau FRANCE.

At last Menut Laurent, Chimere's father, gave himself the advice that horizontal data, such the ones that MODIS gives, are not sufficient as data input, and that I should also use vertical data to mix all information.

The CALIPSO group studied the rise of aerosols in regions before the monsoon using both data.

In the days and weeks before the monsoon, heat builds over India. Hot air rises over the baked earth and westerly winds rush in to fill the void, bringing dust-laden air from the deserts of southwest Asia and the Arabian Peninsula. Through April, May, and June, as monsoon conditions build, the air over the Ganges River plain grows thick with dust, smoke, and haze. Air quality over India is at its worst at this time of year. Finally, from mid- to-late June, the winds shift and cleansing monsoon rains fall.

Fig.22 below provides a profile of the pre-monsoon air over India on May the 12th, 2007.

The lower image was made with data from the CALIPSO satellite (one of the so called satellite A-train Satellites, where AQUA and ARIA are the head and tail of the satellite train), which sends pulses of light laser through the atmosphere at night and measures the light signal that returns to the sensor. CALIPSO sensor provides a vertical laser profile.

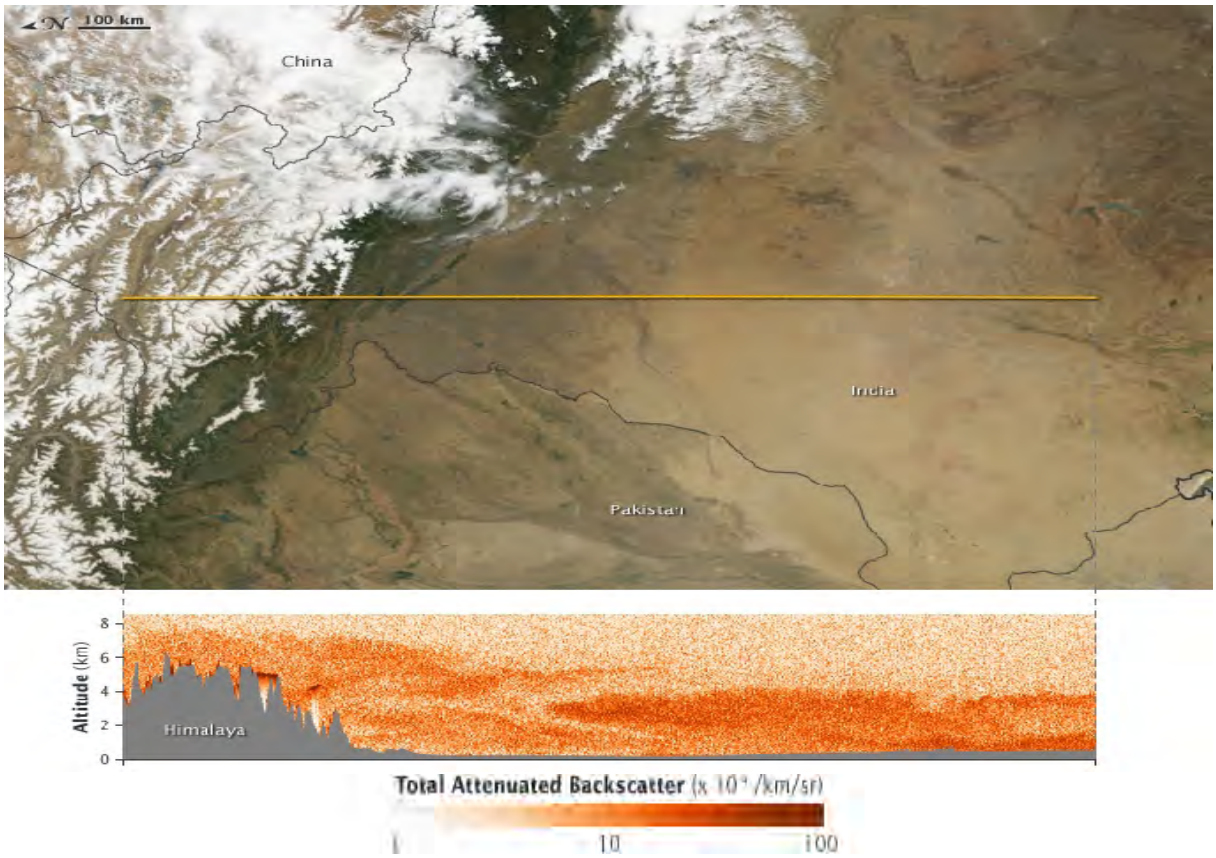

Fig. 22 – Top Image is a daytime MODIS; bottom image provides a profile of the pre-monsoon air CALIPSO laser night sensor. Both over India on May the 12th, 2007.

This measurement reveals the concentration of particles—ice, dust, soot, and so forth—in the atmosphere. The dark orange areas in the profile show where the particle concentration was most dense. Pale orange and white areas reveal fewer particles.

The top image is a daytime scene captured that same day by MODIS on the Terra satellite. The yellow line across the top image shows the path of the satellite on May the 12th when it collected the profile in the lower image.

The dense particle concentration included a combination of dust, smoke from fires, and urban smog. Measurements from other satellites and ground-based instruments revealed that the bulk of the pollution was dust.

Dust transported by westerly winds moves over the Ganges Plain and hits a barrier: the massive Himalayas. Trapped against the mountain front, the dust builds until concentrations are higher than at any other time of year. The rising of hot air from the land, combined with the incoming winds, pushes the dust and haze high into the atmosphere along the front of the Himalaya. In this image, the bulk of the dust reaches about four kilometers in altitude; along

the mountains, it reaches six to seven kilometers. (The particles over the mountains and the Tibetan Plateau are probably ice clouds, but may also contain some dust.)

This dust and haze over the Ganges Plain may increase the intensity of monsoon rains. Both soot and dust particles absorb energy, heating the atmosphere. The added heat pushes the air higher than it would otherwise rises. The rising air sucks up more air, and when that air is moist, the monsoon circulation may strengthen, leading to more rainfall during the early summer.

The high dust and haze also might hasten the melting of snow in the Himalayas. Particles settle on the surface, darkening the snow. White snow reflects energy, but the particle-darkened surface absorbs it, causing the snow to melt faster. This has been demonstrated in other regions.

The crucial point is, that in order to complete MODIS data, in site measurements to validate images data and quality considerations or, in alternative, vertical Satellite data (such as LIDAR, and CALIPSO) are needed to really fulfill the algorithm and the routine.

4.7 PERFORMING ALGORITHM DATA SET

The collection of algorithm' performed data is showed belowe.

Sardinia Modis Image 2009 091
MYD021KM.A2009091.0100.005.2009091204610.hdf

Linear combinations 20-31

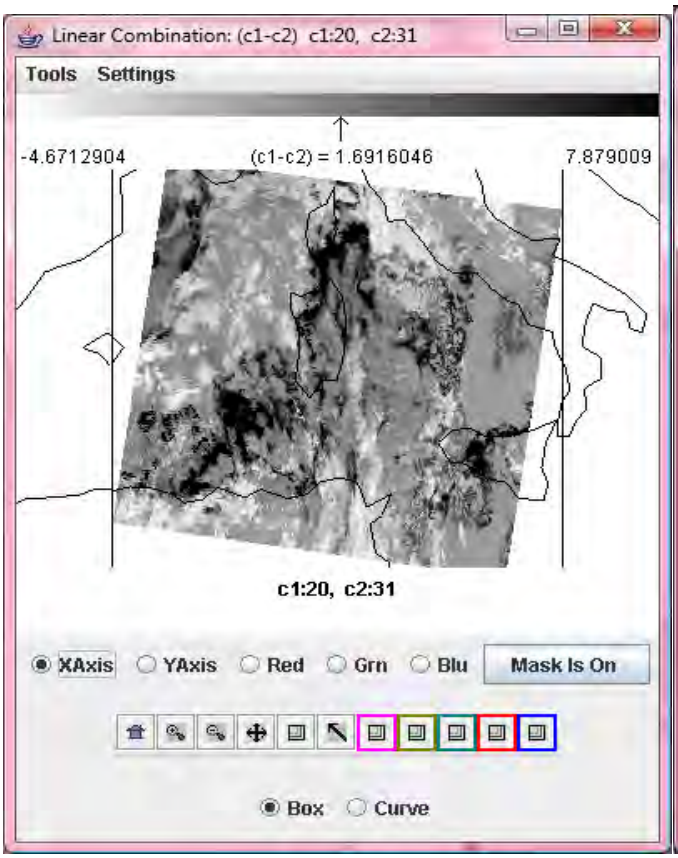

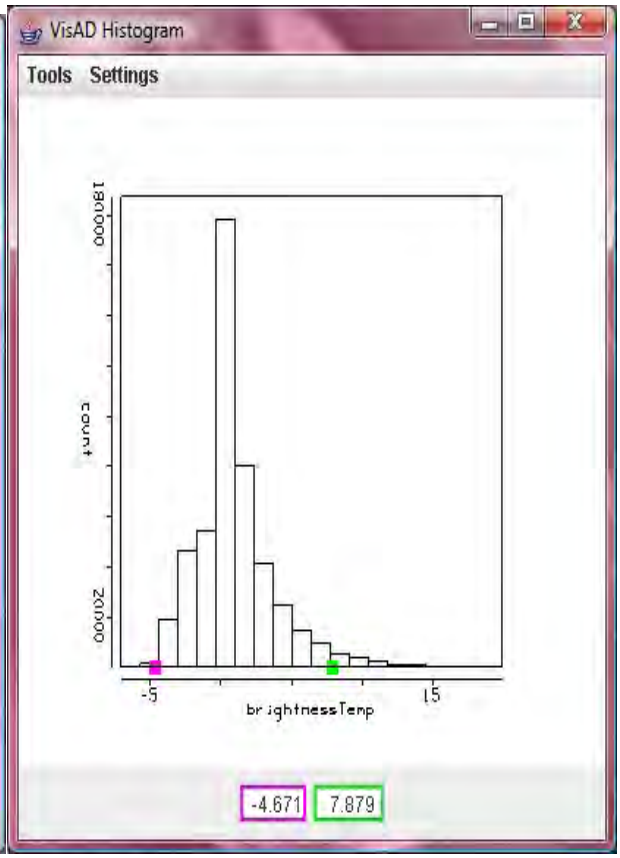

linear combinations 29-31

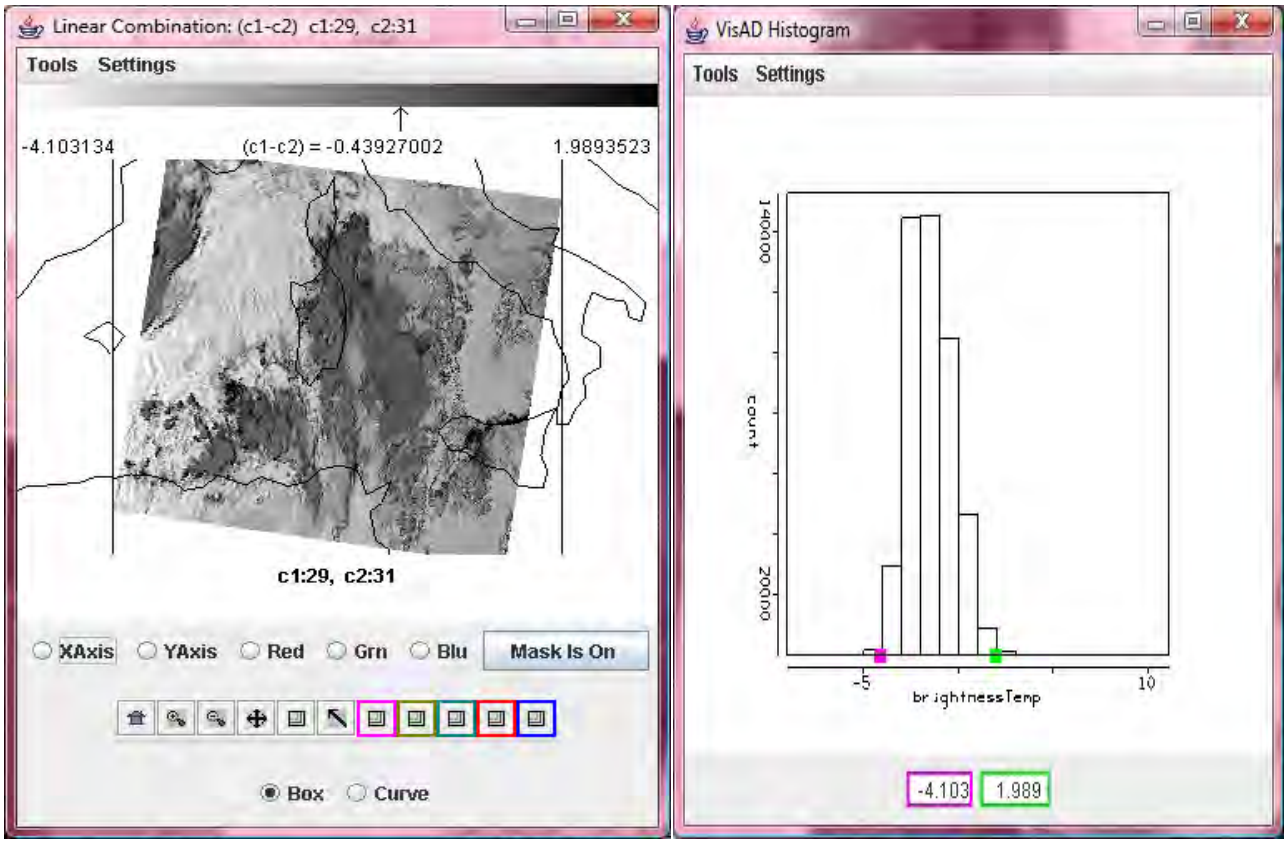

linear combo 31-32

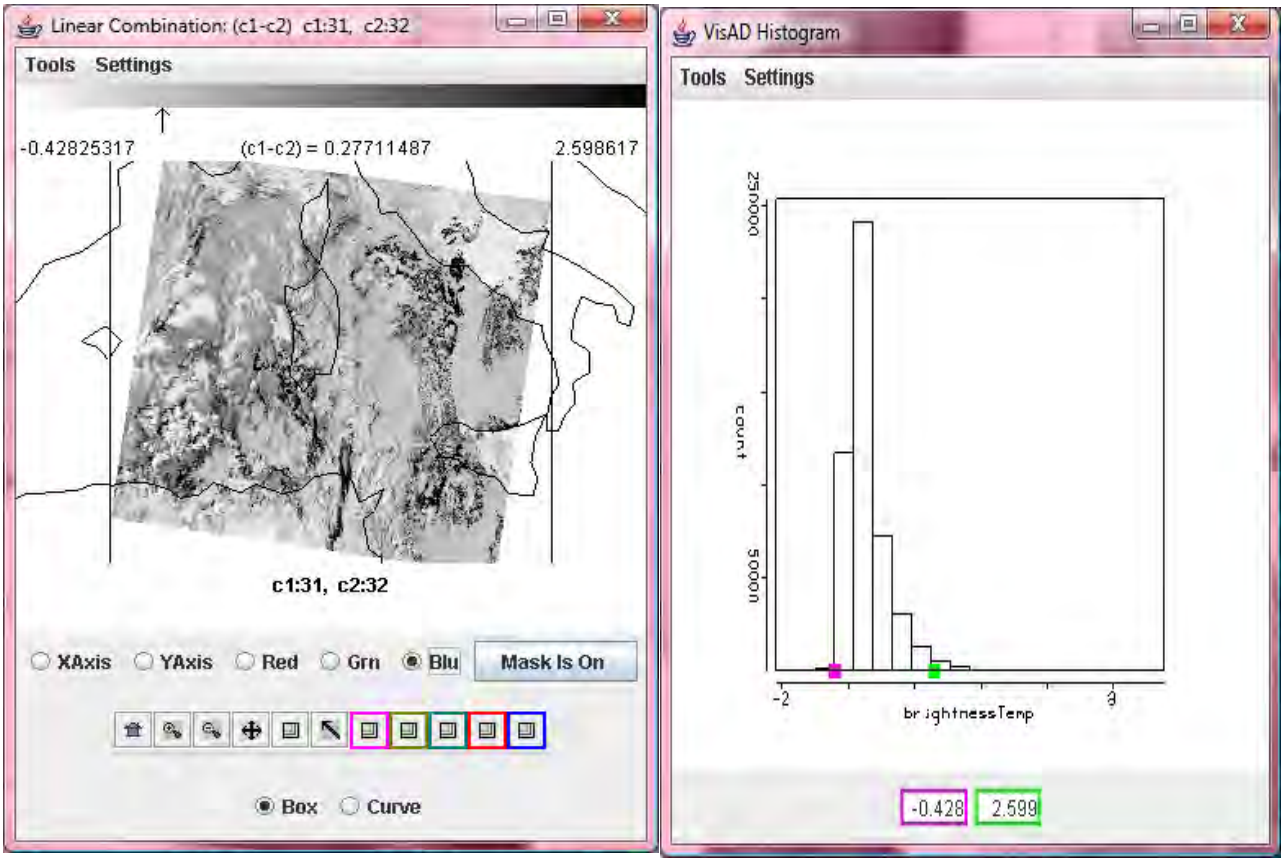

The Scatter Plot of the 3 axes Red/X, Green/Y and Blu/Z

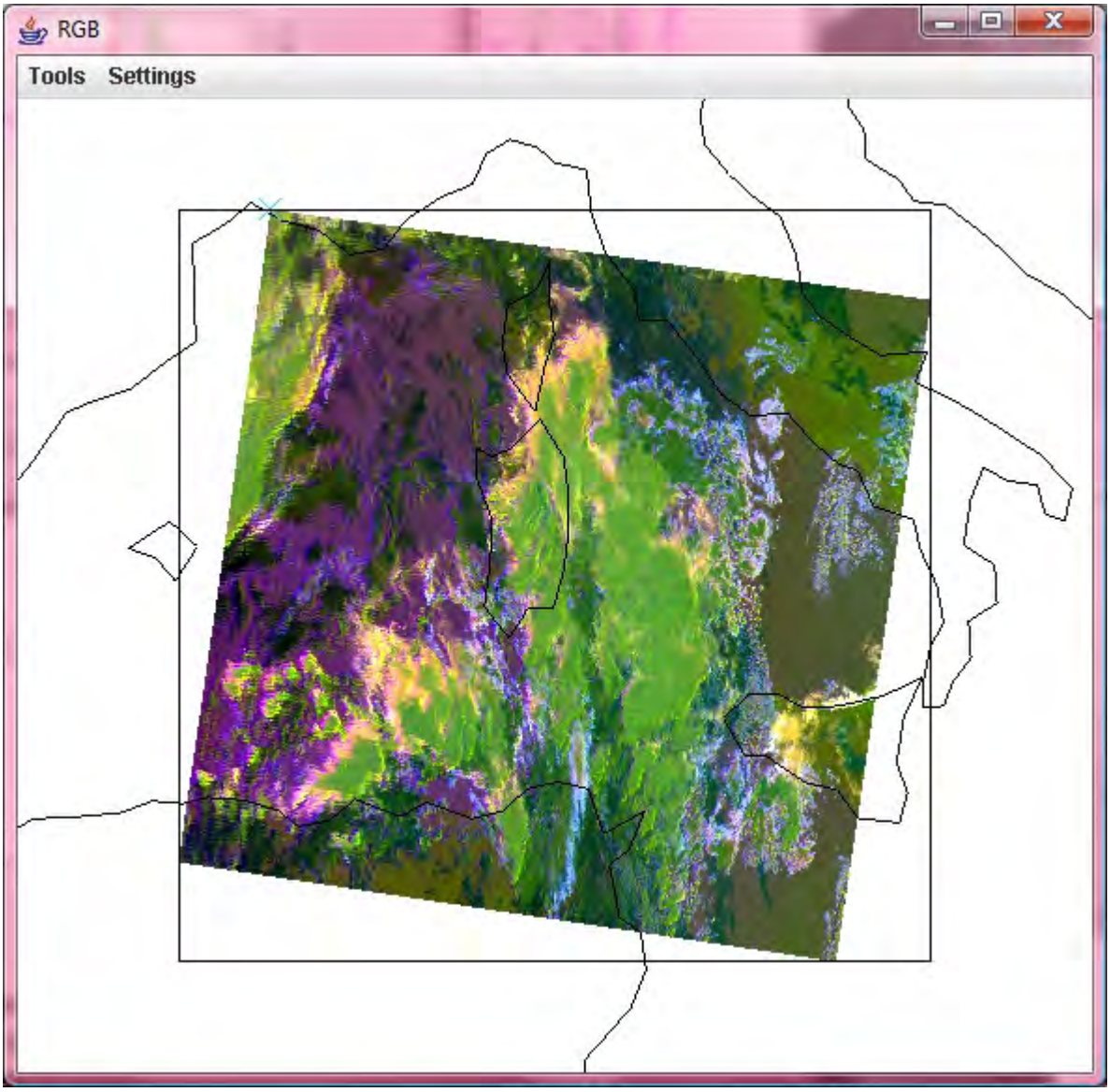

No dust only clouds.

MYD021KM.A2009091.1205.005.2009092162919.hdf

RGB

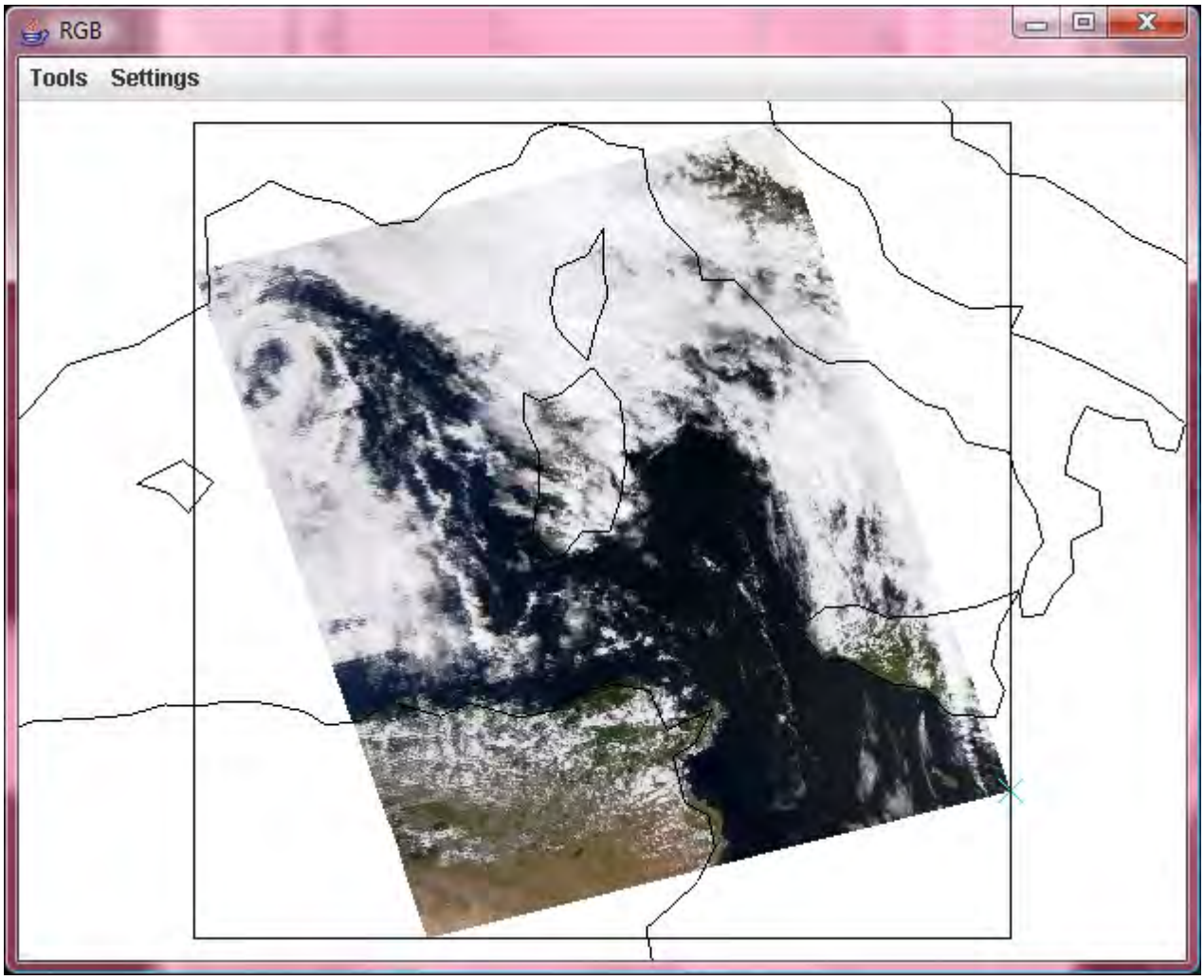

linear combinations 20-31

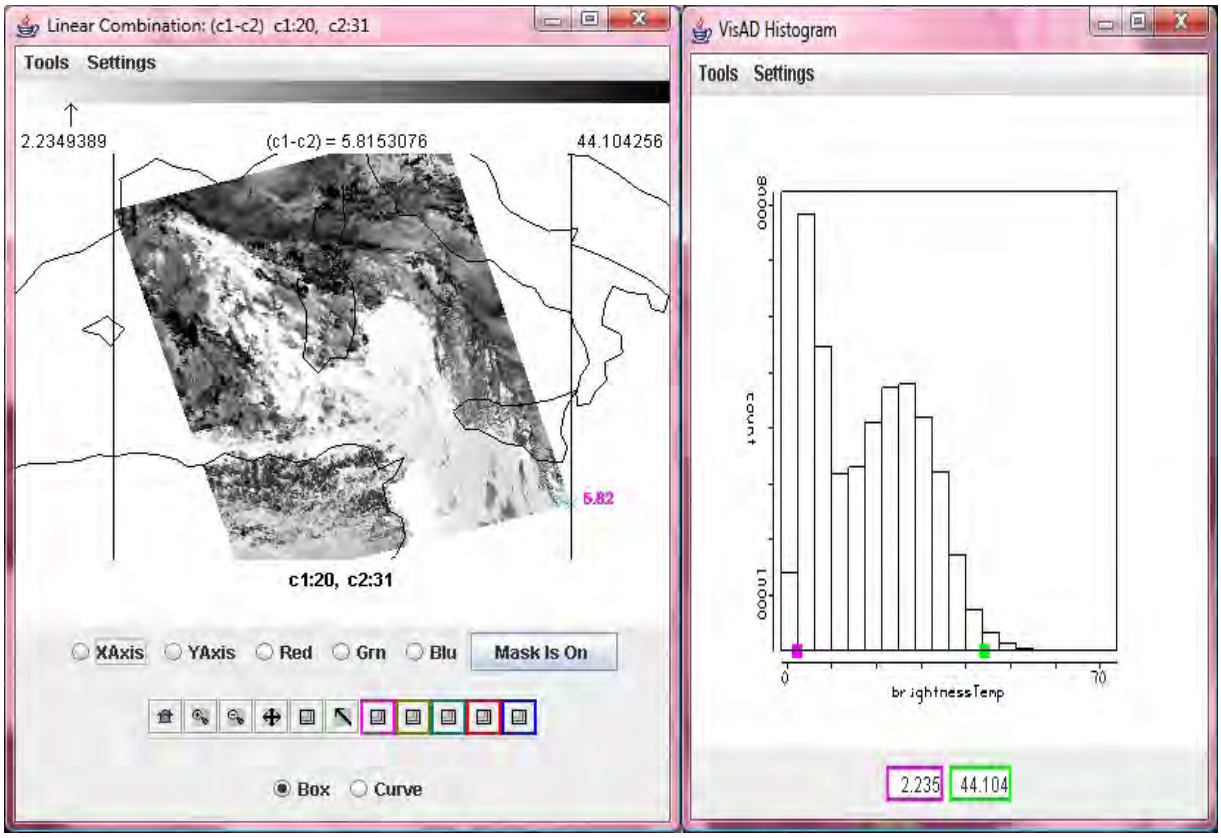

linear combinations 29-31

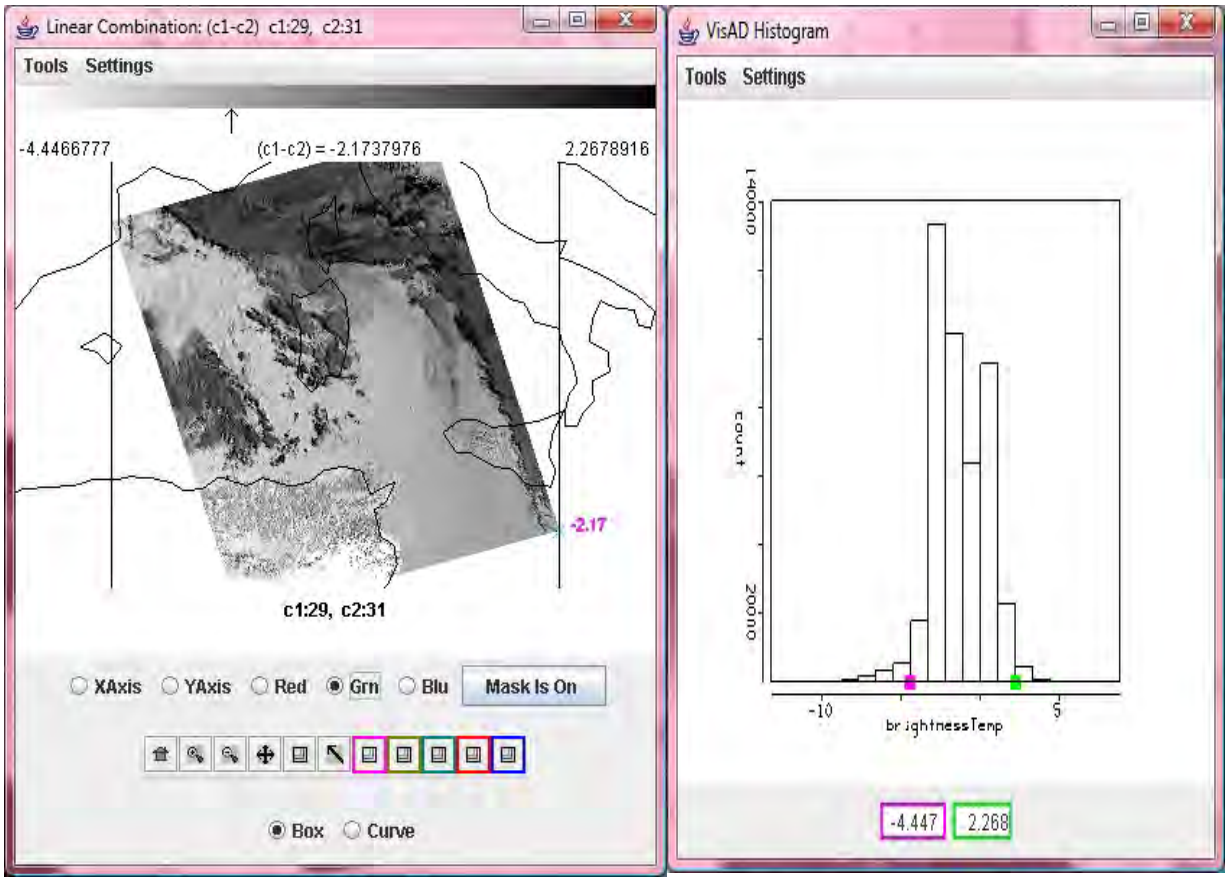

linear combo 32-31

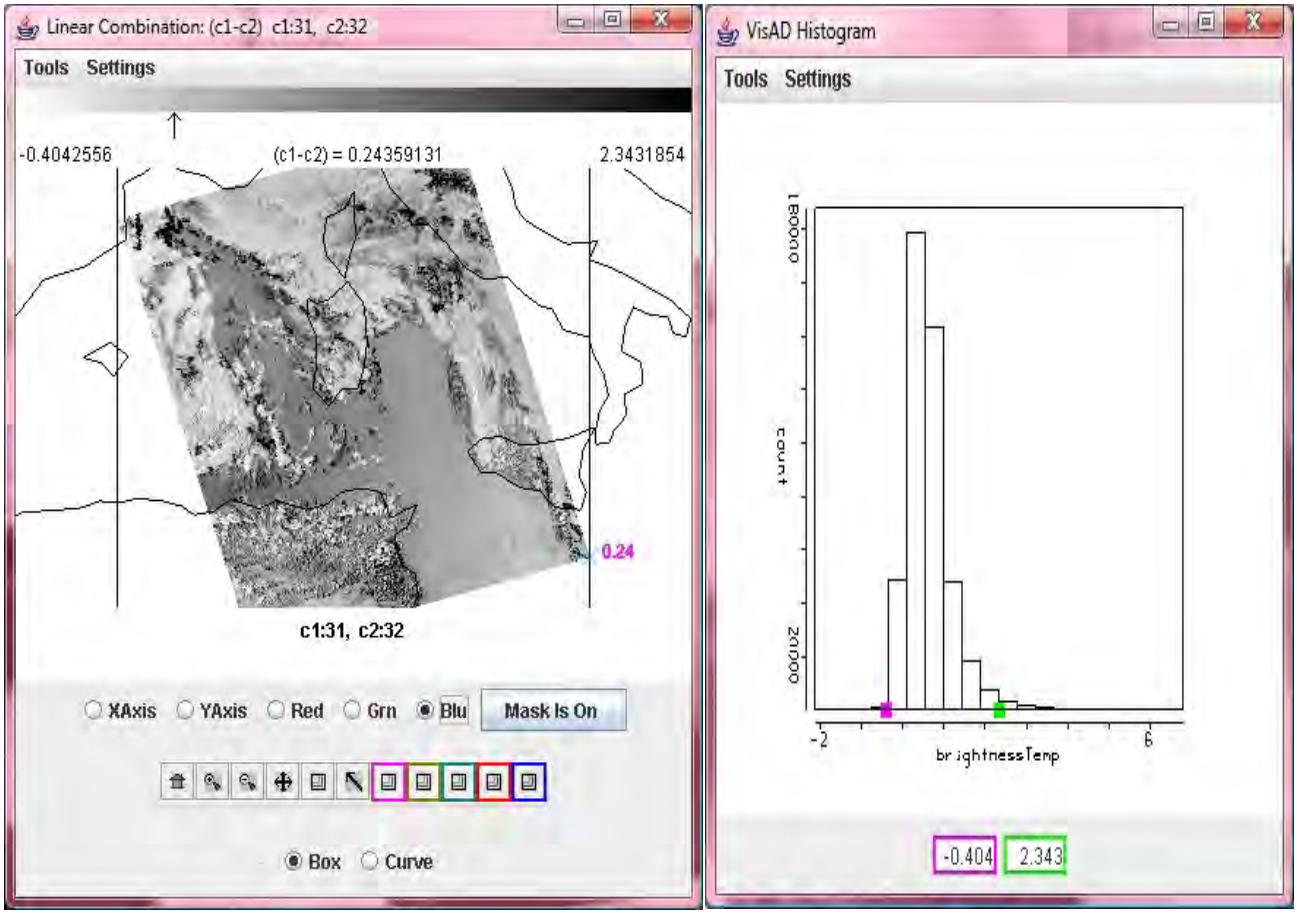

the Scatter Plot

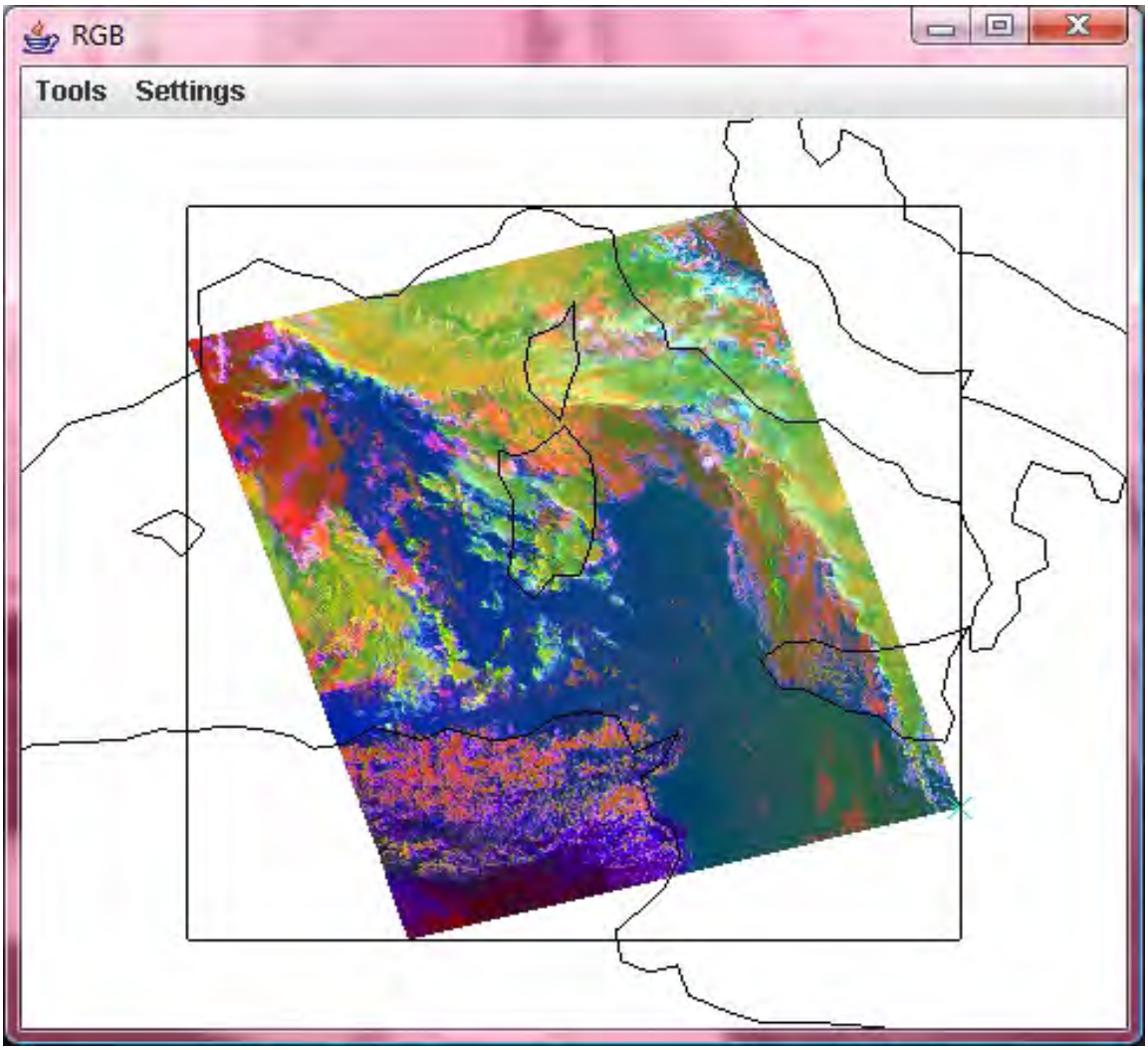

Clould' surface differing temperatures.

MYD021KM.A2009092.0145.005.2009092164413.hdf

RGB

no data in the range 1-19 visible and near ir

20-31

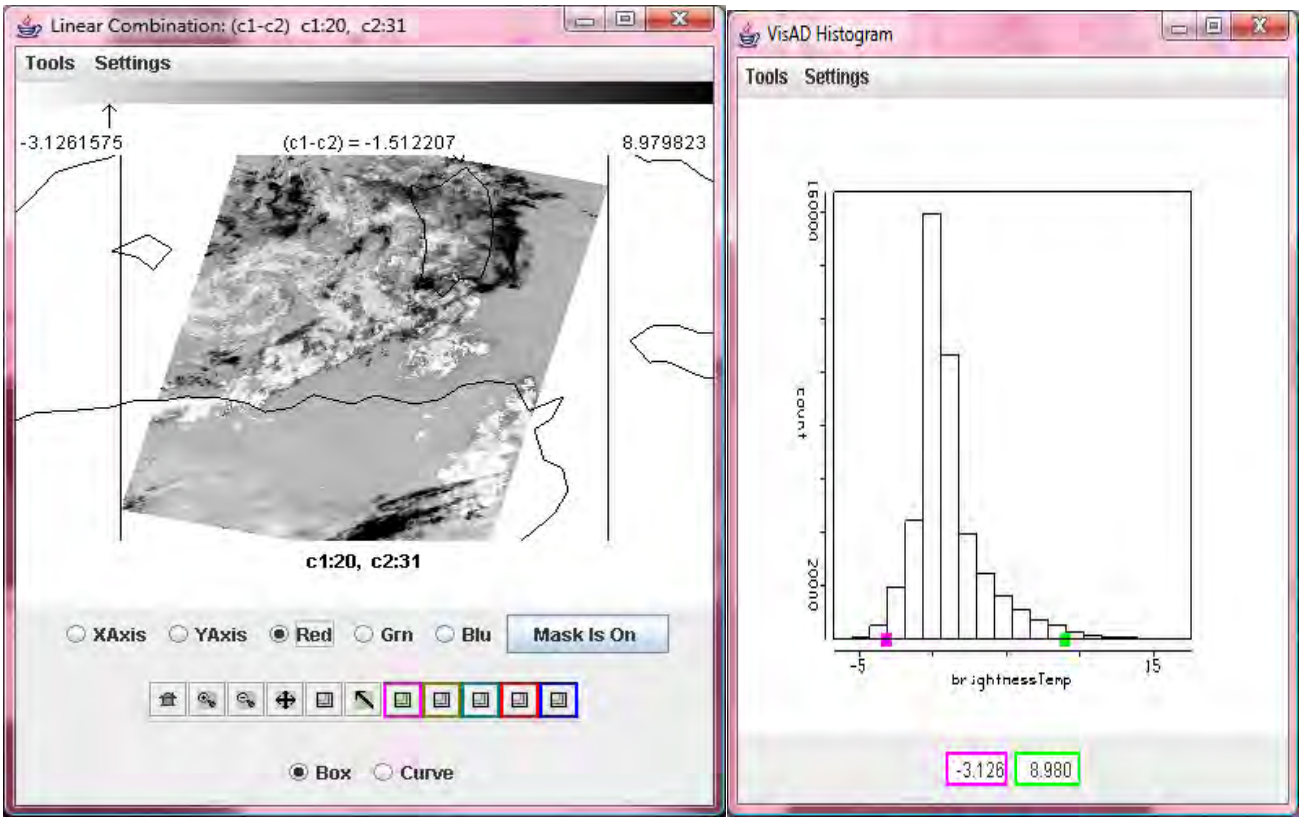

29-31

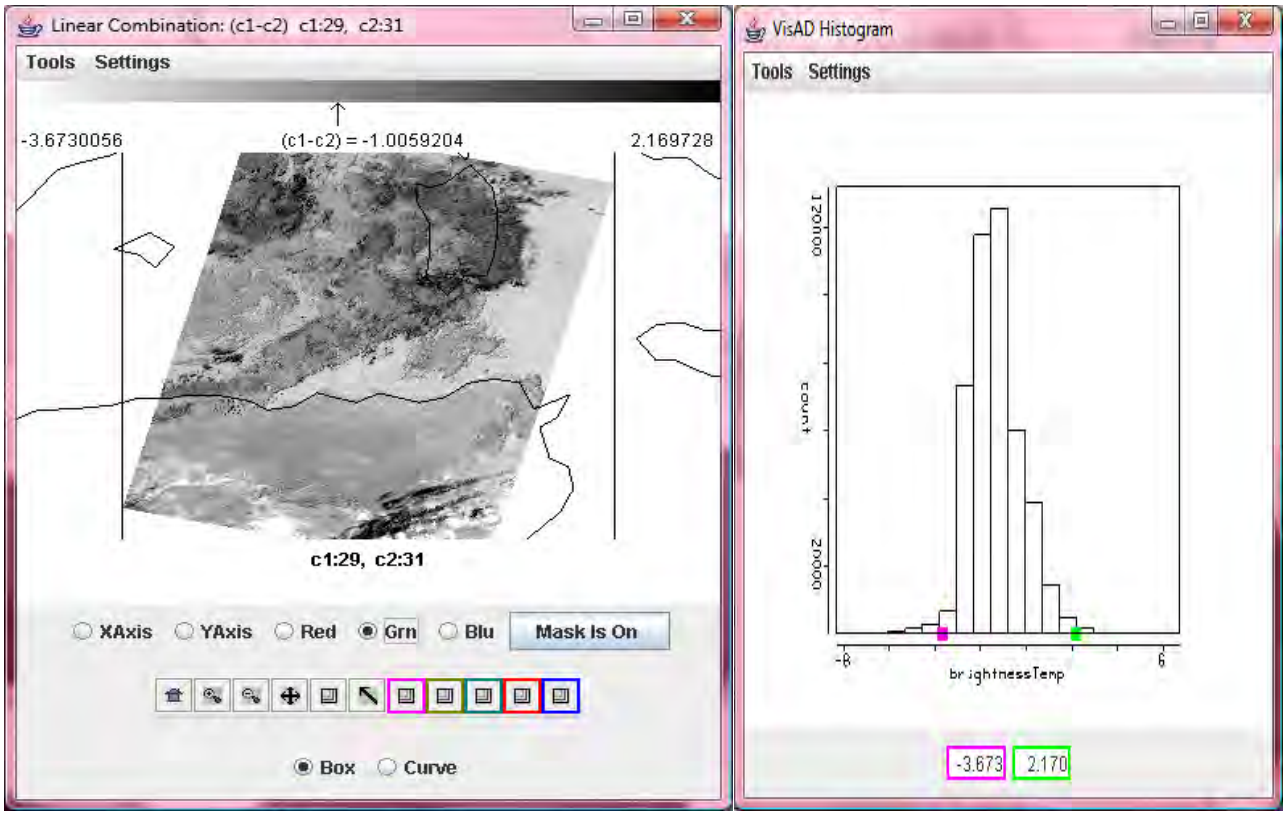
Linear Combination: (c1-c2) c1:29, c2:31
Tools Settings
-3.6730056
(c1-c2) = -1.0059204
2.169728
c1:29, c2:31
XAxis YAxis Red Grn Blu Mask Is On
Box Curve
VisAD Histogram
Tools Settings
120000
count
20000
brightnessTemp
-3.673
2.170

32-31

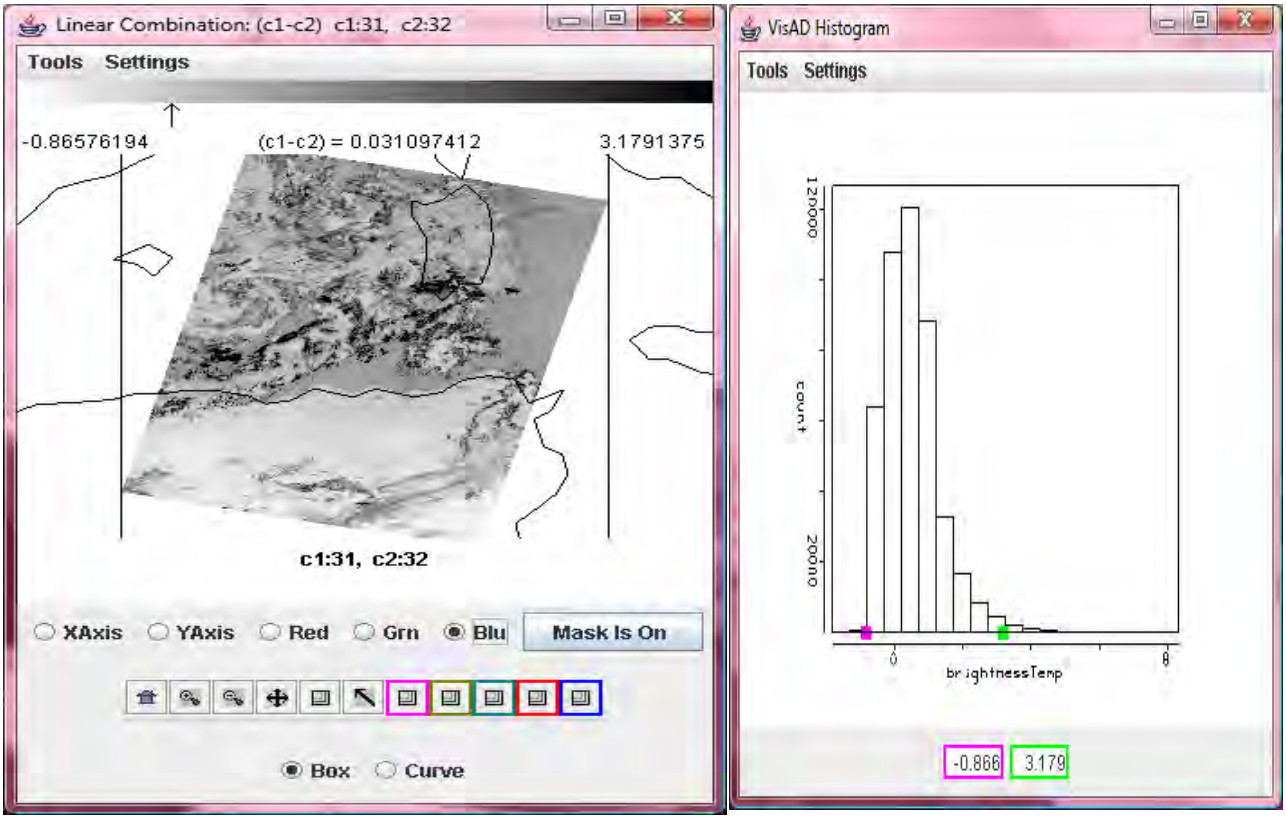
Linear Combination: (c1-c2) c1:31, c2:32
Tools Settings
-0.86576194
(c1-c2) = 0.031097412
3.1791375
c1:31, c2:32
XAxis YAxis Red Grn Blu Mask Is On
Box Curve
VisAD Histogram
Tools Settings
120000
count
20000
brightnessTemp
-0.866
3.179

scatter plot

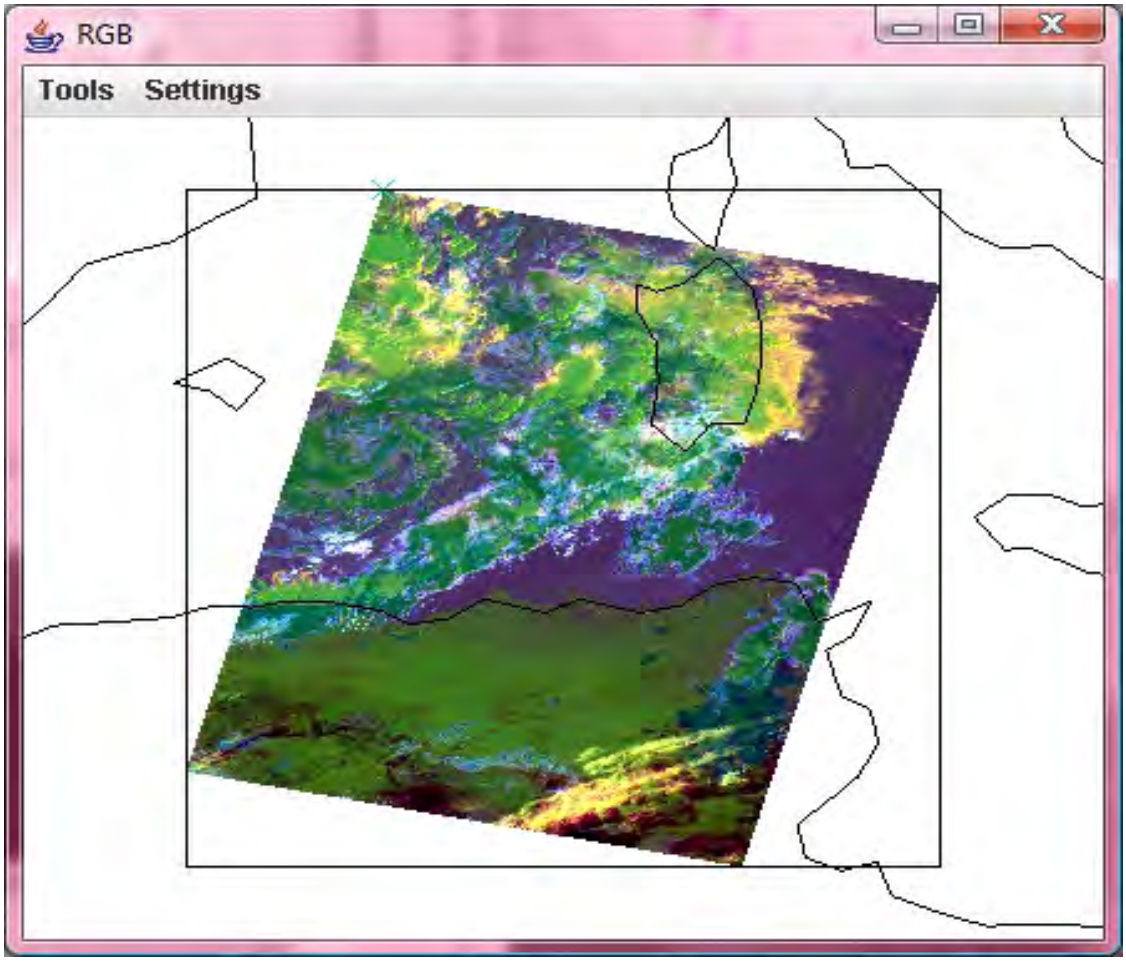

Dust leaving Sardinia from South West to North East.

MYD021KM.A2009092.1110.005.2009093171920.hdf

RGB

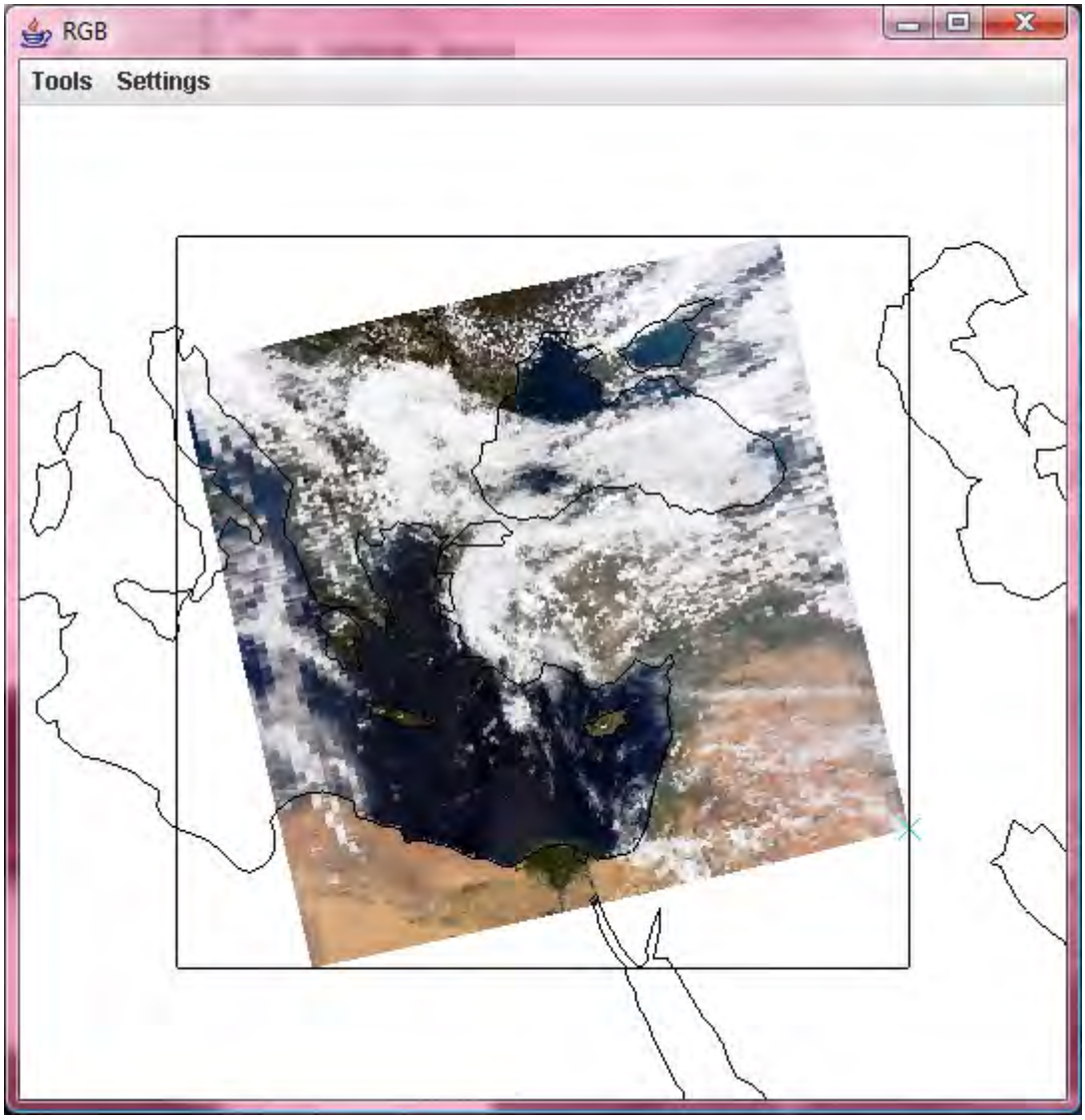

20-31

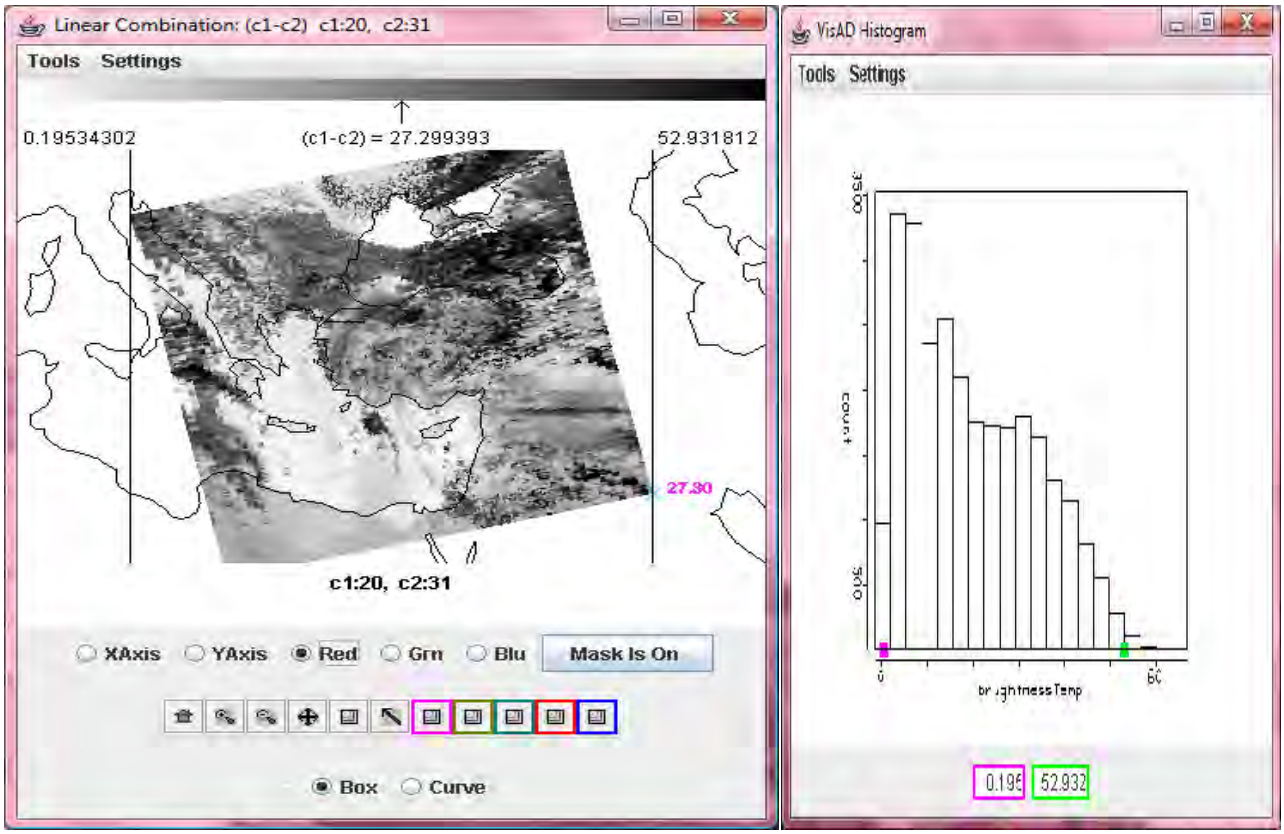
Linear Combination: (c1-c2) c1:20, c2:31
Tools Settings
0.19534302
(c1-c2) = 27.299393
52.931812
27.30
c1:20, c2:31
XAxis YAxis Red Grn Blu Mask Is On
Box Curve
VisAD Histogram
Tools Settings
count
brightnessTemp
0.19
52.932

29-31

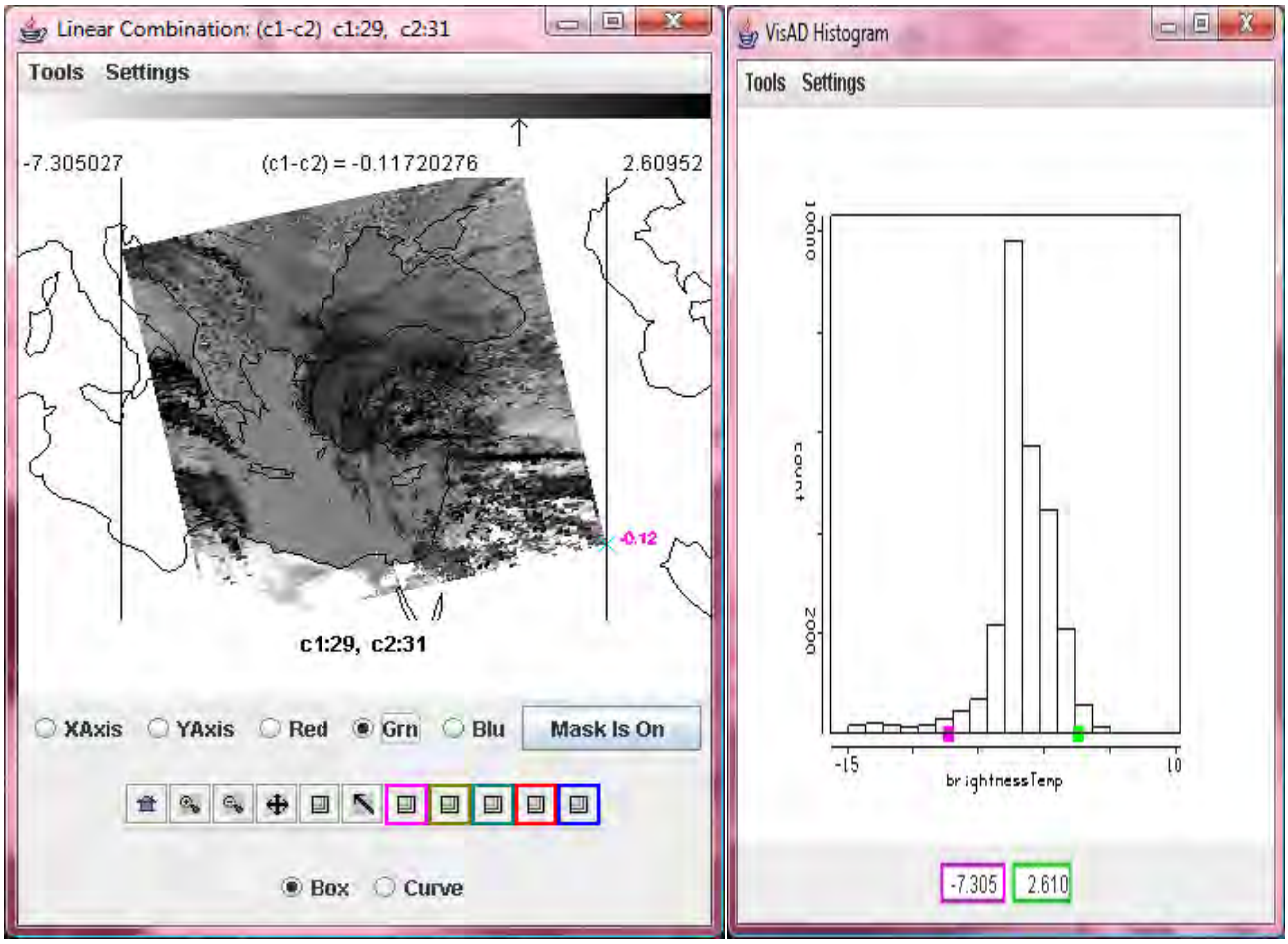
Linear Combination: (c1-c2) c1:29, c2:31
Tools Settings
-7.305027
(c1-c2) = -0.11720276
2.60952
-0.12
c1:29, c2:31
XAxis YAxis Red Grn Blu Mask Is On
Box Curve
VisAD Histogram
Tools Settings
count
brightnessTemp
-7.305
2.610

31-32

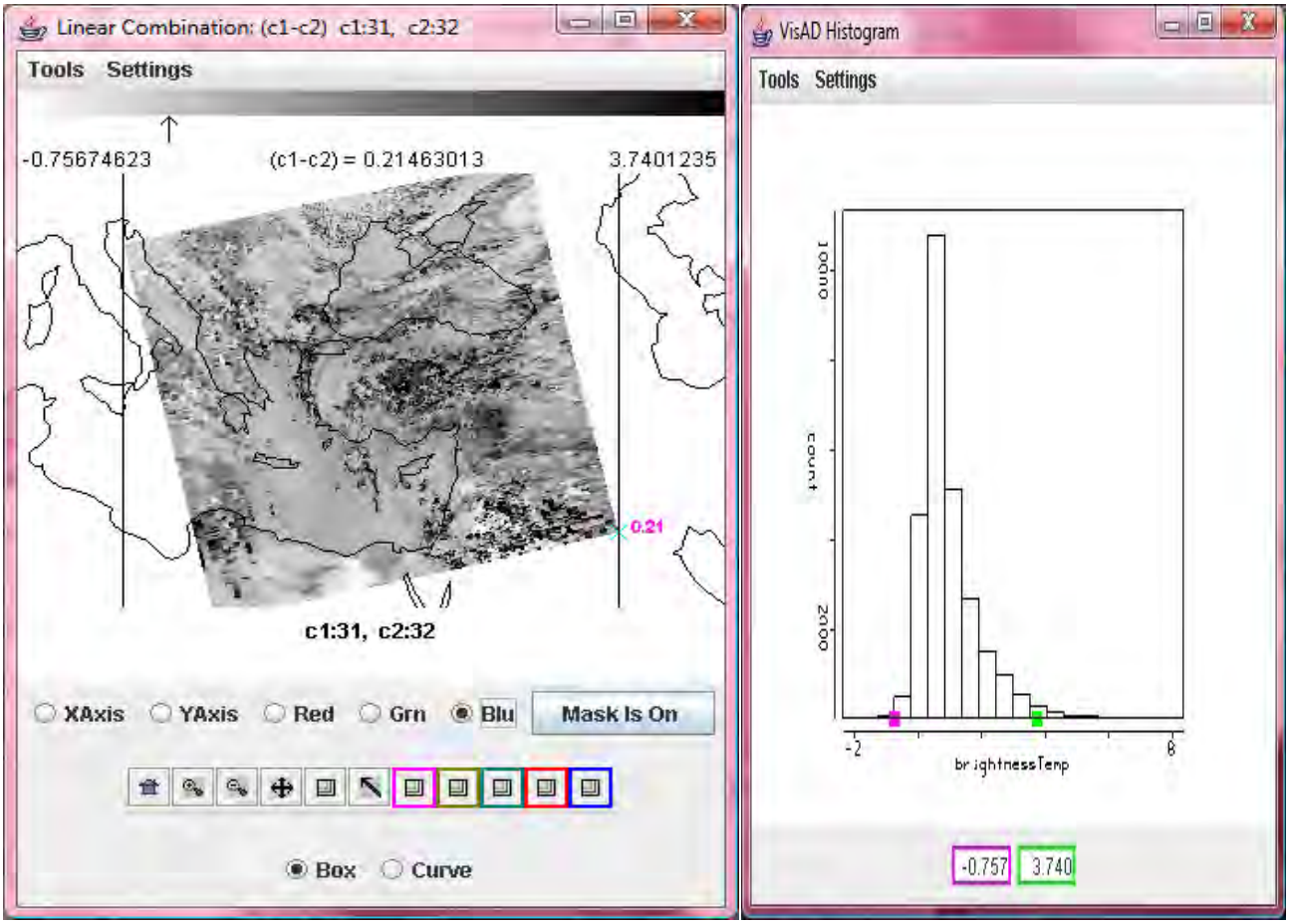
Linear Combination: (c1-c2) c1:31, c2:32
Tools Settings
-0.75674623
(c1-c2) = 0.21463013
3.7401235
0.21
c1:31, c2:32
XAxis YAxis Red Grn Blu
Mask Is On
Box Curve
VisAD Histogram
Tools Settings
1000
count
2000
-2
0
brightnessTemp
-0.757
3.740

Scatter

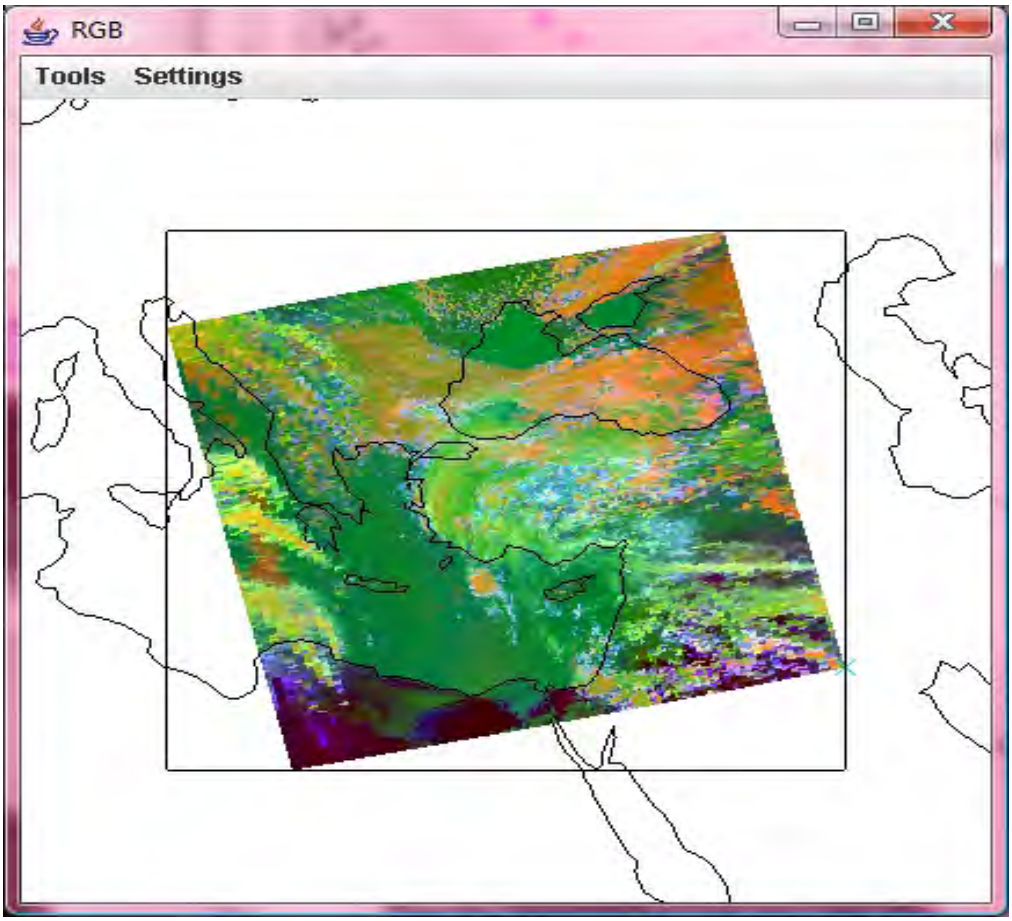

The orange here is the cloud' temperature.

MYD021KM.A2009093.0050.005.2009093183255.hdf

RGB
no data in the visible bands

20-31

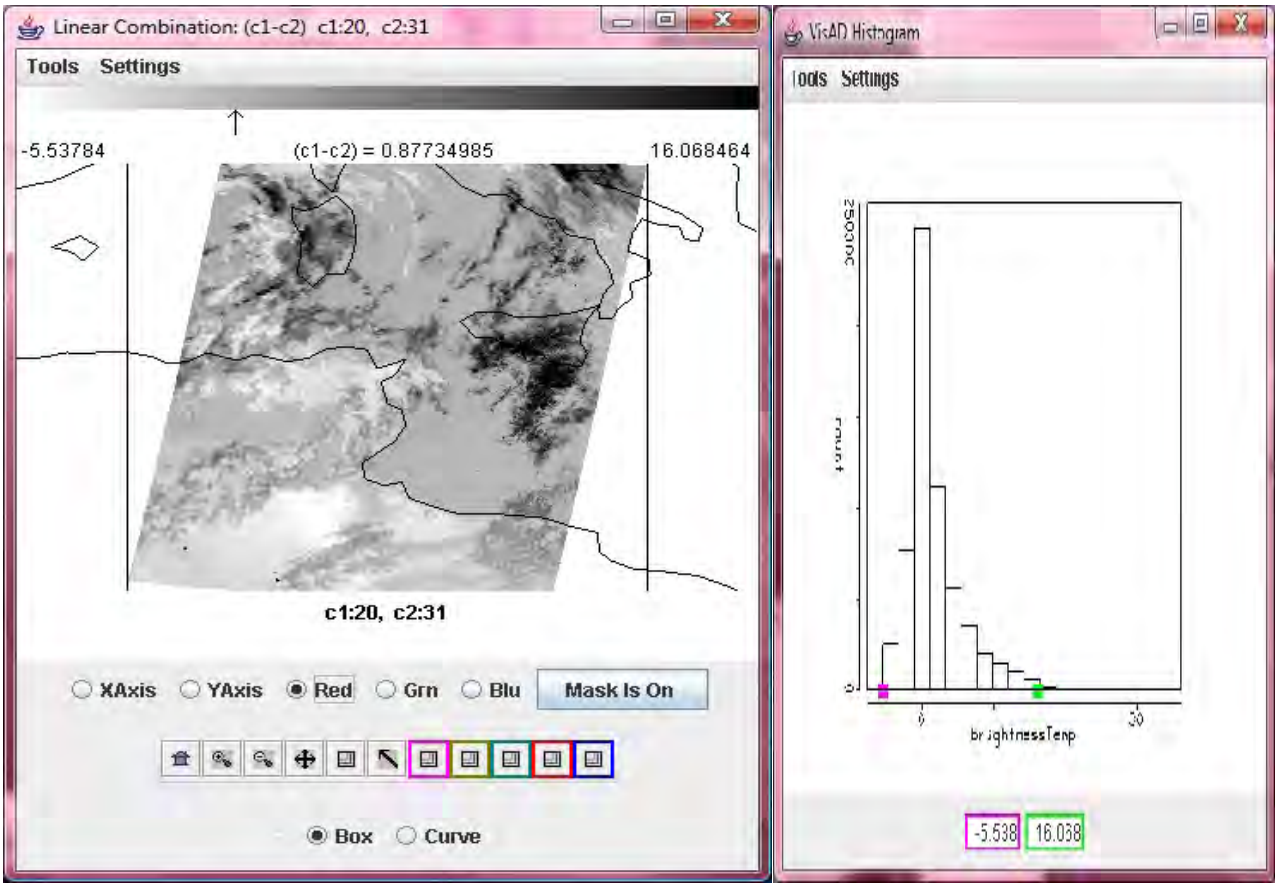

29-31

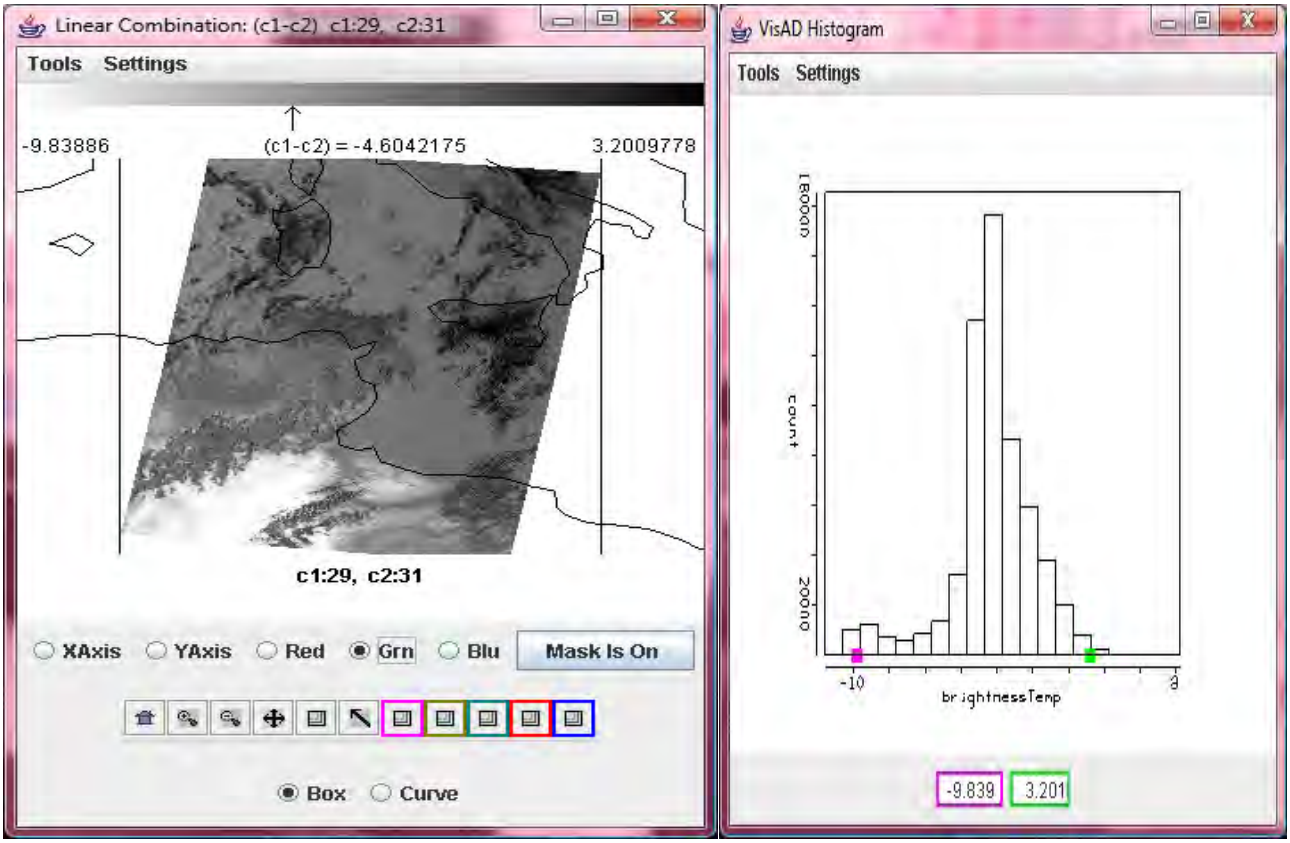
Linear Combination: (c1-c2) c1:29, c2:31
Tools Settings
-9.83886
(c1-c2) = -4.6042175
3.2009778
c1:29, c2:31
XAxis YAxis Red Grn Blu Mask Is On
Box Curve
VisAD Histogram
Tools Settings
count
brightnessTemp
-9.839
3.201

31-32

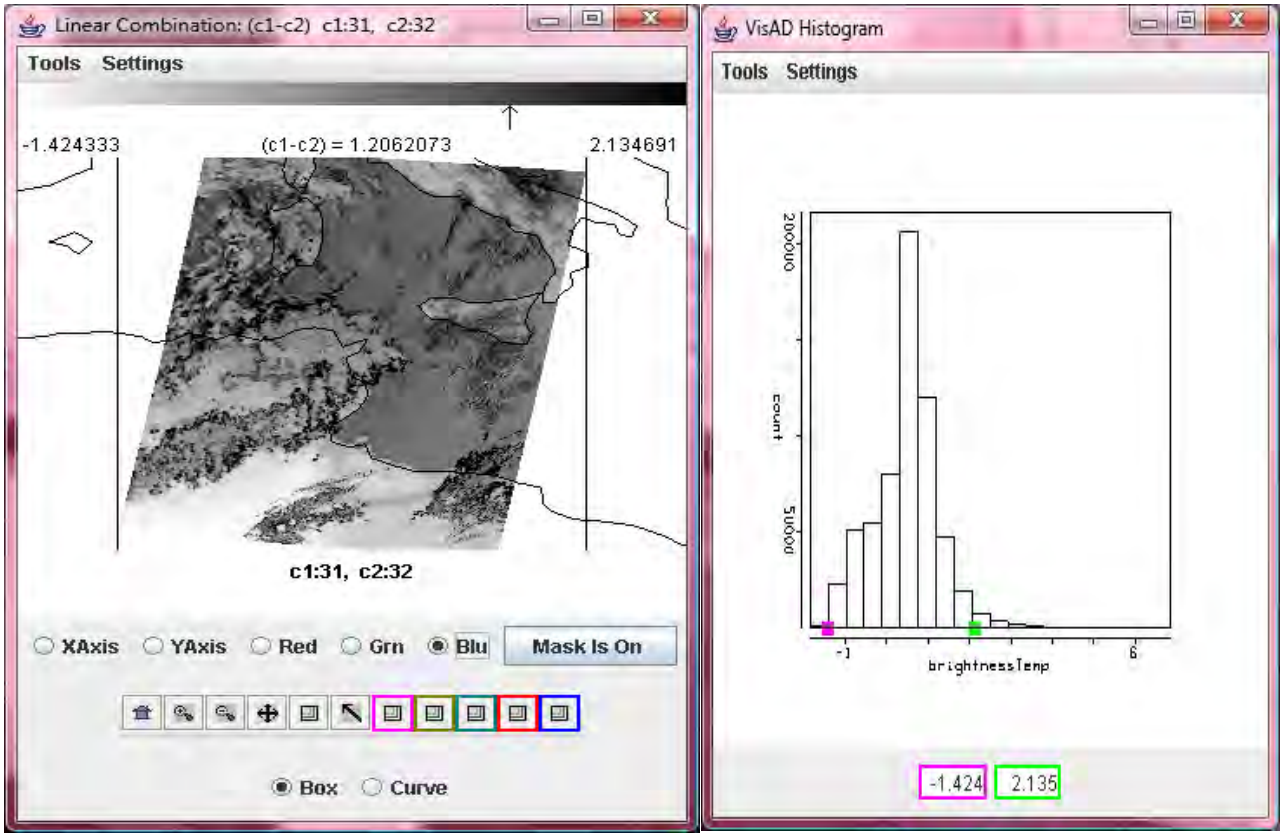
Linear Combination: (c1-c2) c1:31, c2:32
Tools Settings
-1.424333
(c1-c2) = 1.2062073
2.134691
c1:31, c2:32
XAxis YAxis Red Grn Blu Mask Is On
Box Curve
VisAD Histogram
Tools Settings
count
brightnessTemp
-1.424
2.135

Scatter

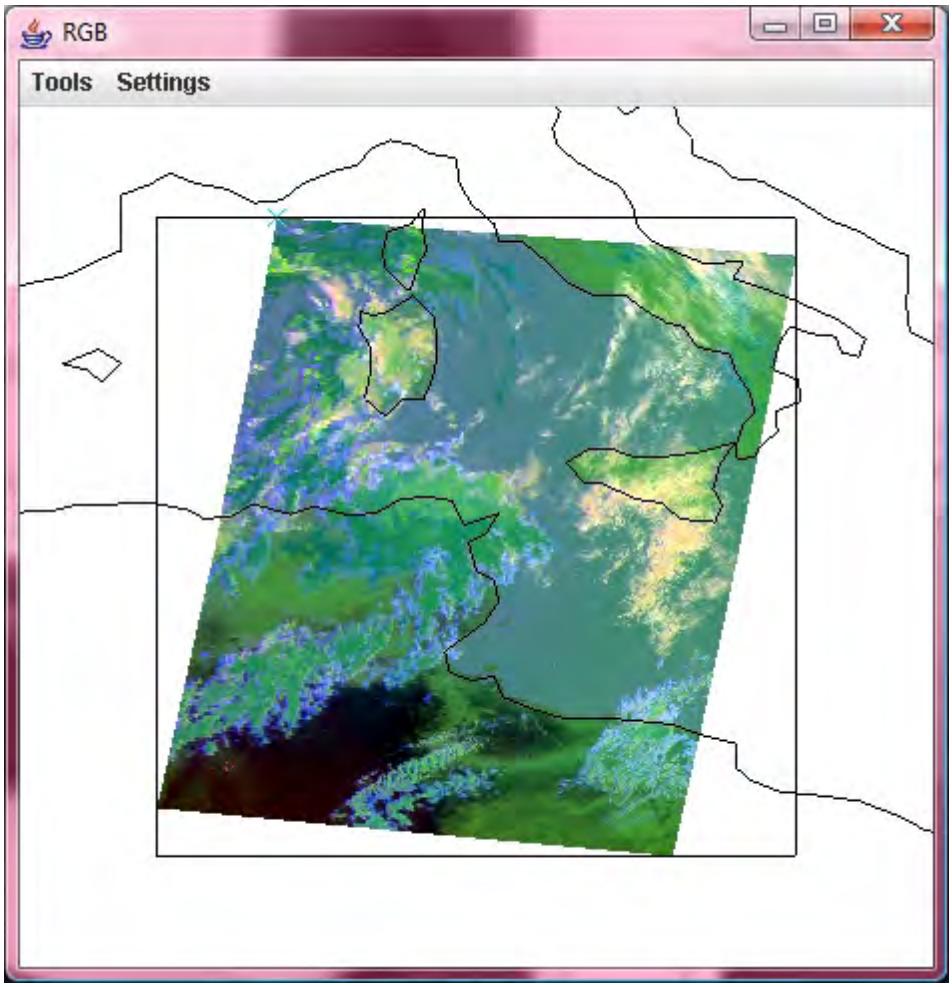

No dust presence.

MOD021KM.A2008215.1035.005.2008215194002.hdf

2008 luglio

RGB

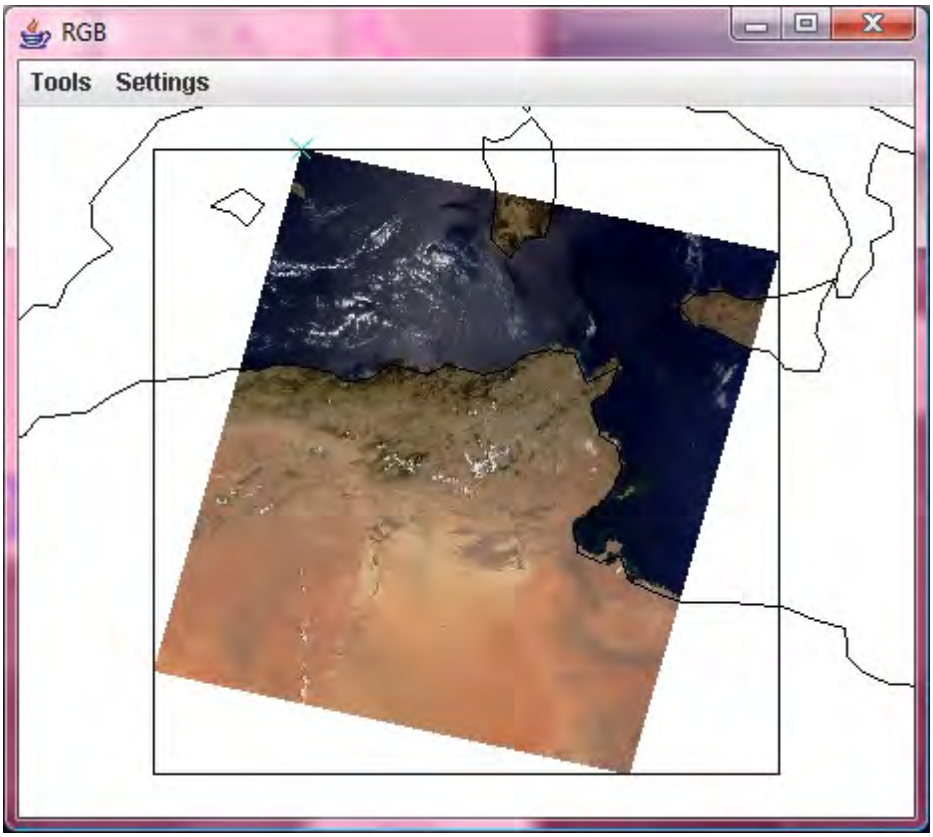

20-31

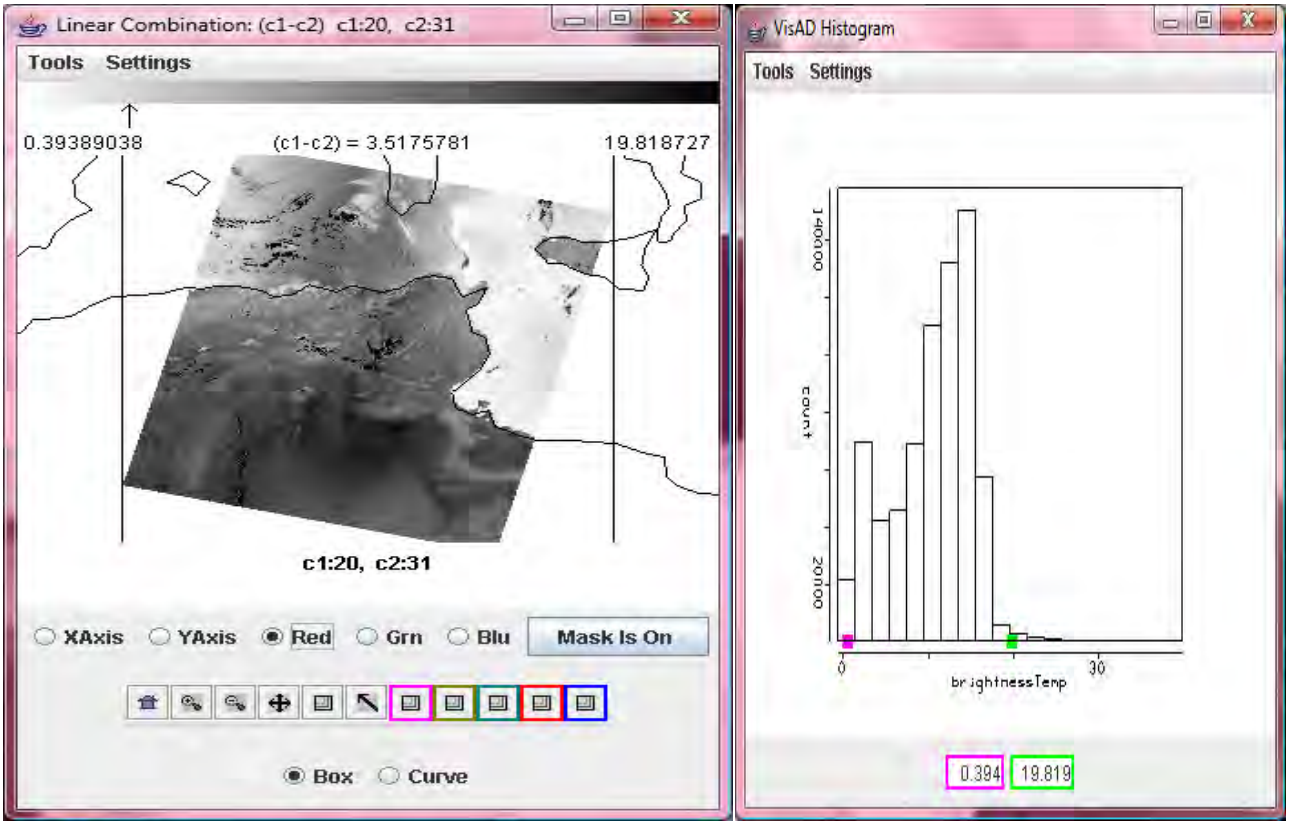
Linear Combination: (c1-c2) c1:20, c2:31
Tools Settings
0.39389038
(c1-c2) = 3.5175781
19.818727
c1:20, c2:31
XAxis YAxis Red Grn Blu Mask Is On
Box Curve
VisAD Histogram
Tools Settings
count
brightnessTemp
0.394
19.819

29-31

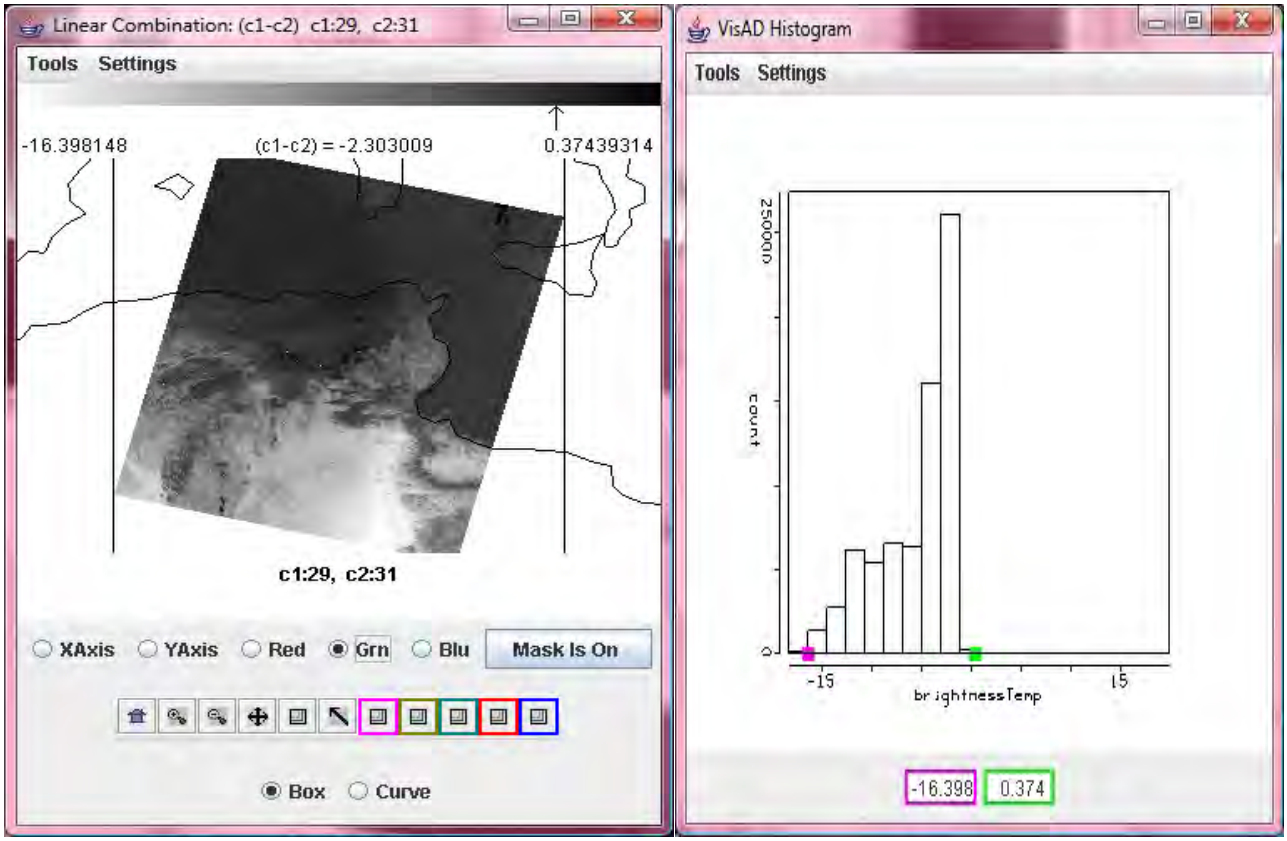
Linear Combination: (c1-c2) c1:29, c2:31
Tools Settings
-16.398148
(c1-c2) = -2.303009
0.37439314
c1:29, c2:31
XAxis YAxis Red Grn Blu Mask Is On
Box Curve
VisAD Histogram
Tools Settings
250000
count
0
-15
15
brightnessTemp
-16.398
0.374

31-32

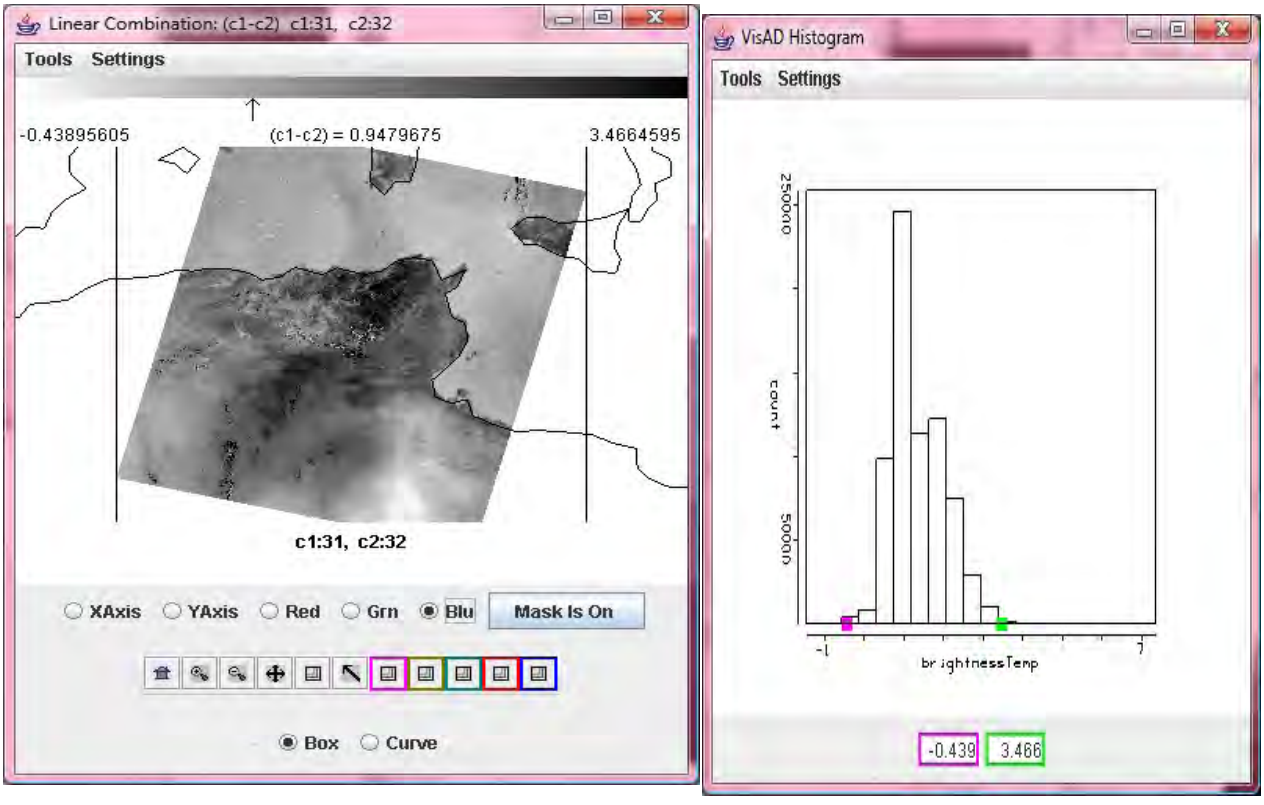
Linear Combination: (c1-c2) c1:31, c2:32
Tools Settings
-0.43895605
(c1-c2) = 0.9479675
3.4664595
c1:31, c2:32
XAxis YAxis Red Grn Blu Mask Is On
Box Curve
VisAD Histogram
Tools Settings
250000
50000
count
-1
1
brightnessTemp
-0.439
3.466

Scatter

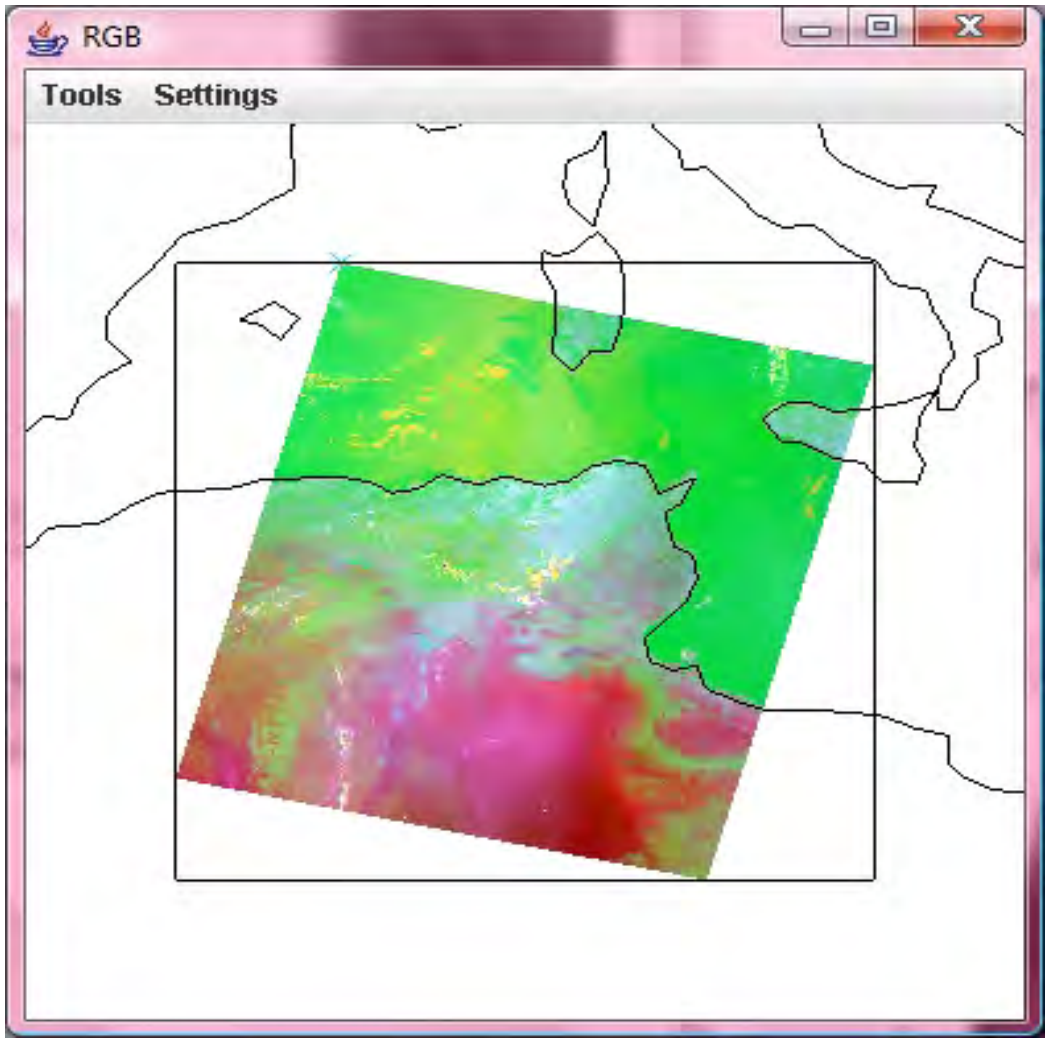

Very low presence of dust leaving Africa reaching Mediterranean Sea.

REFERENCES

Duda David P, Minnis P, Trepte Q, Sun-Mack S. *The continous monitoring of desert dust using an infrared based dust detection and retrieval method.* Abstract for the 12th AMS Conference on atmospheric radiation, Madison july 2006.

Sodemann H, Palmer AS, Schwierz C, Schwikowski M, Wernli H: *the transport history of two Saharan dust events achived in an Alpine ice core.* Atmos. Chem. Phys, 6, 667-688, 2006.

Balis D, Amiridis V, Kazadzis S, Papayannis A, Tsaknakis G, Tzortzakis S, Kalivitis N, Vrekoussis M, Kanakidou M, Mihalopoulos N, Chourdakis G, Nickovic S, Perez C, Baldasano J, Drakakis M: O*ptical characteristics of desert dust over the east Mediterranean during summer: a case study.* Ann. Geophys., 24, 807-821, 2006.

White Kevin. *Remote Sensing of Aeolian Dust Production and Distribution*. Desertification and Risk Analysis Using high and medium Resolution Satellite Data. NATO Science for Peace and Security series - C: Environmental Security, 59-67.

Goudie AS, Middleton NJ. *Saharan Dust storm: nature and consequences*. Earth Science Reviews 56, 179-204, 2001.

Menzel Paul. *Remote Sensing Applications with Meteorological Satellites.* NOAA Satellites and Information Services, University of Wisconsin, Madison WI, Feb 2006.

Kalashnikova O, Kahn R. *Mineral dust plume evolution over the Atlantic from MISR and MODIS aerosol retrievals*, Journal of Geophysical Research, 113, D24204. 2008.

King M. D., Si-CheeTsay, Platnik S. E., Wang Mencghua, Kuo-Nan Liou *Cloud Retrieval Algorithms for MODIS: Optical Thickness, Effective Particle Radius, and Thermodynamic Phase,* MODIS Algorithm Theoretical Basic Document No. ATBD-MOD-05 and MOD06-Cloud product, version 5, dec 1997.

Ilea C G, Kisinski P, Hoffman A C, *3-D Eulerian Lagrangian simulation of Dust lifting*, ICNAAM, 2006 extended abstract 1-4.

Nickovic S, Kallos G, Papadopoulos A, Kakaliagou O: *A model for prediction of desert dust cycle in the atmosphere*. J Geophys Res, 106, 18113-18130, 2001.

Koren I, Kaufman Y J: *Direct wind measurement of Saharan dust events from Terra and Aqua satellites*, Geophys. Res, Lett 31, L06122, doi 10.1029/2003GL019338, 2004.

J-P Béthoux, B Gentili, D Tailliez, *Warming and freshwater budget change in the Mediterranean since the 1940s, their possible relation to the greenhouse effect*, Geophysical Research Letters, 1998.

D A Metaxas, A Bartzokas, A Vitsas. *Temperature fluctuations in the Mediterranean area during the last 120 years*. Int. J. Climatology, 11:897-908, 1991.

J-P Béthoux, B Gentili, *The Mediterranean Sea, coastal and deep-sea signatures of climatic and environmental changes*. J. Mar. Systems, 7:383-394, 1996.

Gautam R., Hsu N.C., and Lau K.M.. *Premonsoon aerosol characterization and radiative effects over the Indo-Gangetic Plains: Implications for regional climate warming*. Journal of Geophysical Research, 115, D17208, sept 2010.

Gautam, R., Hsu, N.C., Lau, K.M., and Kafatos, M. *Aerosol and rainfall variability over the Indian monsoon region: distributions, trends, and coupling.* Annales Geophysicae, 27, 3691-3703, sept 2009.

Gautam, R., Hsu, N.C., Lau, K.M., Tsay, S.C., and Kafatos, M.. *Enhanced pre-monsoon warming over the Himalayan-Gangetic region from 1979 to 2007.* Geophysical Research Letters, 36, L07704, apr 2010.

Lau, K. M., M. K. Kim, and K. M. Kim. *Asian monsoon anomalies induced by aerosol direct forcing: The role of the Tibetan Plateau*. Climate Dynamics, 26, 855–864, feb 2006.

Lau, K. M., M. K. Kim, K. M. Kim, and W. S. Lee. *Enhanced surface warming and accelerated snow melt in the Himalayas and Tibetan Plateau induced by absorbing aerosols*. Environmental Research Letters, 5, 025204, apr 2010.

Yasunari, T. J., Bonasoni, P., Laj, P., Fujita, K., Vuillermoz, E., Marinoni, A., Cristofanelli, P., Duchi, R., Tartari, G., and Lau, K.-M.. *Preliminary estimation of black carbon deposition from Nepal Climate Observatory-Pyramid data and its possible impact on snow albedo changes over Himalayan glaciers during the pre-monsoon season*. Atmospheric Chemistry and Physics. 10, 9291-9328, 2010.

Luisa Marelli, *Contribution of natural sources to air pollution levels in the EU – a technical basis for the developement of guidance for the member States*. Institute for Environment and Sustainability, EUR 22779 EN, 2007.

HYDRA Project

http://www.nationsencyclopedia.com/Africa

National drought Mitigation Centre

http://www.ssec.wisc.edu/

http://cimss.ssec.wisc.edu

Council Directive 1999/30/EC

GEOS-Chem (global scale): http://www.as.harvard.edu:16080/ctm/geos/

Chimere (EU): http://www.lmd.polytechnique.fr/chimere/

CNR – Italy - INAA

TeleGIS Laboratory Unica

ATTACHEMENTS

PHD's OUTCOMES

During the PhD I realise two international publications, a Poster with a short presentation a 2 hours lecture on portable radiometer during an international course, and a speech during a workshop in Cagliari, Italy, Physics Dep.

Here below the publications and the poster.

Features on Present Environment and Suistainable Development n°4/2010

ISSN 1843-5971 (http://www.pesd.ro/Pesd%20vol%204%20-%202010.html **):**

7. MARZIA BOCCONE - Dust detection algorithm using MODIS data and HYDRA software

10. FRANCESCA GIORDANO, MARZIA BOCCONE - Forest fragmentation, urbanization and landscape structure analysis in an area prone to desertification in Sardinia (Italy)

Poster presented at the 4th International Symposium *Present Environment and Sustainable Developement.*

7.

Dust Detection Algorithm using MODIS data and HYDRA software

Marzia Boccone [1]
[1]Telegis Laboratory, Department of Earth Science and PhD in Environmental Science and Engineering at the University of Cagliari, 09100 Cagliari, Italy (boccone@unica.it)

Keywords: modis, remote sensing, dust, linear combination bands, hydra, algorithm

Abstract
It is globally achieved that dust is part of natural aerosols quantity in air, with dimension from 1 to 10 microns, and could affect both human health, for breath disease, and local climate system, or global as well. Dust could reach Mediterranean and South European countries because of the local meteorology, the source points are often in the Sahara desert. Using Satellites Spectroradiometry we could detect and visualise dust over land and oceans. We used three Modis combination bands into the multispectral data analysis toolkit HYDRA (HYperspectral data viewer for Development if Research Application): a simple algorithm is showed with the help of HYDRA software, that help scientists to see dust easly without any other processed data. A case study is showed over the South West Mediterranean Area, near Tunisia and Lybia, but could be used for any other case and area of the world.

1. INTRODUCTION

It is globally achieved that dust is part of natural aerosols quantity in air, with dimension from 1 to 10 microns, and could affect human health, for breath disease, and local climate system, or global as well. The erosion, transport and deposition of this kind of particle matter creates hazards when it affects human activities. Locally, dust stormes result in a low visibility, creating dangers for road and air transport. There is also an environmental concerne because of the severe dust erosion occurring trought those years, and also because has an impact on the nutrient budget of oceanic ecosystems by providing a source of Fe to fertilize ocean regions that would otherwise be nutrient-starved. It is well known that dust mineral particles influence the earth's radiation balance and the climatology mainly in two ways: the first one by reflecting and absorbing incoming and outgoing radiation and the second one by acting as cloud condensation nuclei, but the direction of that affected radiative forcing is unknown. It is important to remind that dust moves around in the atmosphere following meteorological conditions and patterns, infact Eulerian-Lagrangean back-scatter methods and Chemistry-Transport Parallel models use this informations to develop trajectories for dust and other Particle Matter. The first is used to find centre of dust origin or Spot, the second is useful for air quality forecast or simulation, especially used around the most populated area. The Saharan desert is the world's most important natural source of dust. In the Mediterranean sea we can detect between 10 to 20 dust cases per years. In the low Mediterranean region, nearby North African Dust Spots, cases are normally more frequent and more heavy than in the upper regions. Meteorological observations from space are made from the electromagnetic radiation leaving the atmosphere. Outgoing radiation from earth to space varies with wavelength for the Energy Planck function dependent on wavelength and for the absorption by atmospheric gases of differing molecular structures. Energy transfer from one place to another is accomplished by any of three processes. Conduction is the transfer of kinetic energy of atoms or molecules by contact among them travelling at varying speeds. Convection is the physical displacement of matter in gases or liquids. Radiation is the process whereby energy is transferred across space without the necessity of a medium. Remote sensing is the observation of a target by a device separated by some distance. With satellites for meteorological research has been largely confined to passive detection or radiation emanating from earth-atmosphere system. Satellite remote sensing can provide long time series of observations of atmospheric dust, which can help evaluating the importance of different sources. Using data from the Moderate Resolution Imaging Spectroradiometer (MODIS) could be useful to combine different radiation bands, not only to identified specific dust sources. The measurements of aerosols, suspended particles in the atmosphere, such as dust from the Sahara desert, are an important element in describing energy transmission trough the atmosphere. Aerosols are a significant source of uncertainty in climate modelling because they affect

cloud microphysics by acting as condensation nuclei, thereby affecting cloud radiative properties, the hydrological cycle and atmospheric dynamics. They also interact directly with solar radiation, thus affecting the radiative balance. Estimative emissivity of dust is 0.75 between 3.5-3.9 μm, 0.97 between 10.3-11.3 μm and 11.5-12.5μm, so the algorithm studied focuses on those bands. The purpose of this study is to use MODIS data and to develop an algorithm able to show dust by combining spectral bands into a scatter plot or RGB plot. The spectral bands were chosen between the emissivity bands of dust.

2. STUDY AREA

This kind of method could be applied over every part of the world, but to show the methodology we choose South West Mediterranean area because of the increase of mean seasonal temperature, desertification and frequent dust episods during rainfalls. Infact the presence of dust could increase mean seasonal temperature, but also sea surface temperature and general desertification. Tunisia and Libya and the nearby area consists of two climatic belts, with Mediterranean influences in the north and Saharan in the south. Temperatures are moderate along the coast, with an average annual reading of 18° C (64° F), and hot in the interior south. The summer season in the north, from May through September, is hot and dry; the winter, which extends from October to April, is mild and characterized by frequent rains. Temperatures at Tunis range from an average minimum of 6° C (43° F) and maximum of 14° C (57° F) in January, to an average minimum of 21° C (70° F) and maximum of 33° C (91° F) in August. Precipitation in the northern region reaches a high of 150 cm annually, while rainfall in the extreme south averages less than 20 cm a year. The Lybia climate has marked seasonal variations influenced by both the Mediterranean Sea and the desert. Along the Tripolitanian coast, summer temperatures reach between 40 and 46° C (104– 115° F); farther south, temperatures are even higher. Summers in the north of Cyrenaica range from 27 to 32° C (81–90° F). In Tobruk (Tubruq), the average January temperature is 13° C (55° F); July, 26° C (79° F). The ghibli, a hot, dry desert wind, can change temperatures by 17–22° C (30–40° F) in both summer and winter. Rainfall varies from region to region. Rain falls generally in a short winter period and frequently causes floods. Evaporation is high, and severe droughts are common. The Jabal Akhdar region of Cyrenaica receives a yearly average of 40 to 60 cm (16–24 in). Other regions have less than 20 cm (8 in), and the Sahara has less than 5 cm (2 in) a year.

2.1 CLIMATOLOGIC DATA

Here we present the general climatology of the Study Area, South West Mediterranean, choosing two local climatological data and nearby areas, Tripoli and Djerba (Libya and Tunisia). Tripoli lies at the western extremity of Libya close to the Tunisian border. the dominant climatic influences in Tripoli, a coastal lowland city, are Mediterranean. The city enjoys warm summers and mild winters with an average July temperature of between 22 °C (72 °F) and 29 °C (84 °F). In December temperatures have reached as low as 1 °C (34 °F), but the average remains at between 9 °C (48 °F) and 18 °C (64 °F). The average annual rainfall is less than 400 mm (15,7 inch). Here below in Table 1 you can see climatologic data for Tripoli.

Table 1: Weather data for Tripoli

month	jan	feb	mar	apr	may	jun	jul	aug	sep	oct	nov	dec	year
aver H °C (°F)	16 (61)	17 (63)	19 (66)	22 (72)	24 (75)	27 (81)	29 (84)	30 (86)	29 (84)	27 (81)	23 (73)	18 (64)	23 (73)
aver L °C (°F)	8 (46)	9 (48)	11 (52)	14 (57	16 (61)	19 (66)	22 (72)	22 (72)	22 (72)	18 (64)	14 (57)	9 (48)	15 (59)
precip mm (inch)	81 (3.2)	46 (1.8)	28 (1.1)	10 (0.4)	5 (0.2)	3 (0.1)	0 (0)	0 (0)	10 (0.4)	41 (1.6)	66 (2.6)	94 (3.7)	384 (15.1)

Djerba is a beautiful island of Tunisia and it is well known for its mild Mediterranean climate. Average temperature are nearly the same of that of Tripoli, but precipitation is lower. Here below in Table 2 you can see climatologic data for Djerba. And in Fig.1 the two precipitation related together.

Table 2: Weather data for Djerba													
month	jan	feb	mar	apr	may	jun	jul	aug	sep	oct	nov	dec	year
aver H °C (°F)	16 (61)	18 (64)	20 (67)	22 (72)	26 (78)	26 (83)	32 (89)	32 (90)	30 (86)	26 (79)	21 (70)	17 (63)	24 (75)
aver L °C (°F)	9 (48)	9 (49)	11 (52)	13 (56)	16 (62)	20 (67)	22 (71)	23 (73)	22 (71)	18 (65)	14 (57)	10 (50)	16 (60)
precip mm (inch)	28 (1.1)	20 (0.8)	19 (0.8)	13 (0.5)	5 (0.2)	1 (0)	0 (0)	3 (0.1)	19 (0.8)	53 (2.1)	34 (1.3)	36 (1.4)	231 (9.1)

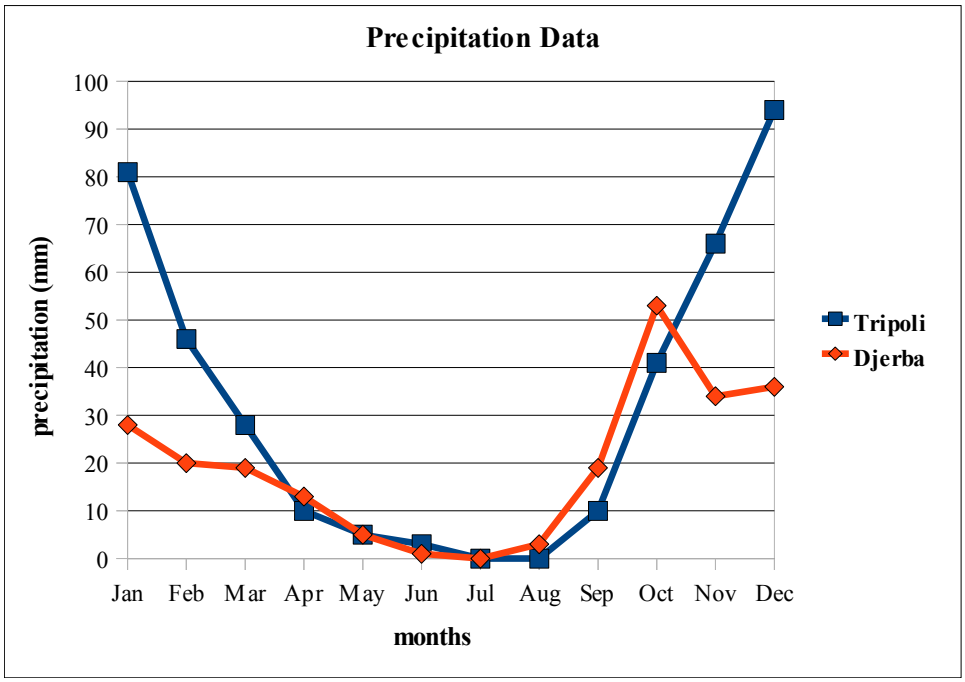

Fig.1 - Monthly precipitation charts of Tripoli and Djerba

Here below is showed the general study area about 41N, 7W, 17E, 35S. And the Reflectance/Brightness Temperature curve of the RGB combination bands versus wavelenght.

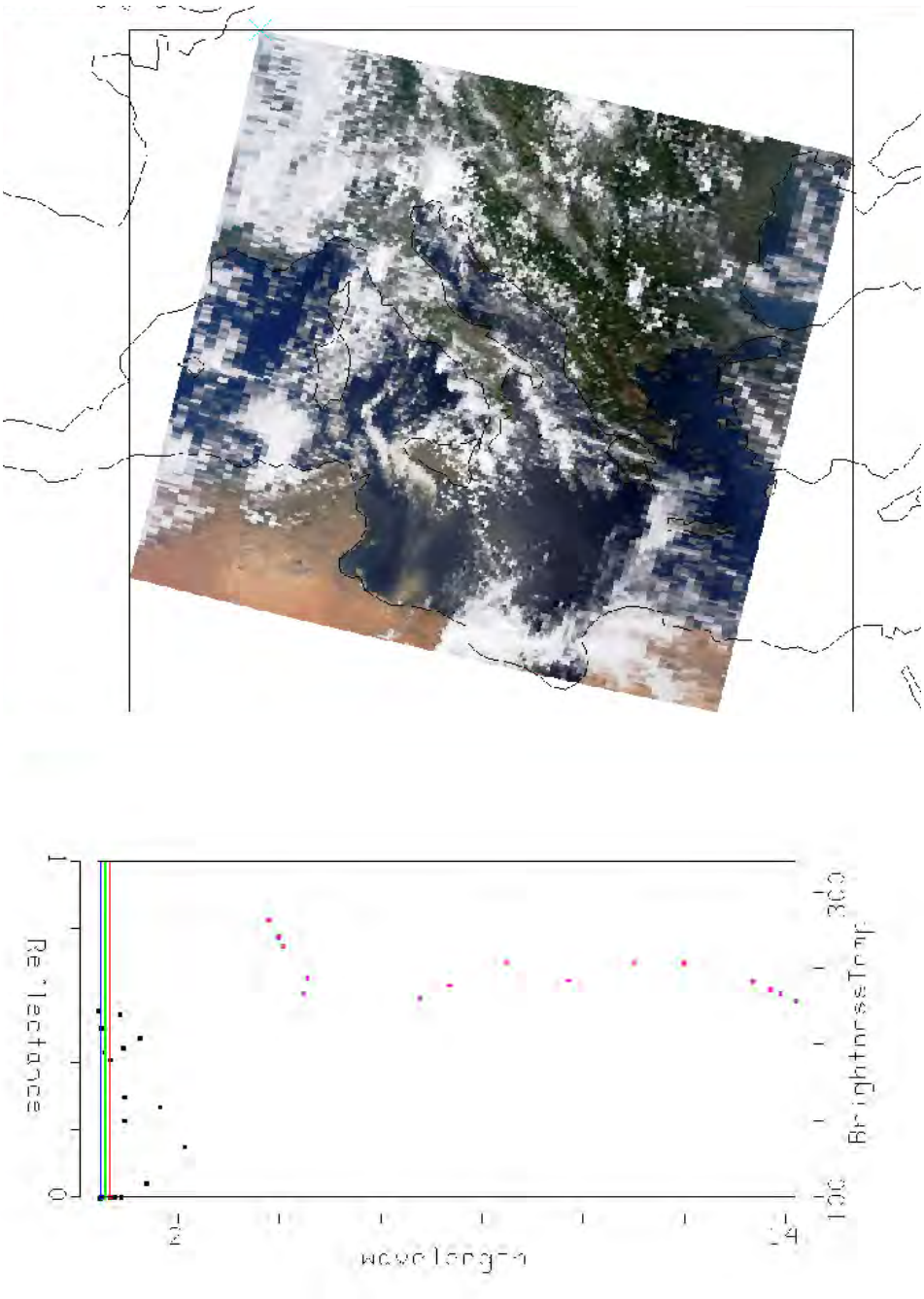

Fig. 2 - Up, RGB image of the Study Area, data: july 14, 2007, and down, the corresponding Reflectance/Brightness Temperature (BT) versus wavelenght: the RGB bands are respectively the first, the second and the third by the left of the diagram.

3 METHODS

3.1 MODIS

The Moderate Resolution Imaging Spectroradiometer (MODIS) is an Earth Observing System (EOS) facility instrument that is currently flying, but in retirement age, aboard the Terra and Aqua spacecraft. Terra began collecting data on February 24, 2000, Aqua, a counterpart of Terra, was launched on May 4, 2002 and began collecting data on June 22, 2002. MODIS is a scanning spectro-radiometer with 36 spectral bands between 0.645 and 14.235 μm. Bands 1 – 2 are sensed with a spatial resolution of 250 m, bands 3 –7 at 500 m, and the remaining bands 8- 36 at 1 km. You can download rough data or processed data from some link to NASA institute or, if you have an Antenna, you can directly broadcast by your own. For this case we use MOD021KM level 1b data at 1km of spatial resolution and with calibrated radiances, from MODIS sensor on Terra. Our general programme focus on Mediterranean Area, due to desertification and dust episodes. So the case study shows the image of Tunisia/Libya region on July 14, 2007.

3.2 HYDRA

We used the freeware multispectral data analysis toolkit, HYDRA (HYperspectral data viewer for Development of Research Application). Infact various spectral channels combination were visualised to detect an algorithm for dust over Mediterranean region, and also multiple channel combinations and scatter plots that help to detect Particle Matter (PM). The software HYDRA can be used for such environmental studies but also for others, especially used to process and manage Meteorological Satellite Data. Such as MODIS, SEVIRI and AIRS data.

3.3 BUILDING THE ALGORITHM

Estimative emissivity of dust is 0.75 between 3.5-3.9 μm, 0.97 between 10.3-11.3 μm and 11.5-12.5μm, so the algorithm studied focuses on those bands combinations, that are 20 (3.7 μm) , 29 (8.5 μm), 31 (11 μm) and 32 (12 μm) MODIS Channels.

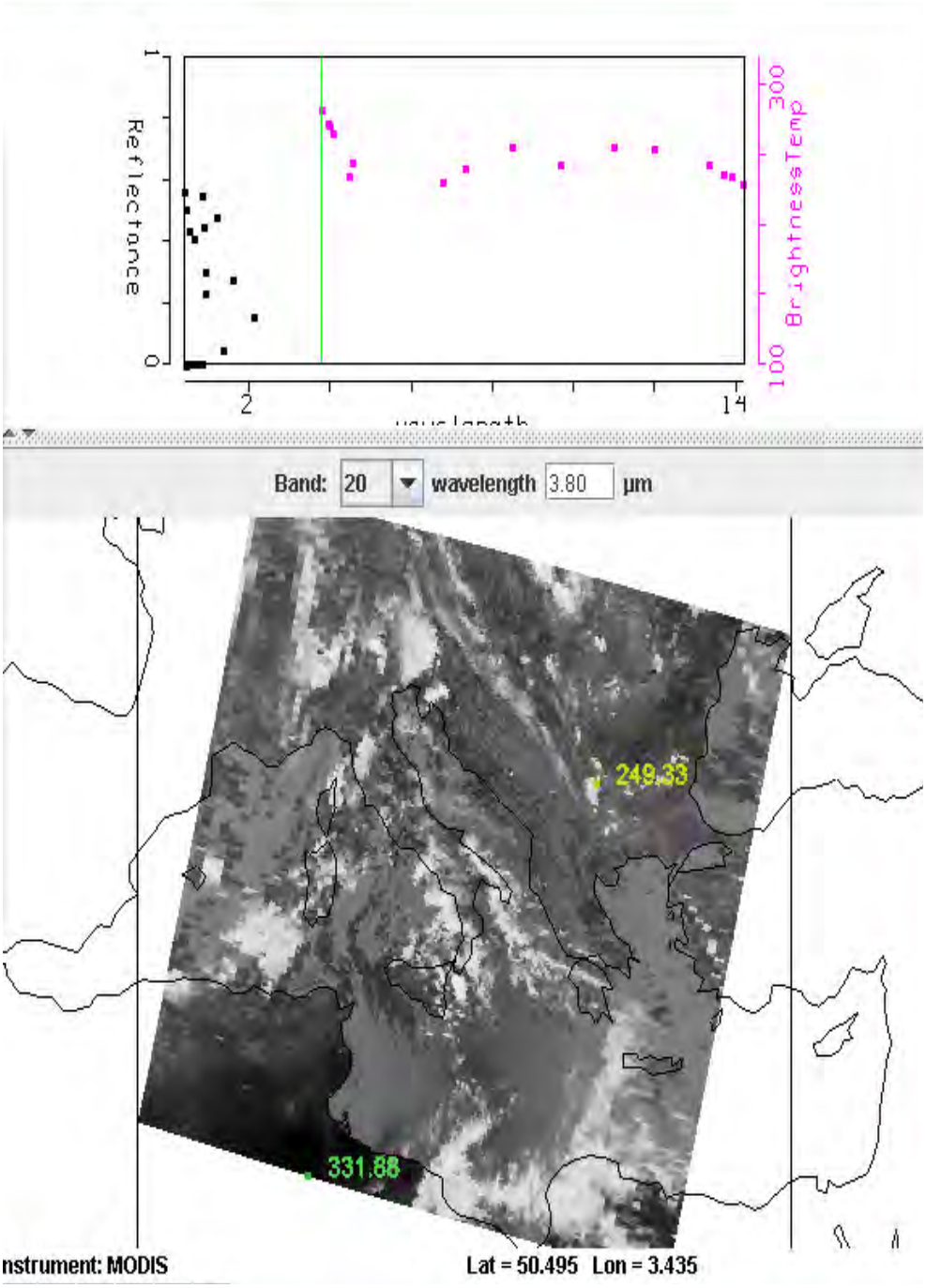

Fig 3.a MODIS image of band: 3.a. 20 (3.7 µm), Visualised using HYDRA-Multichannel-Viewer.

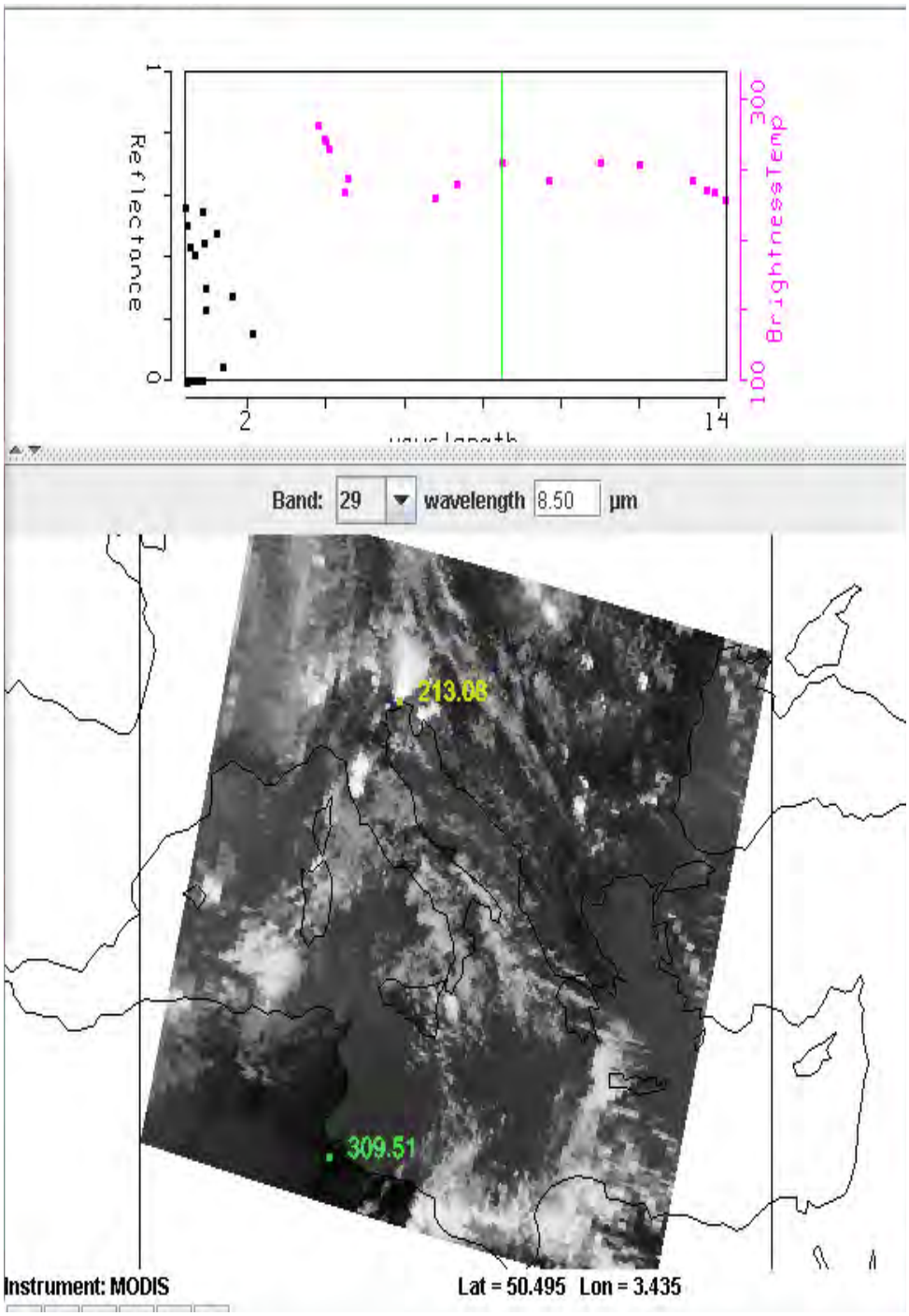

Fig 3.b MODIS image of band: 3.b. 29 (8.5 µm). Visualised using HYDRA-Multichannel-Viewer.

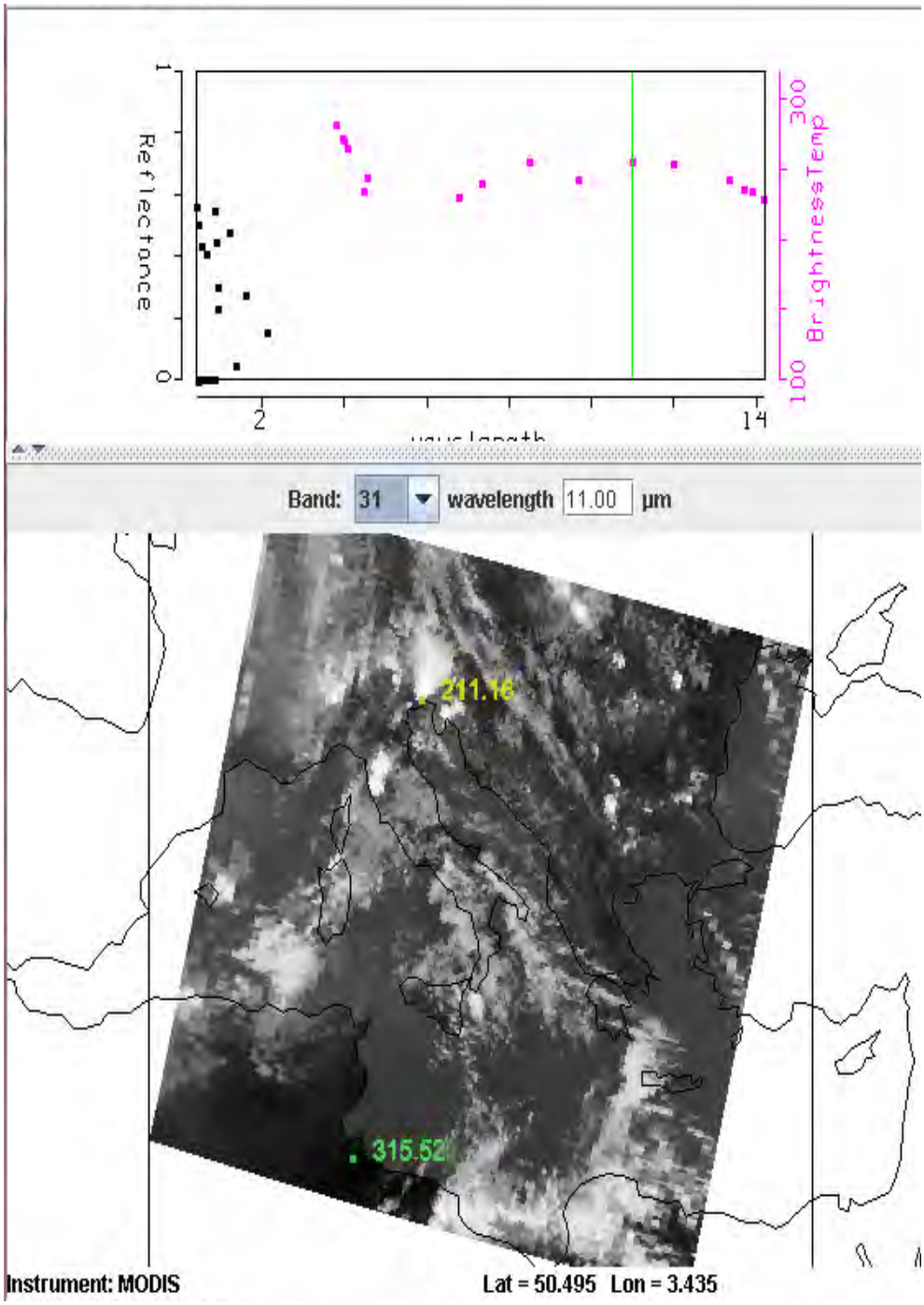

Fig. 3.c - MODIS image of band: 3.c. 31 (11 µm). Visualised using HYDRA-Multichannel-Viewer.

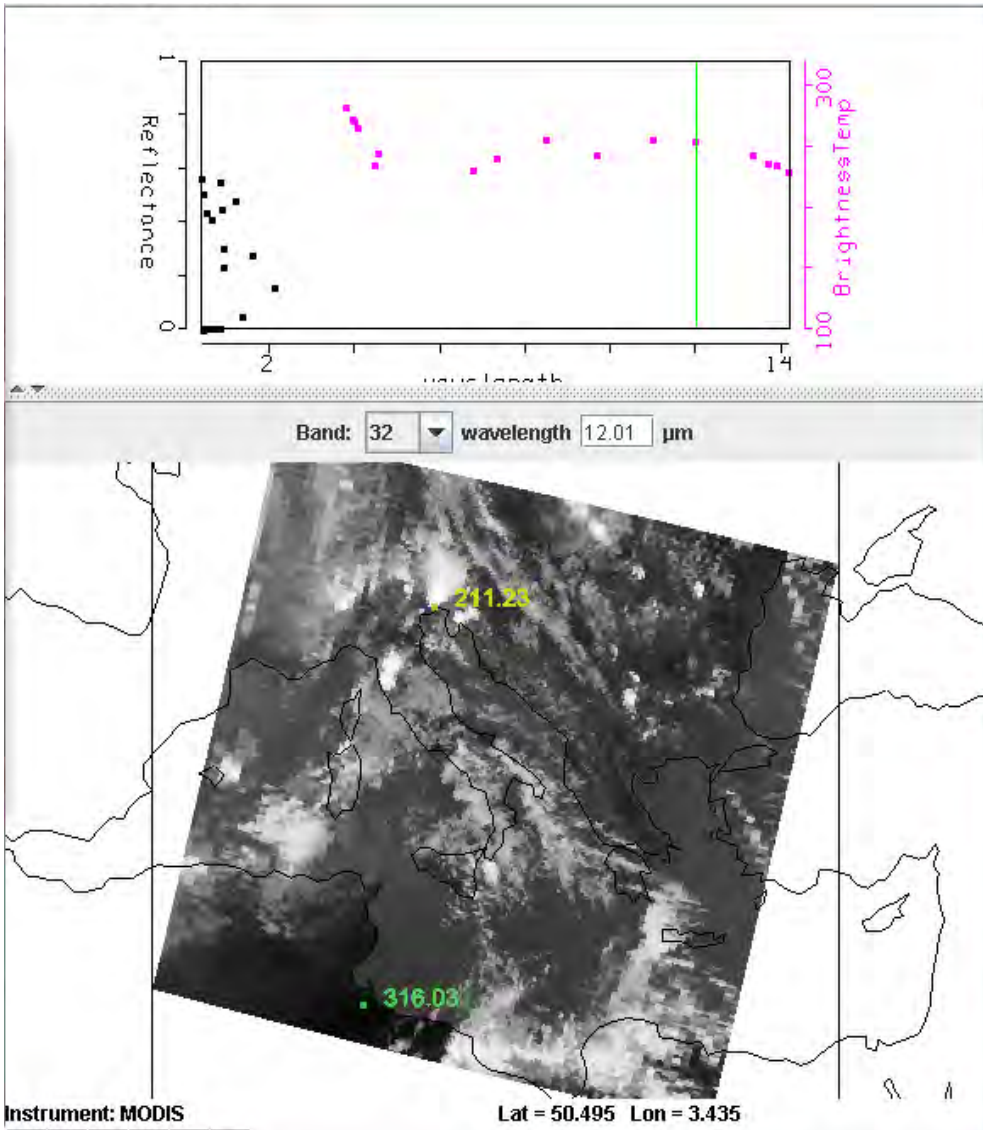

Fig. 3.d - MODIS image of band: 3.d. 32 (12 µm). Visualised using HYDRA-Multichannel-Viewer.

We performed first three linear combination with the help of HYDRA, those linear combinations are X= 20 – 31 (3.7-11µm), Y= 29 – 31 (8.5-11 µm) and Z= 31 – 32 (11 - 12µm). In the next chapter is showed the methodology applied over the case study area and the entire algorithm based on the above mentioned linear combinations bands.

3.4 METODOLOGY TO THE CASE STUDY

The first linear combination bands performed using HYDRA is X= 20 - 31 (3.7-11µm):

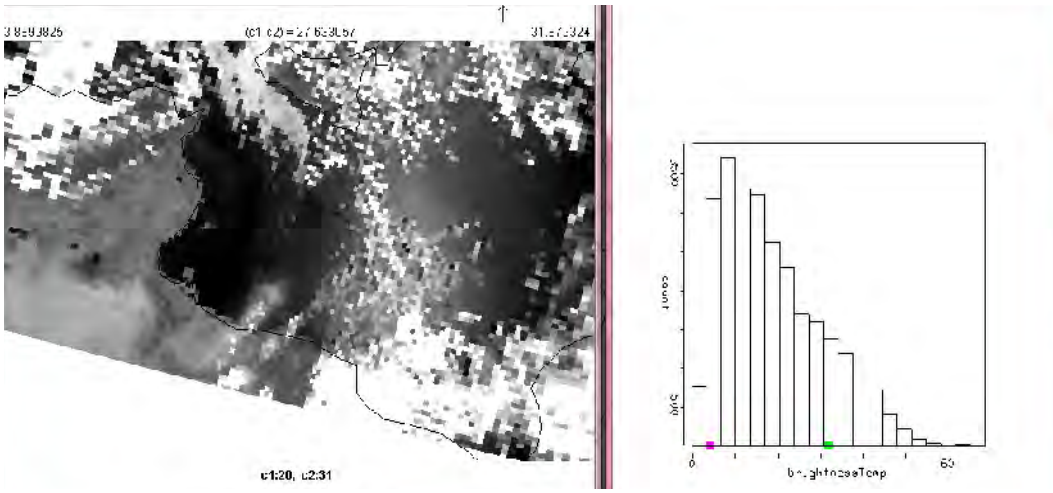

Fig. 4 – Image of the linear combination bands X=20-31 (3.7-11μm). Here the zone selected have the Brightness Temperature (BT) between 3.89 and 31.88. Dust, in the picture, have BT between 10-30, that correspond to 3000-3500 counts on the diagram (right), and very bright and white in the picture (left).

The second linear combination bands performed is Y= 29 - 31 (8.5-11 μm) in the same area:

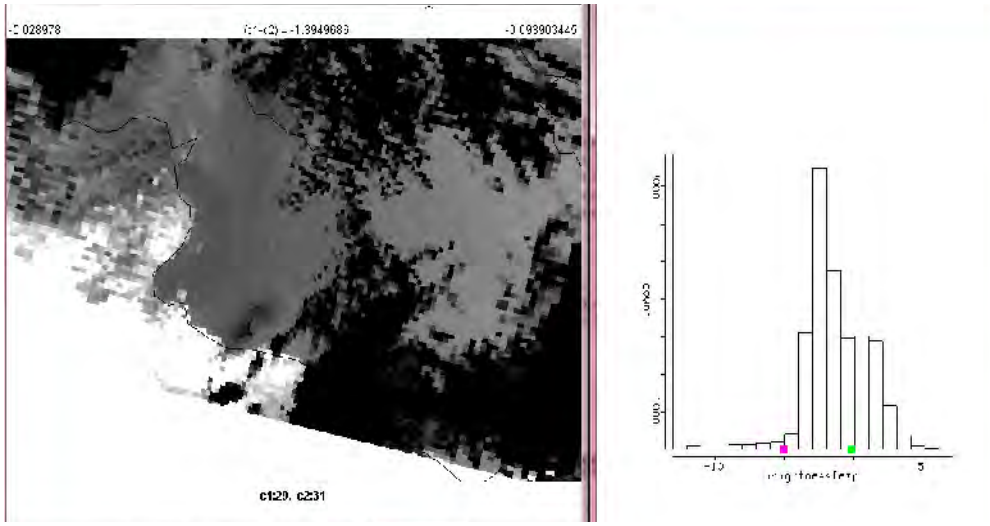

Fig. 5 – Image of the linear combination bands Y=29-31 (8.5-11 μm). Here the zone selected have Bright Temperature between - 5.03 and - 0.10. The picture shows the same dust area of the X combination in Fig. 4, here BT is between -5 and -1.

The third linear combination bands performed is Z= 31 – 32 (11 - 12μm):

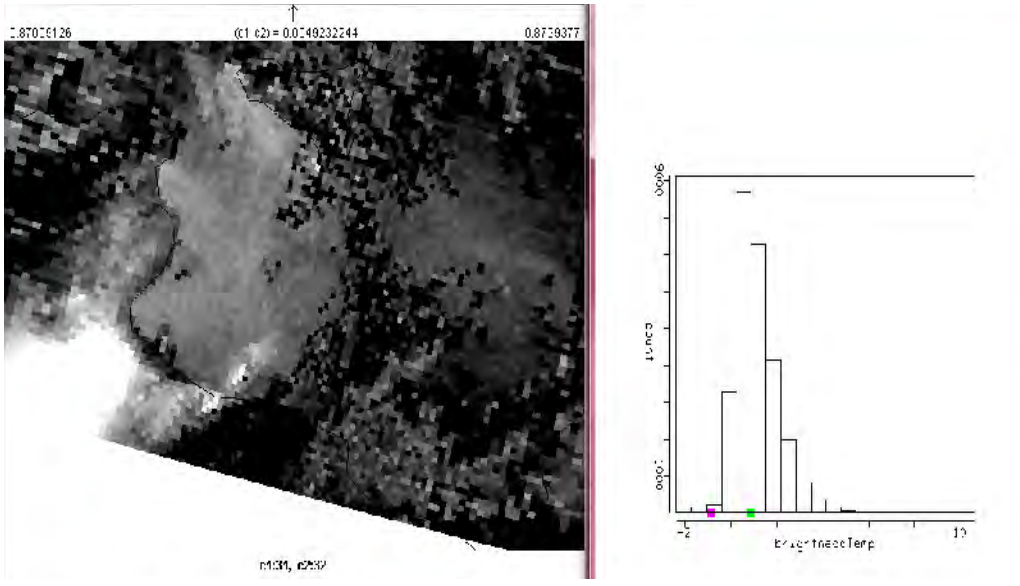

Fig. 6 – Image of the linear combination bands Z=31-32 (11 - 12μm). Here the zone selected have Bright Temperature between - 0.87 and 0.88. The picture shows the same dust area of the combination X and Y (Fig. 4 and 5), here there is the point with highest BT, about -0.91.

Using HYDRA we also compare the first two linear combination bands, X= 20 - 31 (3.7-11μm) and Y= 29 - 31 (8.5-11 μm) in a Scatter Plot in order to see what happens in the dust area zone marked with the elliptic line:

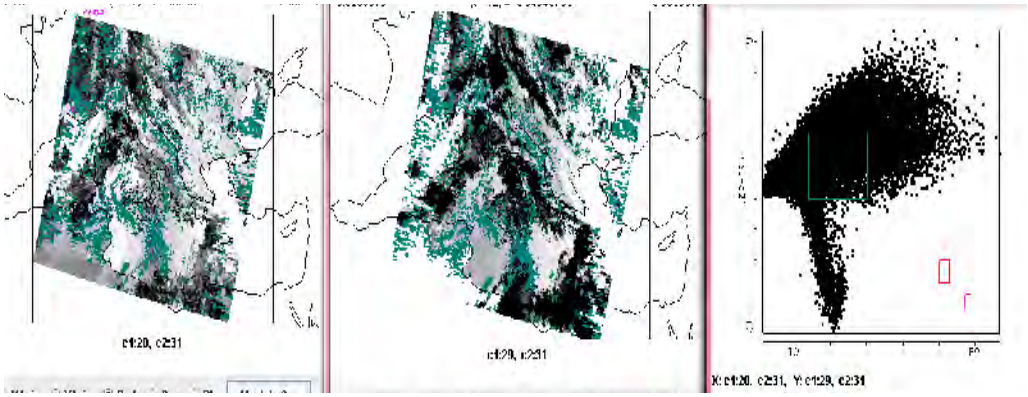

Fig. 7 - Image of the Scatter Plot of the two linear combination bands, X= 20 - 31 (3.7-11μm) and Y= 29 - 31 (8.5-11 μm). Here you see the dust area zone related to bands 20, 29 and 31. In the Scatter Plot on the left there are the corresponding values which contain also the dust area zone (see the square just about in the centre of the Plot).

Using HYDRA we also compare all those combination bands X, Y and Z in a RGB plot, were the three combination above are X, Y, Z like R, G, B:

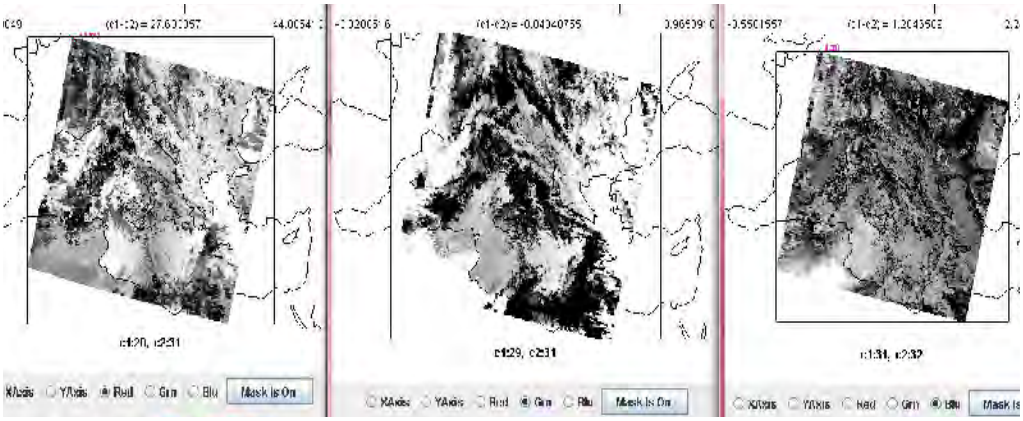

Fig. 8 - Image of the Three linear combinations selected as X, R and Y, G and Z, B using HYDRA multichannel viewer.

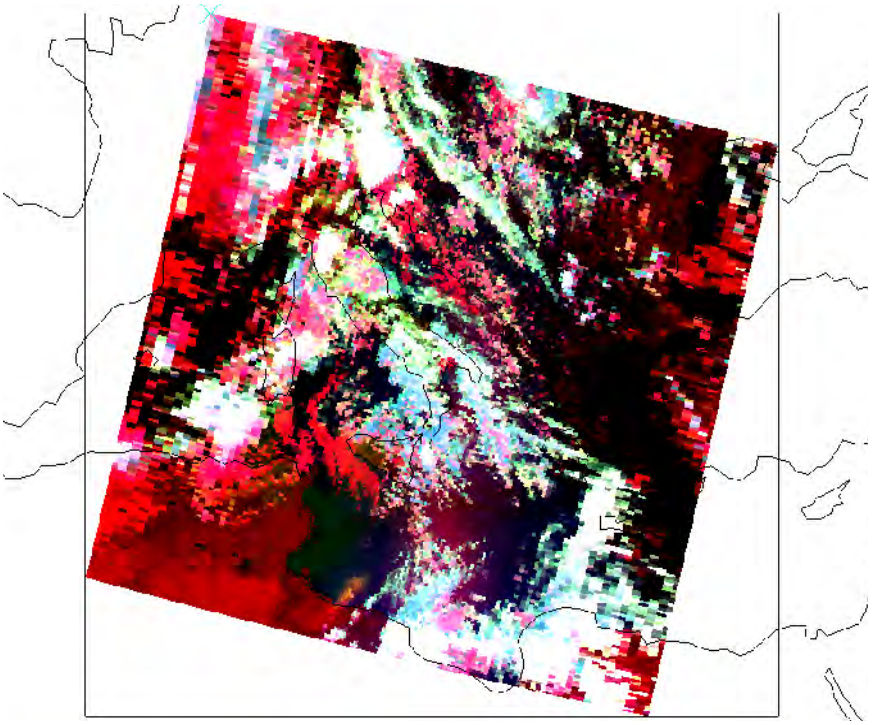

Fig. 9 – RGB Plot of the three combinations X, Y, Z. The picture shows the dust area.
Here the lower and upper values of the colour scale were choosen as: 6.68 - 27.194 for Red [X= 20 – 31 (3.7-11μm)]; -2.10 - 1.26 for Green [Y= 29 – 31 (8.5-11 μm)]; -26.45 - 5.48 for Blue [Z= 31 – 32 (11 - 12μm)].
The great concentration of dust leaving the land is following the weather conditions, the data image choose is well clear by high clouds, even thought there are some ice clouds on the right.

4. CONCLUSIONS

Now that we presented the algorithm performed, focused on the detection of dust of the Saharan desert, as already shown, estimative emissivity of dust is 0.75 between 3.5-3.9 μm, 0.97 between 10.3-11.3 μm and 11.5-12.5μm, so the algorithm presented focuses on combination of those bands. The location of anthropogenic aerosols is an important consideration in their impact on local climate, so the algorithm studied focuses on those MODIS bands 20 (3.7 μm), 29 (8.5 μm), 31 (11 μm) and 32 (12 μm), corresponding to the above mentioned emissivity bands of dust. Here there is the algorithm's summary:

- First of all the collection of data, images over the Mediterranean sea, from night and day from: http://ladsweb.nascom.nasa.gov/data/search.html OR from direct broadcast from the Antenna (as we have at the University of Cagliari)
- Here is showed a part of the Mediterranean Sea, nearby Tunisia and Lybia area july 14, 2007
- Then we combined the MODIS bands 3.7-11, 8.5-11, 11-12, μm (Fig. 4, 5, 6)
- Then we Scatter those combination bands in a X,Y plot (Fig. 7)
- Then we performed an RGB/XYZ Plot (Fig. 8, 9)

It is a simple algorithm that help scientists to detect dust easily without any other processed data only making some consideration about BT values and using HYDRA multichannel viewer toolkit. The same algorithm could be used to detect dust over other regions and study areas. With the final comparison between Scatter plot, XYZ and the original RGB (Fig. 2) you can easily know where there is the largest amount of dust while the RGB give you an idea of the scatter of dust near and far the largest part of it. The next step of the Telegis laboratory research team is to compute the amount of dust detected, in order to compare of dust transported from desert/land to ocean/other land.

5. ACKNOWLEDGEMENTS

This work is part of an international PhD in Environmental Science and Engineering, without financial support. The authors would like to thank Paolo Antonelli of the Space Science and Engineering Center, University of Wisconsin-Madison.

References

Balis D, Amiridis V, Kazadzis S, Papayannis A, Tsaknakis G, Tzortzakis S, Kalivitis N, Vrekoussis M, Kanakidou M, Mihalopoulos N, Chourdakis G, Nickovic S, Perez C, Baldasano J, Drakakis M (2006): O*ptical characteristics of desert dust over the east Mediterranean during summer: a case study.* Ann. Geophys., 24, 807-821

Duda David P, Minnis P, Trepte Q, Sun-Mack S (2006): *The continuos monitoring of desert dust using an infrared based dust detection and retrieval method.* Abstract for the 12th AMS Conference on atmospheric radiation, Madison

Goudie AS, Middleton NJ (2001): *Saharan Dust storm: nature and consequences*. Earth Science Reviews 56, 179-204

HYDRA Project

Menzel P (2006): *Remote Sensing Applications with Meteorological Satellites.* NOAA Satellites and Information Services, University of Wisconsin, Madison WI

National drought Mitigation Centre

http://www.nationsencyclopedia.com/Africa

Sodemann H, Palmer AS, Schwierz C, Schwikowski M, Wernli H (2006): *the transport history of two Saharan dust events achived in an Alpine ice core.* Atmos. Chem. Phys, 6, 667-688

http://www.ssec.wisc.edu/

White Kevin (2007). *Remote Sensing of Aeolian Dust Production and Distribution*. Desertification and Risk Analysis Using high and medium Resolution Satellite Data. NATO Science for Peace and Security series - C: Environmental Security, 59-67.

10.

Forest fragmentation, urbanization and landscape structure analysis in an area prone to desertification in Sardinia (Italy)

Francesca Giordano* and Marzia Boccone
University of Cagliari, Earth Sciences Department, TeleGis Laboratory
Via Trentino, 51 09127 Cagliari (Italy)
*Authors for correspondence (e-mail: fragisi@tin.it, marzia@boccone.it)

Key words: desertification, land cover, landscape ecology, remote sensing, FRAGSTATS.

Abstract
Land degradation and desertification processes represent a serious problem in many Italian regions, as in Sardinia (Italy), and in particular in the north-western part of the island (Nurra region) where urbanization, overgrazing and fires have induced environmental degradation and rapid land-use change.
Purpose of the study was to analyse in depth the forest fragmentation process and the landscape dynamics occurring over the 28-years period between 1972 and 2000 in an area prone to desertification in Sardinia. In this study, using satellite remote sensing, Geographical Information System and the software FRAGSTATS three Landsat satellite images were classified into seven land cover types and a stepwise indicator approach was adopted.
The results have enabled the identification of areas in which specific spatial patterns occurred at some degree of intensity as degradation factors thus explaining, at least in part, the sensitivity to desertification of specific areas.

Introduction

In the last two centuries the impact of human agricultural, industrial and extractive activities on the land has grown enormously, altering entire landscapes with important ecological consequences such as loss of biodiversity, deforestation, soil erosion and desertification.

In Italy about 21,3% of the land is at risk of desertification, as a consequence of both natural and anthropic occurrences (Costantini et al., 2007). Due to its particular geographical position and its extreme climatic events, such as droughts and floods, Sardinia can be considered a representative area of the typical environmental problems of the Mediterranean Basin. In fact, the landscape morphology and the climate make the soil very fragile and sensitive to activities which do not consider soil suitability and its limitations. In the last decades, urban sprawl[1] along the coastal areas has strongly increased due to new tourist settlements and urban infrastructures. Not only urban sprawl, but also loss of fertile soil, massive water exploitation, overgrazing and fires represent other important causes of the environmental problems on the island (Giordano and Marini, 2008).

Research studies are ongoing in order to further investigate where desertification represents a problem, to assess how critical the problem is and finally to better understand the processes of desertification. Desertification indicators[2] have been identified as potentially useful

1 Urban sprawl is commonly used to describe physically expanding urban areas. The European Environment Agency (EEA) has described sprawl as the physical patterns of low-density expansion of large urban areas, under market conditions, mainly into the surrounding agricultural areas.

2 The European Environment Agency (EEA) defines an indicator as a parameter or value derived from parameters, which provides information about a phenomenon. Indicators are quantified information that helps to

tools for both management and monitoring, and the Mediterranean countries are searching for a common methodology for identifying and using such indicators (Desertlinks, 2005).

From this perspective, a change in land cover and landscape represents an important and sensitive indicator that echoes the interactions between human activity and the natural environment (Zhou et al., 2008a). In semi-arid and arid environments, in particular, where fragile ecosystems are dominant, land cover and landscape change often reflects the most significant impact on the environment due to excessive human activity (Zhou et al., 2008b).

Most landscapes of the Mediterranean Basin have been shaped by human-nature interactions over large periods of time. In such cultural landscapes the main driving factor of changes is human impact, especially in terms of land-use and demography. Land-use and population change usually leads to landscape changes with consequences in terms of habitat fragmentation and alteration. As a consequence, a comprehensive assessment of the causes and the extent of landscape change is needed in order to gain a better understanding of the possible ecological consequences such as biodiversity loss, soil erosion and reduced productivity, and as a baseline for setting appropriate management and restoration strategies (Plieninger, 2006).

The role spatial pattern plays in ecological processes has made the development of landscape assessment approaches possible for regional environmental quality assessment and for monitoring land use and land cover types.

Studying the landscape, its current state (structure) and its future changes (dynamics) enables understanding of the ecological mechanisms and processes that drive changes in the landscapes.

Desertification assessment, in particular, has made increasing use of landscape ecology principles but still few examples of landscape metrics, derived from land use and land cover maps and used to quantify environmental change in arid and semi-arid regions, are found in literature (Sun et al., 2007; Sun et al., 2008).

Since information on land cover and landscape is critical to understanding environmental issues and changes in arid and semi-arid regions, the integration of remote sensing with Geographic Information System (GIS) techniques is increasingly important for the assessment of environmental problems such as land desertification (Zhang et al., 2008).

In this scientific context, and based on the assumption that many processes of desertification are typically related to the spatial structure of the landscape and its temporal variation, we drawn up the following general objective of the present research: to explicitly explore the concepts and methodology of a landscape approach for the monitoring of desertification.

Up to now, the key research topics in landscape ecology have focused on ecological flows and processes in landscape mosaics, but landscape ecology has been rarely combined with the issue of desertification, in particular in the Mediterranean region.

The objective of the following research was therefore to set up both a conceptual framework and a methodological implementation for land cover and landscape spatio-temporal detection, characterization and assessment based on remote sensing, GIS and landscape analysis. The integration of such instruments was drawn up in order to enhance the understanding of patterns of desertification processes by setting up appropriate synthetic landscape indexes related to specific spatial patterns which have not been deeply investigated up to now within the

explain how things are changing over time and how they vary spatially. Indicators generally simplify the reality in order to make complex phenomena quantifiable, so that information can be communicated.
Desertification indicators should help to identify where desertification is a current or potential problem and to monitor changes over time.

framework of the most common methodologies for the monitoring of desertification.

Study area

Sardinia, due to its particular geographical position and extreme climatic events such as droughts and floods, is characterized by having a lack of water and can be considered as a representative area of the typical environmental problems of the whole Mediterranean Basin.
The study area (ca 40° 43' N, 8° 34' E) is located in the north-western part of Sardinia (Italy) and includes the municipalities of Sassari, Alghero, Stintino and Porto Torres, comprising approximately 88400 ha (Figure 1).

Figure 1. Study area in the north-western part of Sardinia (Italy).

The area is representative of various land degradation and desertification processes such as urban sprawl, massive water exploitation, overgrazing and fire. Furthermore, it offers a wide availability of data, information and studies derived from many national and international projects (Motta et al., 1999; Kosmas et al., 1999; Bandinelli et al., 2000; Zucca et al., 2003; Pittalis, 2003; Motroni et al., 2004; RIADE, 2002-2005; DesertNet, 2002-2004; DesertNet II, 2005 – 2008, Desertwatch, 2004-2006; Ceccarelli et al., 2006).

The study area is characterized by a high geological and morphological complexity and is mostly in metamorphic rocks partially covered by Tertiary and Neogene sedimentary strata. Human activity has increased the variability of the landscape, by modifying in particular the original structure of vegetation.

The climate is typically Mediterranean dry-subhumid with an abundant amount of rainfall during the autumn-winter period and a small amount of rainfall with very high temperatures during the summer period. Mean annual precipitation values vary between 490 mm and 870 mm. During the period 1961-1990 a mean annual temperature of 16°C was registered. The mean hottest temperature was registered during august with a value equal to 29,7 °C. Due to these climatic characteristics the soil suffers from low water quantities and, as a consequence, in this area sclerophyllous vegetation, surviving in water scarce conditions, is widespread.

The area belongs to the phytoclimatic area of *Lauretum*. Vegetation is characterized by mediterranean scrub such as sclerophyllous evergreen forests (*Cistus, Oleaster, Pistacia Lentiscus, Quercus suber, Quercus ilex*) and other typical mediterranean species (*Calycotome*).
As demonstrated in recent studies (Motroni et al, 2004), the area is strongly sensitive to land degradation and desertification with more than half of the territory belonging to critical Environmentally Sensitive Areas (ESAs) or "*areas already highly degraded through past*

misuse, presenting a threat to the environment of the surrounding areas".

Methods

For the purposes described above, we drawn up a methodology able to provide quantitative data of interest for the monitoring of desertification and related to forest fragmentation, urbanization and landscape structure dynamics.

Hence, we tested the approach in order to assess and to characterise the changes occurred over a period of twenty-eight years in an area prone to desertification, where this kind of investigation has not been experimented on up until now.

The methodology was structured into a multi-step systematic procedure including nine different phases, to be performed one next to another (Figure 2).

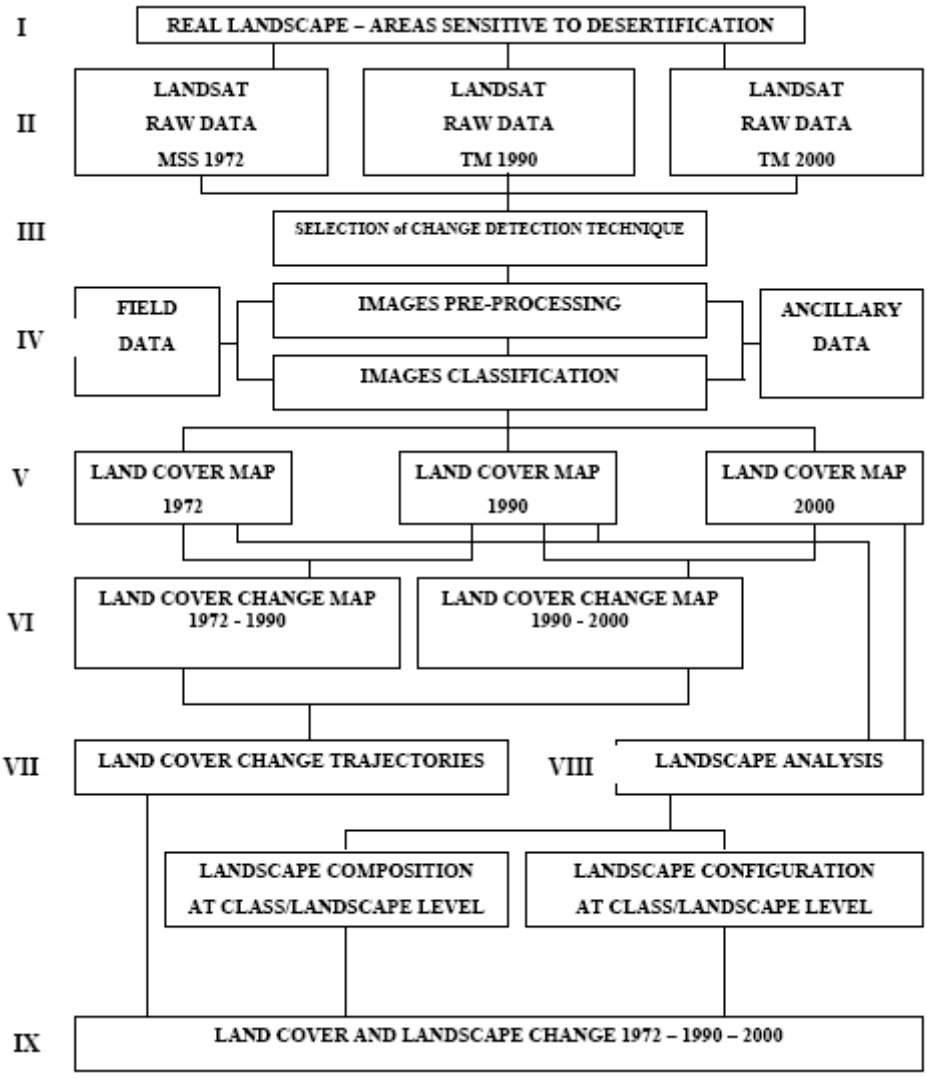

Figure 2. Flow chart of the multi-step systematic procedure set up.

Three Landsat images were selected over the study area: Landsat Multispectral Scanner (MSS) of August 13, 1972; Landsat Thematic Mapper (TM) of May 12, 1990 and Landsat

Thematic Mapper (TM) of June 27, 2000. Furthermore, twelve orthophotos Italia 2000[1]9 at the scale 1:10.000, dating back to 2000 and covering the overall study area, were used as reference source of information required for the classification procedure of the Landsat images. Field data were acquired among the data provided in the framework of the DESERTWATCH Project. In particular, we acquired ground truth points covering the study area and we used them as control points for the assessment of the classification accuracies for the three land cover maps. The ESAs (Environmentally Sensitive Areas) map represented the areas sensitive to desertification in Sardinia at a scale of 1:100.000 (Motroni et al., 2004).

Before performing any procedure, Landsat MSS was resampled to 30m × 30m by means of the nearest neighbour technique in order to make the pixel size comparable with that of the two higher spatial resolution images. In the present study georeferentiation was performed by means of the image-to-image method as the Landsat TM 2000, which was selected as the reference image, was already georeferenced. A set of 30 GCPs was selected throughout the scenes for the georeferentiation of the images, in a dispersed way including the intersection of roads, the airport runway of Alghero, buildings and avoiding landmarks that can vary during time. In the present study a 1st-order transformation was used to perform georeferentiation for both the images. Root Mean Square error was 0,83 pixels for Landsat MSS 1972 and 0,71 pixels for Landsat TM 1990, that means that the reference pixel is 0,83 (24,9 m) and 0,71 pixel (21,3 m) away from retransformed pixel. After georeferentiation the data file values of rectified pixels were resampled to fit into a new grid of pixel rows and columns. Among the resampling methods available in ERDAS Imagine, nearest neighbor was selected.

For the present research we chose the post-classification comparison method among the techniques available in scientific literature. Supervised classification was employed in order to classify individual images independently, using a unified land cover classification scheme to ensure that the classifications of the multi-temporal images well-matched each other. To perform this process the computer system was trained to recognize patterns in the data. Training is the process of defining the criteria by which these patterns are recognized. In the present study a supervised training was performed, in which pixels representing specific land cover features were recognized with the help of ortophotos and available maps. On the basis of the spatial patterns of interest for our research, we defined our land cover classification scheme as it follows: croplands, urban areas, forestlands, barren areas, wetlands and water bodies. By identifying specific patterns, the computer system was then instructed in order to identify pixels with similar characteristics. The result of training was a set of signatures defining training samples representative of the class to be identified. For each class a set of about 50 training sample was identified. The maximum likelihood algorithm was here applied to parametric signatures, which are based on statistical parameters of the pixels that are in the training sample. After the classification was performed the accuracy of the classification was evaluated by comparing it to geographical data that were assumed to be true (ground truth). The classification accuracy obtained for each image, was respectively: 83% for Landsat 1972, 88% for Landsat 1990 and 92% for Landsat 2000.

Following the post-classification procedure, the identification of land cover changes was performed by comparing two-by-two the land cover maps obtained.

The operational phase took the land cover maps resulting from the previous classification as the

1 9 An ortophoto is an aerial photograph that has been geometrically corrected or orthorectified such that the scale of the photograph is uniform and the photo can be considered equivalent to a map. Unlike an uncorrected aerial photograph, an orthophoto can be used to measure true distances, because it is an accurate representation of the earth's surface, having been adjusted for topographic relief, lens distorsion and camera tilt. Terraitaly – IT2000 was carried out by Compagnia Generale Ripreseaeree SpA of Parma (Italy).

sources of further procedures. The three land cover maps of 1972, 1990 and 2000 were converted into GRID format and used as the input image into the FRAGSTATS software.

Once the landscape metrics have been performed we composed specific sets of metrics at class and landscape level based on scientific research literature, in order to improve the understanding of spatial pattern change of interest for the monitoring of desertification and related to forest fragmentation (Geneletti, 2004; Yu and Ng, 2007; Baskent and Kadiogullari, 2007; Gonzalez et al., 2007; Cakir et al., 2008; Kadiogullari and Baskent, 2008), urbanization level (Weng, 2007; Gonzalez et al., 2007; Keles et al., 2008) and landscape structure (Li et al. 2004).
If we consider forest patches as resistant component to desertification, then forest fragmentation weakens this resistance, thus favouring the sensitivity level of the area. Hence, to reinforce the interpretation of forest fragmentation, we consider landscape metrics able to capture the increase in the number of forest patches, the reduction in their mean area and the decrease in the largest forest area. In addition, we required metrics able to assess the isolation of patches and the variation of the physical connectivity of forest ecosystems.
Therefore we selected the following set of metrics:

Forest fragmentation = *NP* + *AREA_MN* + *LPI* + *ENN_MN* + *COHESION* (1)

where:
NP = Number of Patches;
AREA_MN = Mean Patch Area;
LPI = Largest Patch Index;
ENN_MN = Mean Euclidean Nearest Neighbor Distance;
COHESION = Patch Cohesion Index.

Landscape metrics for capturing the spatial pattern of the urbanization degree in areas prone to desertification, were chosen taking into account that the dispersion of buildings leads to a high level of habitat fragmentation. In general, impacts of new buildings may be minor if they are located in close vicinity to existing ones (Gonzalez et al., 2007).
In this sense, urbanization level was analysed by means of the following set of metrics:

Urbanization level = *PD* + *AREA_MN* + *ENN_MN* + *LPI* (2)
where:
PD = Patch Density;
AREA_MN = Mean Patch Area;
ENN_MN = Mean Euclidean Nearest Neighbor Distance
LPI = Largest Patch Index.

Finally, the set of metrics for the analysis of landscape structure was composed on the basis of the main findings of Li (2004). In particular, we combined together landscape metrics able to capture the various aspects of landscape linked to land degradation and desertification, such as landscape fragmentation, land cover diversity and irregularity of patches. Land cover diversity, in particular, is relevant to desertification if we assume that a greater land use diversity, in terms of small and contiguous plots of different land uses, generally implies a smaller risk of land degradation and higher biodiversity (Desertlinks, 2005). The following landscape metrics were therefore used for this purpose:

Landscape structure = *NP* + *AREA_MN* + *SHDI* + *LSI* + *ENN_MN* (3)
where:

NP = Number of Patches;
AREA_MN = Mean Patch Area;
SHDI = SHannon's Diversity Index;
LSI = Landscape Shape Index;
ENN_MN = Mean Euclidean Nearest Neighbor Distance.

In order to obtain final synthetic indexes for each spatial pattern, for each landscape metric we calculated the variation, percentage-wise, occurred between the two study periods investigated. Then we classified them into six classes and we assigned a score on the basis of the positive or negative trend (table 1).

%	**0 – 20 %**	**20 – 40%**	**40 – 60%**	**60 – 80%**	**80 – 100%**	**> 100%**
Positive	0	+ 1	+ 2	+ 3	+ 4	+ 5
Negative	0	- 1	- 2	- 3	- 4	- 5

Table 1 – Classes and scores for the variation of the landscape metrics.

The final indexes were then calculated by means of the algebric sum of the scores and then classified into the following five classes: low (- 25 ÷ –15), medium – low (- 15 ÷ - 5), medium (- 5 ÷ + 5), medium – high (+ 5 ÷ + 15), high (+ 15 ÷ + 25).

The indexes thus obtained have the potential to reflect in a synthetic value various aspects of the spatial pattern investigated and their variation over time.

Results

We analysed the change of the urbanization and forest fragmentation spatial patterns occurred at class level and the change of the landscape structure at landscape level, by means of specific sets of metrics selected in order to reinforce our interpretation.
Furthermore, we set up a classification system for each landscape metrics in order to combine them and to obtain synthetic indexes.
In the following figures the maps of the synthetic indexes are illustrated.

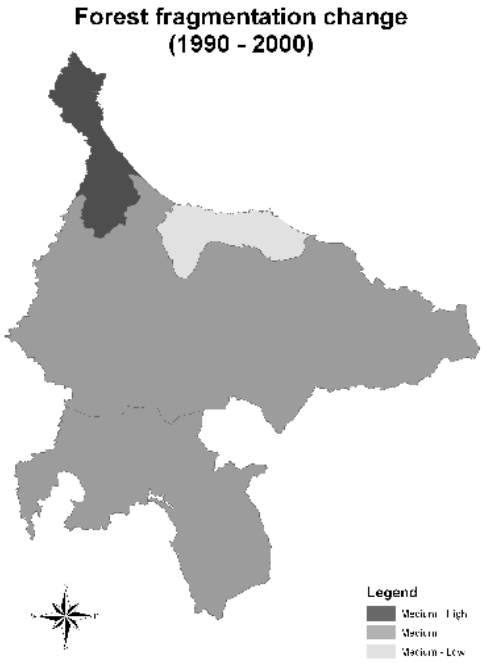

Figure 3 - Synthetic index of forest fragmentation change (1972 – 1990; 1990 – 2000).

Figure 3 illustrates the synthetic index of forest fragmentation for the two periods investigated. As seen in the figures, both the maps indicate the municipality of Stintino as the area in which the process of forest fragmentation was found to be the highest. Here, in fact, a very clear trend toward forest fragmentation was observed with a continuous trend over time toward an increase in the number of forest patches, a decreasing mean patch area and a reduction in the largest forest patch, connected to an increase in the isolation of forest patch and a decline in the forest connectivity.
The high values of the index found in the municipality of Stintino clearly reflect a persistent process over time, in which all the landscape metrics experimented negative trends.

In figure 4 the change of the urbanization level that occurred in the area over time is illustrated.

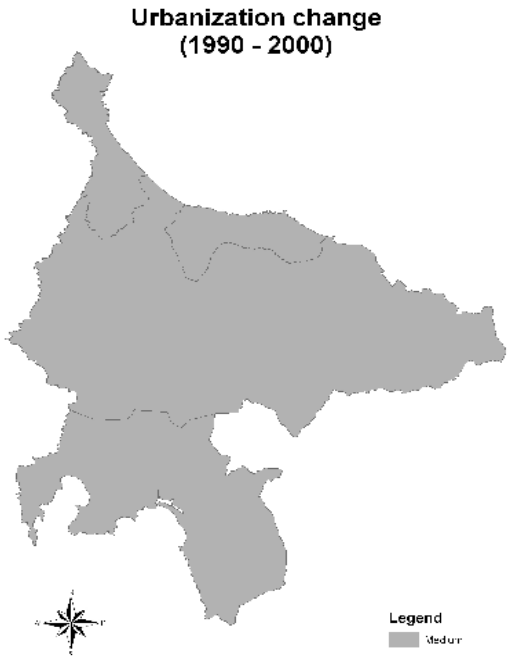

Figure 4 - Synthetic index of urbanization change (1972 – 1990; 1990 – 2000).

The synthetic index of urbanization change does not reflect only the enlargement of urban areas, but the way how it took place over time. As illustrated in the figure the municipalities of Porto Torres and Sassari showed a medium – high level of urbanization between 1972 and 1990. As enlightened in Weng (2007), the degree of fragmentation of urban areas is positively related to the degree of urbanization.
In these areas, the fragmentation of urban landscape is clearly linked to the strong increase in the urban density of the area and the strong reduction in the mean urban areas. New small urban areas are in some way dispersed in the landscape and not adjacent to each other, thus leading to an increase in the habitat fragmentation and to more severe impacts (Gonzalez-Abraham et al., 2007).

In figure 5 the synthetic index of landscape structure change is represented.

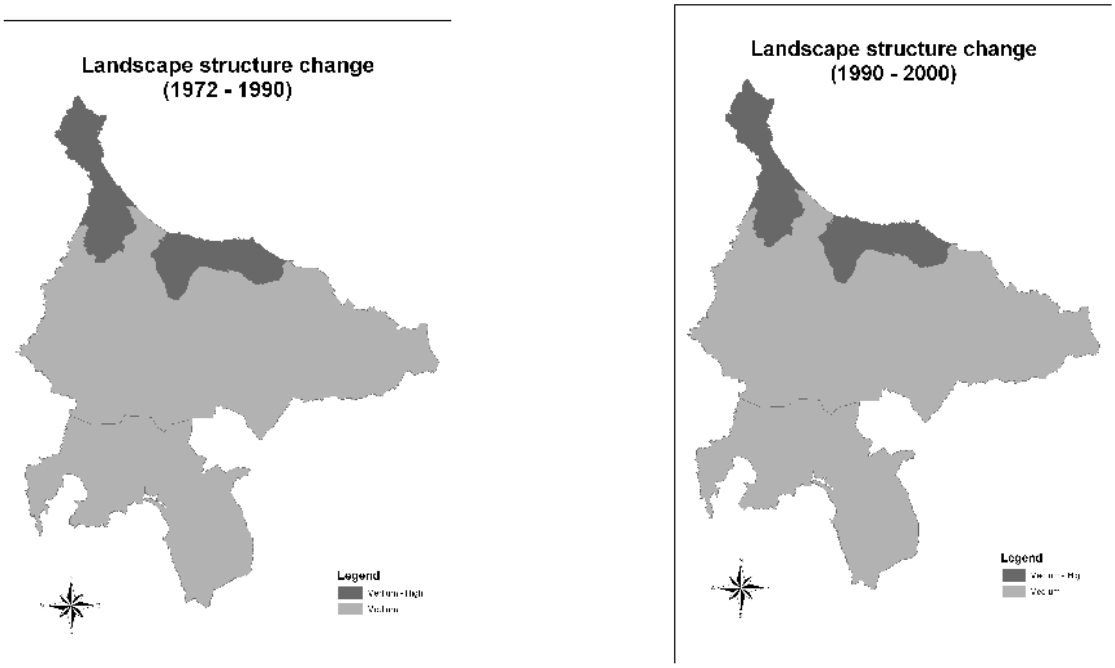

Figure 5 - Synthetic index of landscape structure change (1972 – 1990; 1990 – 2000).

As seen in the figure 5 the municipalities of Stintino and Porto Torres showed the highest level of change in the landscape structure toward a more fragmented landscape characterized by increasingly smaller and contiguous patches per unit area, decreasingly heterogeneous land cover structure, more irregular patches and closer links with each other. These results were found to be in accordance with the research findings found in literature for areas prone to desertification and land degradation (Li et al., 2004; Herzog et al., 2001).
In particular, the municipality of Stintino was the only municipality in which the diversity index continuously decreased over time, according to the assumption that the greater land use diversity is, in terms of small and contiguous plots of different land uses, the smaller the risk of land degradation and the higher biodiversity (Desertlinks, 2005).

Discussion and conclusions

On the basis of the analysis and comparison of the landscape metrics at different levels, and by means of an appropriate combination of landscape metrics into synthetic indexes, we identified areas in which specific spatial patterns related to land degradation occurred in a more intense way. By means of the methodology implemented we assessed and characterised the spatial patterns as they occurred in the study area over the twenty-eight years period investigated.

In the present research study, we explored and tested the concepts and methodology of a landscape approach in areas prone to desertification, where this kind of investigation has not been experimented on up until now. Up to now, the key research topics in landscape ecology have focused on ecological flows and processes in landscape mosaics, but landscape ecology has

been rarely combined with the issue of desertification, in particular in the Mediterranean region.

The study provided an example of the integration of remote sensing, Geographical Information Systems and landscape analysis in order to monitor the environmental changes that took place over a period of twenty-eight years. The methodology implemented and the indicators set up proved to be powerful tools for the characterisation of the spatio-temporal dynamic of landscape in an area prone to desertification. The use of a landscape approach allowed for an assessment of specific spatial patterns related to land degradation and desertification that can be used in developing practicable application plans at the regional level in desertification prevention planning and decision-making. Furthermore, the landscape indicators investigated and set up in the present research represent important tools able to integrate the standard approach commonly used until now for the monitoring of desertification, as they represent rather new indicators able to provide additional and complementary information to those provided by the most common approaches and indicators. In particular, the analysis of forestlands and urban areas and the use of indicators related to forest fragmentation, urbanization and landscape structure allowed us to identify noteworthy differences among the municipalities.

The synthetic index performed for forest fragmentation analysis, clearly demonstrated that the forest landscape of the municipality of Stintino has moved into a more fragmented structure, with more small fragments of forests that are more isolated, more irregular and less spatially connected. Here, in fact, forested areas were broken-up into smaller, more fragile, more irregular and more isolated units in favour of urban and crop areas, thus reducing their ability to resist the desertification and to recover from disturbances. Larger and better connected ecosystems, in fact, are typically more fitting at conserving biodiversity and preventing from soil erosion and land degradation than smaller and more isolated ones.
The tourist vocation of Stintino represented the main driving force behind the changes occurred, as new tourist settlements were built mainly along the northern side of the coastal areas. Rapid development of urbanization and tourism thus increased the demand for proper infrastructure such as roads, water facilities and utilities. As a result, areas used for settlements have expanded in extreme proportions, as planned urbanization. The obvious consequence was that this kind of urbanization consumed areas of agricultural land and forested areas that could be the cause of many harmful impacts on ecosystem structure, function and dynamics with negative consequences on biodiversity, biogeochemical cycles and land resources.

In the municipality of Sassari between 1972 and 1990 the new urban settlements grew in a sparse way, thus making the landscape more fragmented and denoting a high degree of urbanization with potential negative effects on the properties and functions of the ecosystem (Gonzalez-Abraham et al., 2007). This process was found to be similar to that occurred in the municipality of Porto Torres. The urban sprawl that occurred around the city of Sassari, which is the second city of Sardinia, was the obvious consequence of the process of urbanization from small rural villages to the urban centres. Urbanization has been quickening due to an increase in population and to migration from rural to urban areas, due to employment opportunities in the main urban center. As the city grew, the increasing concentration of population and economic activities demanded that more land be developed for public infrastructure, housing, industrial and commercial uses.

The synthetic index performed for the analysis of landscape structure change provided useful information about the evolution of the territory toward a more fragmented landscape characterized by increasingly smaller and contiguous patches per unit area, decreasingly heterogeneous land cover structure, more irregular patches and closer links with each other. These results were found to be in line with the research findings found in literature related to

desertification and land degradation (Li et al., 2004; Herzog et al., 2001). This type of landscape structure did not facilitate the conservation of landscape, as larger and connected ecosystems are typically better at conserving biodiversity and at preventing from soil erosion and land degradation than smaller and more isolated ones (Desertlinks, 2005).

The results obtained derived by the synthetic indexes set up and performed for the purpose of the present research, demonstrated to be able in identifying the areas in which specific spatial patterns occurred at some degree of intensity as degradation factors thus explaining, at least in part, the sensitivity to desertification of specific areas.
The results of the study that actually achieved analyses and monitoring of land cover and landscape change over time have, therefore, made an important step towards warning the authorities of the features of the past and current land cover and landscape changes and their consequences.

References

Bandinelli G. et al., 2000. Metodologia per la redazione di una carta in scala 1:250000 sulle aree vulnerabili al rischio di desertificazione in Sardegna, sulla base di parametri meteorologici, fisiografici e pedologici.

Baskent E. Z. and Kadiogullari A. I., 2007. Spatial and temporal dynamics of land use pattern in Turkey: a case study in Inegol. Landscape and Urban Planning, Vol. 81, pp. 316-327.

Cakir G., Sivrikaya F., Keles S., 2008. Forest cover change fragmentation using Landsat data in Macka State Forest Enterprise in Turkey. Environmental Monitoring Assessment, 137: 51-66.

Ceccarelli T., Giordano F., Luise A., Perini L., Salvati L., 2006. La vulnerabilità alla desertificazione in Italia: raccolta, analisi, confronto e verifica delle procedure cartografiche di mappatura e degli indicatori a scala nazionale e locale. APAT, CRA UCEA, Manuali e linee guida 40/2006, ISBN – 88-448-02010-4.

Costantini E. A. C., Urbano F., Bonati G., Nino P., Fais A. (curatori), 2007. Atlante nazionale delle aree a rischio di desertificazione. INEA, Roma, pp. 108.

DESERTLINKS, 2005. http://www.kcl.ac.uk/projects/desertlinks/

DesertNet, 2002-2004. http://www.desertnet.org/.

DesertNet II – Implementazione di una Piattaforma di servizi per la lotta contro la siccità e la desertificazione attraverso un sistema di azioni pilota nelle Regioni del Mediterraneo, 2005-2008. http://www.desertnet.org/.

Desertwatch, 2004-2006.
http://www.esa.int/esaEO/SEMHLU3J2FE_environment_0.html#subhead4

Geneletti D., 2004. Using spatial indicators and value functions to assess ecosystem fragmentation caused by linear infrastructures. International Journal of Applied Earth Observation and Geoinformation Vol. 5 (2004), pp. 1-15.

Giordano F., Marini A., 2008. A landscape approach for detecting and assessing changes in an area prone to desertification in Sardinia (Italy). International Journal of Navigation and Observation, Vol. 2008, 5 pp.

Gonzalez-Abraham C. E., Radeloff V. C., Hammer R. B., Hawbaker T. J., Stewart S. I., Clayton M. K., 2007. Building patterns and landscape fragmentation in northern Wisconsin, USA. Landscape Ecology, Vol. 22, pp. 217 – 230.

Herzog F., Lausch A., Muller E., Thulke H., Steinhardt U. and Lehmann, S., 2001. Landscape mtrics for assessment of landscape destruction and rehabilitation. Environmental Management, Vol. 27, pp. 91 – 107.

Kadiogullari A. I. and E. Z. Baskent, 2008. Spatial and temporal dynamics of land use pattern in Eastern Turkey: a case study in Gumushane. Environmental

Keles S., Sivrikaya F., Cakir G., 2008. Urbanization and forest cover change in regional directorate of Trabzon forestry from 1975 to 2000 using landsat data. Environmental Monitoring Assessment, Vol. 140, pp. 1 – 14.

Kosmas C., Kirkby M., Geeson N., 1999. The MEDALUS Project. MEditerranean Desertification And Land USe. Manual on key indicators of Desertification and mapping environmentally sensitive areas to desertification. European Commission, Brussels.

Li Z., Li X., Wang Y., Ma A., Wang J., 2004. Land-use change analysis in Yulin prefecture, northwestern China using remote sensing and GIS. International Journal of Remote Sensing, Vol. 25, No. 24, pp. 5691-5703.

Motroni, A., Canu, S., Bianco, G., Loj, G., 2004. Carta delle aree sensibili alla desertificazione (Environmentally sensitive areas to desertification, ESAs), Servizio Agrometeorologico Regionale per la Sardegna, Aprile 2004.

Motta M., D'Angelo M., Galli A., Zucca C., 1999. Studio di sensibilità alla desertificazione in area Mediterranea mediante telerilevamento e GIS. Atti della III Conferenza Nazionale ASITA (Federazione delle Associazioni Scientifiche per le Informazioni Territoriali e Ambientali). Napoli, 9-12 novembre, pp. 985-986.

Pittalis D., 2003. Applicazione di una metodologia per l'individuazione di aree sensibili alla desertificazione nel territorio comunale di Sassari mediante elaborazione GIS. Tesi di laurea, A. A. 2001 – 2002. Università degli Studi di Sassari – Facoltà di Agraria.

Plieninger T., 2006. Habitat loss, fragmentation and alteration – Quantifying the impact of land-use changes on a Spanish dehesa landscape by use of aerial photography and GIS. Landscape Ecology (2006) 21:91-105.

RIADE – Nuove tecnologie per la lotta alla desertificazione, 2002-2005. http://www.riade.net/.

Sun D., Li H., Li B., 2008. Landscape connectivity changes analysis for monitoring desertification of Minqin county, China. Environmental Monitoring and Assessment (2008) 140: 303-312.

Weng Y. C., 2007. Spatiotemporal changes of landscape pattern in response to urbanization: Landscape and Urban Planning, Vol. 81, pp. 341-353.

Yu X. J. and Ng C. N., 2007. Spatial and temporal dynamics of urban sprawl along two urban-rural transects: a case study of Guangzhou, China. Landscape and Urban Planning, Vol. 79, pp. 96-109.

Zhang Y., Chen Z., Zhu B., Luo X., Guan Y., Guo S., Nie Y., 2008. Land desertification monitoring and assessment in Yulin of Northwest China using remote sensing and geographic information systems (GIS). Environmental Monitoring Assessment, 147: 327-337.

Zhou Q., Li B., Kurban A., 2008a. Spatial pattern analysis of land cover change trajectories in Tarim Basin, northwest China. International Journal of Remote Sensing, Vol. 29, No. 19, pp. 5495-5509.

Zhou Q., Li B., Kurban A., 2008b. Trajectory analysis of land cover change in arid environment of China. International Journal of Remote Sensing, Vol. 29, No. 4, pp. 1093-1107.

Zucca C., Madrau S., Deroma M., Pittalis D., 2003. Il metodo ESAs per la modellizzazione del rischio di desertificazione. Applicazione in un'area della Sardegna nord-occidentale. Convegno ASITA, 2003.

POSTER

October 2010 – Iasi (Romania)

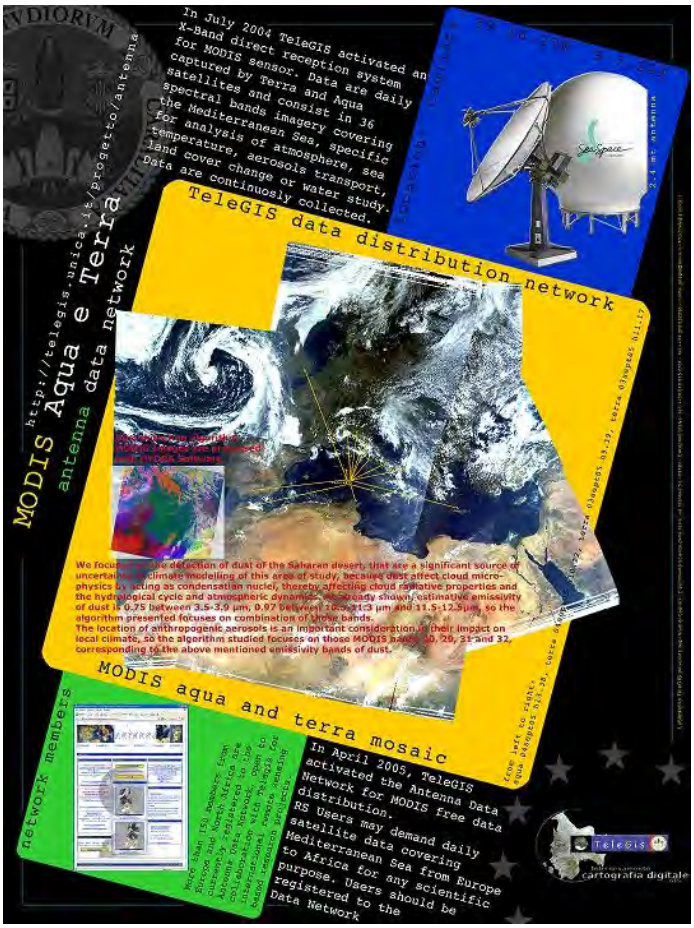

"Dust signatures in MODIS data" poster, was presented at the 4th International Symposium *Present Environment and Sustainable Developement.* The paper presented as poster was accepted for publishing in the 4th volume of the review *Present Environment and Sustainable Developement.*

CONTACTS

Personal Home Page: http://www.boccone.it
TeleGis Lab Unica : http://telegis.unica.it/

Laboratorio TELEGIS
Dipartimento Scienze della Terra
Università di Cagliari
Via Trentino 51
09127 - CAGLIARI - Italy

Tel: +39 070 675 7701
Fax: +39 070 282236
e-mail: telegis@unica.it

Marzia Boccone email: marzia@boccone.it
boccone@unica.it